Interfering of Two Tandem Cylinders Undergoing VIV: Mathematical Modelling and Experiments

by

Milad Armin

Department of Naval Architecture, Ocean and Marine Engineering

University of Strathclyde

This thesis is submitted for the degree of Doctor of Philosophy at

University of Strathclyde

September 2016

I hereby declare that this thesis is the result of the author's original research. It has been composed by the author and has not been previously submitted for examination which has led to the award of a degree. The copyright of this thesis belongs to the author under the terms of the United Kingdom Copyright Acts as qualified by University of Strathclyde Regulation 3.50. Due acknowledgement must always be made of the use of any material contained in, or derived from, this thesis.

Milad Armin

Abstract

Behaviour of two cylinders in tandem subjected to a stream of steady uniform flow is investigated. This research includes experimental and mathematical simulation so that a better understanding of the interaction between two bodies undergoing vortex induced vibration (VIV) can be achieved while one is submerged in the wake of the other. Amplitude and frequency of oscillation are observed for both cylinders when they are placed at different distances from each other. Positioning cylinders at various spacings can help to shed some light on the interaction mechanism of the upstream wake and trailing cylinder.

An experimental investigation was carried out in sub-critical Reynolds number and low mass-damping to simulate the conditions in which offshore structures are deployed. Initially, two identical cylinders are placed in-line with the stream at various spacings. The response of leading cylinder is observed to be similar to that of an isolated cylinder experiencing VIV at all spacings. On the other hand, trailing cylinder response is observed to increase with flow velocity at small and medium spacings. Moreover, as the spacing grows large downstream response becomes more similar to that of the leading cylinder. Motion trajectory of trailing cylinder is significantly influenced by the leading body, and does not follow the typical figure of eight observed for an isolated cylinder at all velocities. Frequency power spectrum of obtained time histories reveals that two sources of excitation exist for trailing cylinder. Corresponding motion to each excitation source is determined using Fast Fourier Transform.

The second set of experiment was conducted using similar cylinders with different natural frequencies to observe how it influences the interaction between two cylinders. It was observed that behaviour of trailing cylinder alters in comparison with initial set

up. However, two sources of excitation are still detected in this set-up.

Mathematical simulation is pursued by modelling the oscillating cylinders with a simple mass-spring-damper system. Furthermore, the force exerted to cylinders by wake is simulated by wake oscillators which can capture the self-exciting and self-limiting nature of VIV phenomenon. Two equations are coupled together by assuming that wake force is proportional to cylinder acceleration. Then, the system of equations is solved analytically,and results are compared to those obtained by a SimuLink model of the system. SimuLink model is solved by numerical RungeKutta method.

It was observed that model is successful in simulating leading cylinder vibration amplitude, while it, initially, fails drastically to predict the oscillation amplitude of trailing cylinder due to buffeting vortices. Two terms were added to accommodate the effect of upstream wake on the trailing cylinder, to modify the force in the equation of motion which is respectively proportional to acceleration and velocity of the cylinder. Moreover, acceleration term is determined by fitting a linear function of the variable to the difference between upstream and downstream wake force obtaining from the experimental investigation results. Additionally, the damping term is determined by optimization of variance between simulation and experiment results. Such an observation can confirm that upstream turbulent wake has a significant influence on added mass coefficient of the trailing cylinder which both are observed to be dependent on upstream Strouhal number.

Overall, the agreement between mathematical model and experimental results is evaluated for both cylinders. Model error for trailing cylinder is calculated between 20% to 30% in cross-flow direction. This error is lower than that of the leading cylinder which is a well established method in literature for simulating VIV of an isolated cylinder.

Contents

List of Figures

List of Tables

Acknowledgements

I would like to offer my sincere gratitude to my supervisors, Dr Mahdi Khorasanci and Professor Sandy Day, whose ample support enabled me to accomplish my research. It was not possible for me to finish PhD without guidances from Dr Khorasanchi. He always trusted me to accomplish my tasks. I appreciate countless hours he spent with me to discuss every single challenge I face during my stay at Strathclyde to help me move further in my studies. The support I received from Professor Sandy Day, the Head of Naval Architecture, Ocean and Marine Engineering Department, was of great importance to me. He trusted and encouraged me in the least hopeful days. I hold myself deeply indebted to him.

The staff of Kelvin Hydrodynamic Laboratory had a great impact on my success in this research. It was impossible to conduct the experiments in this study with such level of precision without their expertise. I wish to thank all of them for their technical inputs and valuable assistance.

I also want to thank all the staff in Naval Architecture, Ocean and Marine Engineering Department as they create a wonderful atmosphere for all the student in Henry Dyer Building to work and leave.

The most important people who made it possible for me to success in my studies and my life are my parents. This research was not only completed over past three years but is the outcome of many years of planning and hard work which I owe all that to my parents. They not only support me through my journey with their love and compassion but put all their resources at my disposal and I am grateful to them for the rest of my life. Past few years were not only tough for me but even harder to my parents as they had to comfort themselves in my absent as they witnessed my struggles trough PhD

and went to extreme measures to help me conquer each challenge. Although I can never repay you, I always love you.

Nomenclature

Abbreviations

CFD	Computational fluid dynamics
DFT	Discrete Fourier transform
DOF	Degrees of freedom
FFT	Fast Fourier transform
FIV	Fluid induced vibration
RMS	Root mean square
STD	Standard deviation
VIV	Vortex induced vibration
WIV	Wake induced vibration
fo8	Figure of eight trajectory

Roman symbols

A	Cylinder cross section
A_r	Supporting rod cross section
A_x,A_y	FIV amplitude in cross-flow and stream-wise directions respectively, none-dimensionalised by cylinder diameter
A_X, B_Y	Added mass modification coefficient in stream-wise and cross-flow respectively for trailing cylinder.
C_1	Mean drag modification coefficient of trailing cylinder.

c	damping
c_a	fluid added damping
c_s	structural viscose damping
C_a	Added mass coefficient
C_D	Oscillating drag coefficient
C_{D_0}	Mean drag coefficient
C_L	Oscillating lift coefficient
C_{L_0}	Stationary cylinder oscillating lift coefficient
D	Circular cylinder diameter
D_r	Supporting rod diameter
e_x, e_y,e_t	Average simulation error, in stream-wise, cross-flow and combined respectively, of the mathematical model from experimental results at various reduced velocities.
E	Modulus of elasticity
E_X, F_Y	Fluid added damping modification coefficient in stream-wise and cross-flow respectively for trailing cylinder.
f_i	Frequency index
f_n	Natural frequency
f_r	Response motion frequency
f_s	Vortex shedding frequency
I	Supporting rod's moment on inertia about bending neutral axis
k	Supporting rod's stiffness
L	Longitudinal distance from centre of the leading to trailing cylinder
L_c	Length of cylinder
L_r	Length of supporting rod
m_s	Structural mass
m_a	Added mass of a cylinder
M	equivalent of structural and added mass at the centre of gravity
Re	Reynolds number: $Re = UD/\nu$

St	Strouhal number:$St = f_n D/U$
T	Transverse distance between centre-to-centre of pair of side-by-side cylinders
T_s	Sampling rate
U_r	Reduced velocity:$U_r = U/f_n D$
X_i	Damped oscillation amplitude response

Greek symbols

α, ϵ	Empirical coefficients
β	Angle between free stream and cylinder relative velocity
δ	Logarithmic decrement
γ	Fluid added damping coefficient $\gamma = \dfrac{C_D}{4\pi St}$
ν	Water kinematic viscosity
ω_a, ω_d	Analogue and digital cut-off frequency
ω_n	Natural frequency
ω_s	Shedding frequency
ω_0	$\dfrac{\omega s}{\omega_n}$
ψ	Angle of incident
ϕ_1 and ϕ_2	Phase difference between up and downstream wake forces and leading cylinder motion
ρ_w	Specific mass of water
τ	Non-dimensional time
θ	Phase difference between leading and trailing cylinders motion
ξ	Structural reduced damping ratio

Chapter 1

Introduction

Long slender structures are parts of many complex engineering systems. Power transmission cables in Electrical Engineering, a stack of chimneys and suspension cables of a bridge in Civil Engineering, slender tubes inside a heat exchanger in Mechanical Engineering, riser and mooring lines in Offshore Engineering are few examples of such structures attractive to engineers in different fields. Most of these structures are subjected to some fluid current, whether it is water or air, thus interaction of these structures with fluid is of all engineers concern.

As the current passes a slender structure, separation happens at high *Reynold number* (Re) which exerts a force on the structure due to asymmetric pressure distribution around it. This force induces a sinusoidal motion in a bluff body. The *fluid induced vibration* (FIV) could be beneficial (source of renewable energy) or could endanger structural integrity by reducing the fatigue life drastically.

FIV has been attractive to engineers for many years especially for past two decades. There is an accelerated growing rate of studies being conducted in recent years due to technological advancement in the field of Offshore Engineering. Exploration and production of hydrocarbons in deep water require risers and mooring lines that can reach water depth up to $3000m$. These long slender cylindrical structures have a complex interaction with the fluid medium surrounding them. This complexity is not only due to the length of these structures but also because of the coupled interaction between fluid and structure through the forces they apply to each other (from fluid to the structure and vice versa). Understanding the physics governing this phenomenon is still a

challenge due to this mutual interaction. The nature of this interaction depends on characteristics of both structure and fluid. For instance, if an external steady flow passes an uniform bluff body which is constrained in a way that it can freely oscillate, the structure may respond with vibration caused by vortices shedding from its aft side which is called *vortex induced vibrations* (VIV).

VIV motion is very common for offshore structures and oscillation amplitude can reach as large as $2D$. The importance of understanding and controlling VIV is truly understood when it is realised that such vibration could bring a drilling operation into halt due to abrasion of drilling riser and the drilling pipe or reduction of a production riser's fatigue life from 25 years to only matter of days. This dramatic effect attracts researchers to study VIV extensively.

1.1 Objectives

Most of the studies conducted on FIV have tried to isolate a cylindrical structure and subject it to a fluid current to observe its behaviour while undergoing FIV. The set-up of these studies varies based on structure's *degrees of freedom* (DOF). Many researchers constrained a rigid structure in all directions except cross-flow (perpendicular to stream direction) and studied the structural response in this direction as well as hydrodynamic forces acting on the structure. However, it is known now that allowing the structure to oscillate in both cross-flow and stream-wise directions yield more accurate results since 1DOF systems have smaller response amplitude in comparison to that of a system with 2DOF at the same Re. Moreover, some researchers consider a flexible structure which means FIV could be observed in all three directions including along the length of the structures where mode shapes become significant. On the other hand, some studies considered a fixed structure to simplify the system. By eliminating the effect of structural motion on the flow regime it becomes possible to focus on the effect of hydrodynamic forces on the structure in an uncoupled system.

Nevertheless, considering an isolated structure does not simulate a real engineering system. In most of the engineering applications that were mentioned earlier two or more structures are placed in proximity to each other, thus, considering only a single cylin-

Figure 1.1: Production TLP on Statoil's Heidrun field, Norwegian Sea. Courtesy of www.offshoreenergytoday.com.

der will ignore the interaction between these structures. Figure1.1 shows a production *tensioned leg platform* (TLP) on Heidrun field in which it can be seen how wakes of two legs are merging into each other (affecting the flow regime around each leg) as well as how closely all risers are arranged in an array at midsection of the platform.

Recently more researchers are trying to address this issue and consider multiple structures (mostly cylindrical) in close proximity so that FIV of a bluff body in the wake of another structure could be observed. However, most of these studies have not gone any further than observation and classification of flow regimes. In this study, we are trying to observe how different FIV of two tandem structures is from VIV of an isolated cylinder. In this context, the main objectives of this research are:

1. Understanding the physics governing FIV of two flexibly mounted rigid cylinders in tandem. It is necessary to comprehend how turbulent wake of the leading cylinder affects FIV of the following body. Moreover, most of the previous works have considered a fixed leading cylinder so by considering two oscillating cylinders it is possible to study the effect of interaction on leading cylinder as well.

2. Observing the effect of spacing between two cylinders. It is well known that the flow velocity in the wake of a structure gradually increases. It is important

to observe how velocity gradient in the wake could aggravate or suppress FIV of a trailing body. This observation can determine what the optimum distance between two offshore (or any other engineering application) structures in tandem arrangement could be.

3. Parametric study on the effect of two cylinders' structural property on their FIV. In the current study, we consider how a change in natural frequency could alter the nature of cylinder's interaction with each other. The outcome could provide engineers with insight into how to arrange structures in clusters in respect to fluid stream direction.

4. Producing a fast and accurate predictive mathematical model. Many studies have been conducted recently to employ a non-linear differential equation to describe VIV phenomenon of a single cylinder. Van der Pol and Rayleigh equations are two popular wake oscillators that have been considered to model the hydrodynamic forces from vortices acting on a cylindrical structure undergoing VIV. Solving any of these equations along with structural motion equation would provide a prediction of frequency and amplitude of the vibration. In the present research, we will try to adopt such a notion for predicting FIV of the trailing cylinder. This method could provide reliable predictions in the early stages of design process.

1.2 Methodology

It is not possible to model a full-scale risers cluster, which could run up to $2000m$ of water depth, in a laboratory, in a way that it could represent all the original structural properties. Considering a riser with different stiffness, damping and natural frequency in each direction shows us how complicated a riser system is to be simulated numerically. Different wave heights with varying frequencies along with marine currents make it almost impossible to model an FIV phenomenon fully. For these reasons researchers have been trying to simplify the model by considering a rigid cylinder as the representative of one section of a long slender, flexible riser. Besides, different studies have tried to limit motion of the structure to gain a better understanding of how hydrody-

namic forces can excite the structure into FIV. A rigid cylinder could be fixed or free to oscillate in cross-flow or/and stream-wise direction(s).
There are three common methods to study FIV, experimental investigation, computational fluid dynamics (CFD) and mathematical modelling.
In the present study, two rigid identical cylinders are considered in tandem, each is allowed to vibrate freely in both directions, cross-flow and stream-wise.

- An experimental investigation was conducted at various spacings. The experiment apparatus will be verified by comparing the results from only one of the cylinders isolated, with the data available in the literature.

- Using the understanding gained through the experiment; this study will adopt the wake oscillator idea and apply it to a pair of cylinders in line. The solution of wake oscillator coupled with a structural motion equation will be used to predict the behaviour of the system at different *Re*. This mathematical model will be solved via Runge-Kutta method, using SimuLink package in Matlab software which will be validated against analytical solution obtained by the author. The model will also be validated against our experiment results in order to evaluate the empirical coefficients of the wake oscillators.

1.3 Structure of the thesis

The structure of present work can be divided into five chapters including this chapter.

- Chapter 2 includes an overview of previous studies focused on FIV. The first part looks at VIV of an isolated bluff body. The second part is a literature review on two cylinders in proximity.

- Chapter 3 describes of the experimental investigation, the apparatus design and set-up. The method used for post-processing the experimental data is presented as well. Moreover, preliminary results obtained are shown with extensive discussion about the physics of the interaction between two cylinders.

- Chapter 4 includes discussion on mathematical modelling, initial analytical solution and its comparison with SimuLink model. A parametric study is carried out

on the original model to observe the effect of different variables and to adjust the model for the trailing cylinder.

- Chapter 5 includes a comparison between the hydrodynamic force of the wake for both cylinders. This comparison leads to identifying two new terms to account the disturbance trailing cylinder experiences in the wake of the leading body.

- Chapter 6 is the conclusion of this study and summarise the main findings. Additionally, some suggestions have been made here for future works that author believes would shed more light on FIV and interaction of multiple structures in close proximity.

Chapter 2

Critical Review

This chapter is a review of previous researches with the focus on FIV of bluff bodies. This review is made up of three sections, "An isolated Cylinder", "Wake Interference" and "FIV of Two Cylinders in Tandem". First section focus is on a single cylinder subjected to steady fluid stream and its vortex shedding mechanism and response to this excitation as well as gradual increase of interest to systems with one and two DOF which was confirmed to be of significant interest to offshore engineers.
The second section includes a brief review of more complex arrangements where two cylinders are in close vicinity. Three categories are reviewed based on the location of structures concerning each other.

2.1 An Isolated Cylinder

In fluid mechanics an object is categorised as a *bluff body* when flow separation occurs over the main surface. A circular cylinder which is the subject of this study is a classic example of a bluff body.

2.1.1 Vortex Shedding Mechanism

As a stream of fluid encounters a circular cylinder, it has to change its path and passes over the upper and lower faces of the cylinder. Viscosity reduces the flow velocity until fluid flow stops on the surface and creates a pressure gradient. At this point, the bound-

ary layer that has been developing from the stagnation point in front of the cylinder separates from the surface and creates a shear layer. There are two separation points on each side of the cylinder where the pressure gradient around the cylinder is zero. It should be mentioned that boundary layer is a layer close to cylinder wall with a shear velocity profile. At low velocities the shear layer does not acquire enough momentum so viscous forces dominate. Thus the layer cannot separate from the surface.

By increase in velocity fluid particles gain enough momentum for separation and increases the vorticity gradient between stagnation point and back of the cylinder. The shear layer vorticity causes this layer to roll behind the cylinder where each shear layers form a vortex on either side of the body with opposite signs. Such a symmetric flow regime persists over a wide range of velocities; however, further growth of velocity results in unstable flow regime, therefore, flow eventually becomes asymmetric, and vortex generation sequence becomes Intermittent (figure 2.1), in other words one vortex develops larger (vortex A) than the one on the other side of the cylinder (vortex B).

As vortex A is stronger, it pulls its counterpart into the cylinder wake until the second vortex is strong enough to pull back and detaches vortex A from the cylinder shear layer (figure 2.1a). However, shear layer continues to roll up behind the cylinder and creates a smaller vortex (C) with the similar sign as A [2]. Interaction between vortex B and C undergoes similar steps as A and B which results into detachment of B. Such an alternative sequence of individual shed vortices forms a pattern in the aft of cylinder which is the characteristic of von Kármán vortex street.

2.1.2 Governing Parameters

Strouhal number

The aforementioned cycle generate vortices at a specific frequency f_s that is commonly expressed in a non-dimensional form as a *Strouhal number* [3].

$$St = \frac{f_s D}{U} \tag{2.1}$$

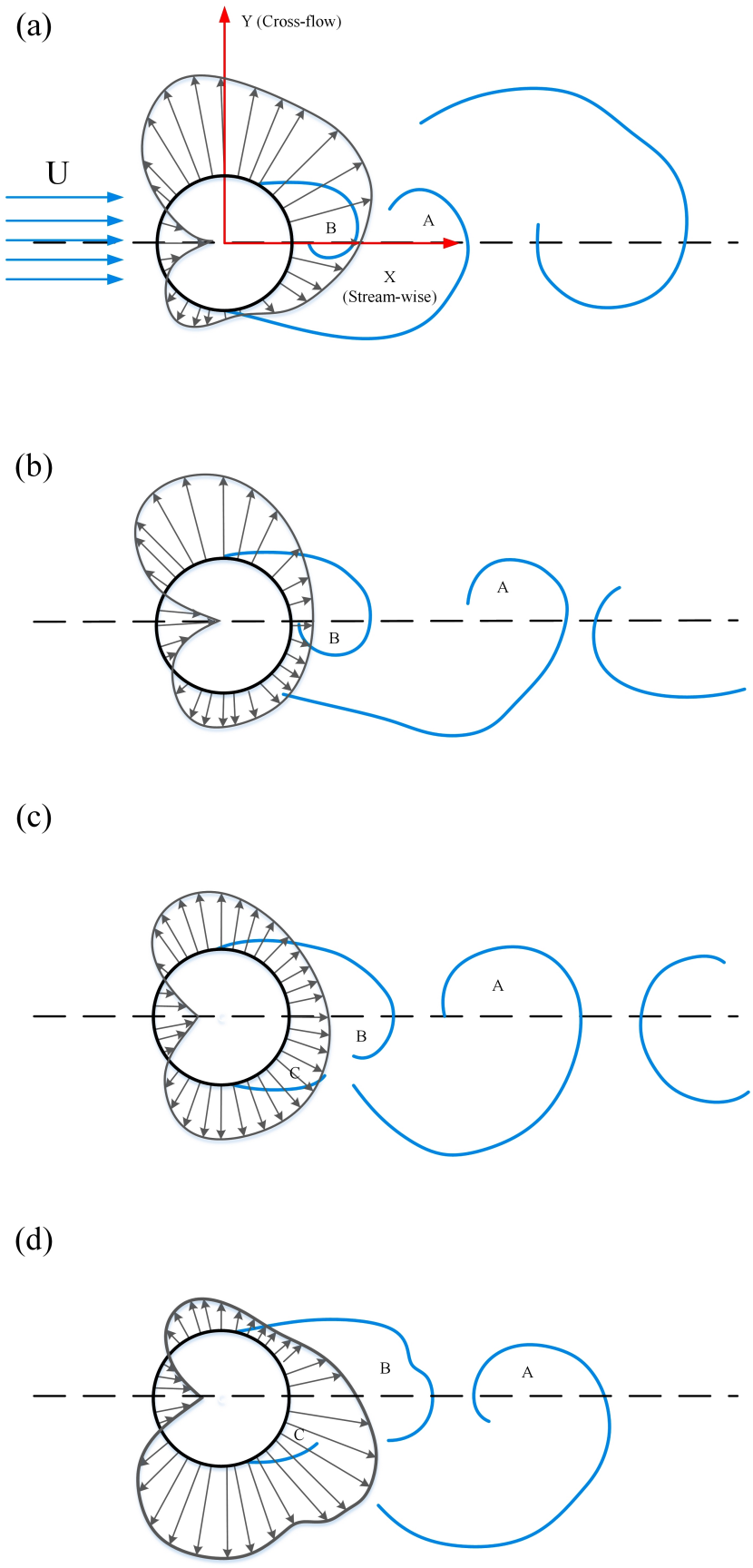

Figure 2.1: Pressure contribution diagram around a cylinder and vortex shedding sequence. Adopted from [1].

Strouhal value has been measured to be approximately 0.2 for a smooth cylinder in wide range of Re in sub-critical regime which is the scope of this research [4].

Reynolds number

The transition between flow regime with symmetric and the one with alternative vortices can be distinguished by another non-dimensional term known as *Reynolds number* (Re).

$$Re = \frac{UD}{\nu} \tag{2.2}$$

where U is stream velocity; D is the cylinder diameter, and ν is the kinematic viscosity of the fluid medium. It has been established that when $Re < 5$ there is no detached shear layer from the surface of cylinder (figure 2.2a) [1] this regime is referred to as *creeping flow*. As it grows large, within the range of $5 < Re < 40$ the flow regime is similar to what has been described as symmetric with two vortices at each side of the cylinder(figure 2.2b). Further increase of Re causes instability in the wake of the cylinder and the von Kármán vortex street forms in the wake however wake is still laminar (figure 2.2c). The transition of the wake from laminar to turbulent happens at $Re < 150$ however the boundary layer is still laminar. The focus of this study is falling into $300 < Re < 1.5 \times 10^5$ which is called subcritical region where a fully developed von Kármán vortex street is visible (figure 2.2d). The range of Re between 1.5×10^5 to 3.5×10^6 is referred to as critical range due to the transition of the boundary layer from laminar to turbulent. Turbulent boundary layer has more kinetic energy and can travel further into the pressure diagram thus the separation is delayed; the wake in this region is narrow and chaotic (figure 2.2e). Due to such a chaotic wake, the Strouhal number can reach up to $St = 0.5$ [1, 5]. Nevertheless, after boundary layer transition to turbulent regime, von Kármán vortex street would be re-established by turbulent vortices (figure 2.2f).

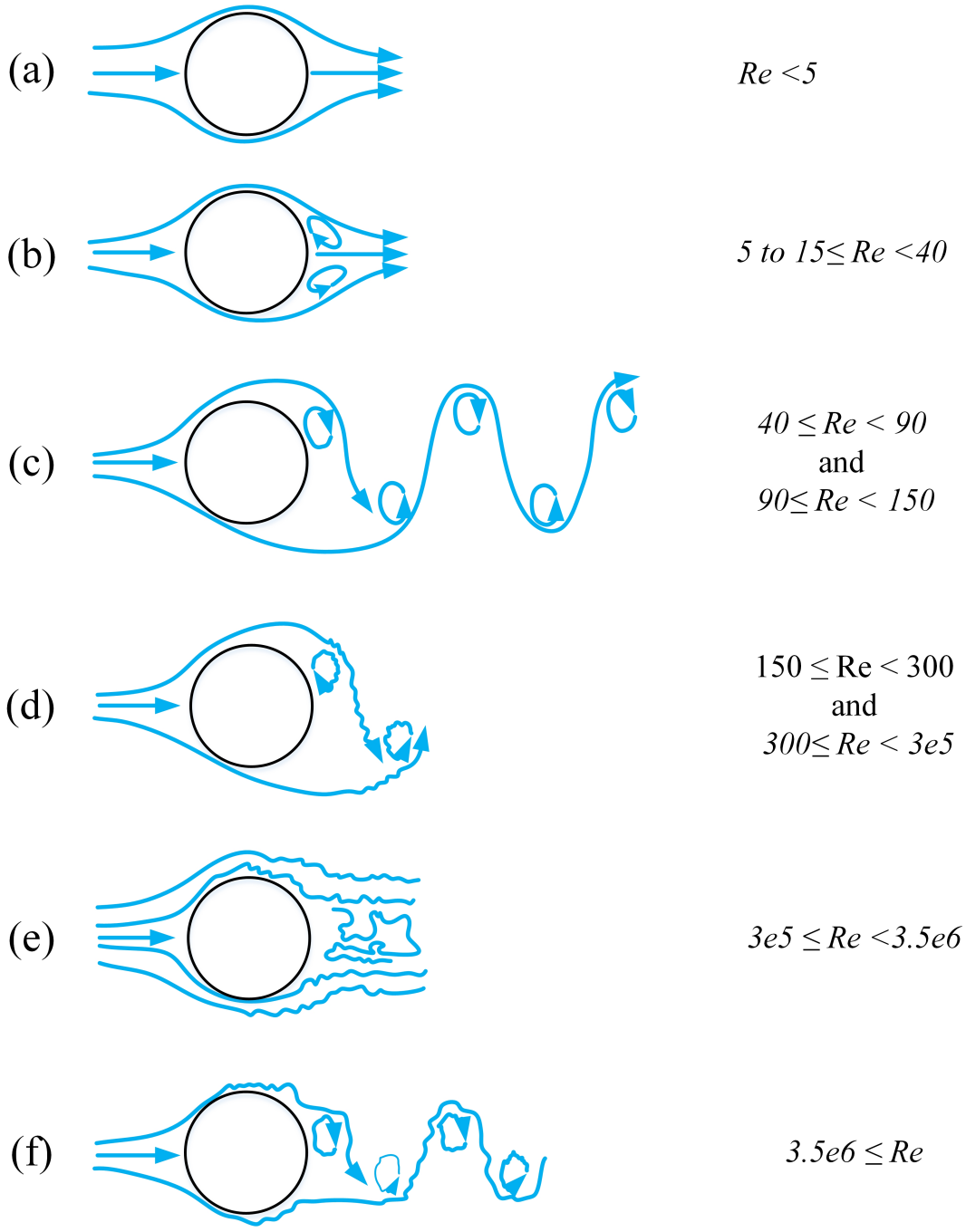

Figure 2.2: Development of flow regime around a bluff body as a function of *Re* in sub-critical region. Adopted from [1].

Hydrodynamic coefficients

The diverse pressure distribution around the cylinder, that is caused by geometry of the bluff body, is shown in figure 2.1. Failure in recovery of the base point pressure at the aft of cylinder creates a stream-wise constant mean drag on the cylinder. Additionally vortex shedding exerts an extra drag force on the body which has similar alternative nature. Combination of these two drag components is considered as drag force (F_D) and can be non-dimensionalised by dynamic pressure head:

$$C_D = \frac{F_D}{\frac{1}{2}\rho U^2 D} \tag{2.3}$$

Figure 2.3 demonstrates the variation of mean drag coefficient $\left(\overline{C}_D\right)$ and oscillating drag coefficient $\hat{C}_D$ against Re [6]. It can be observed that in scope of this paper $\left(\overline{C}_D = 1.2\right)$. The abrupt drop of $\left(\overline{C}_D\right)$ in critical region of Reynolds number is outstanding which is caused by delayed separation, which Zdravkovich [6] called it *drag crisis*.

The asymmetric flow around the body exerts another force on the body which is in cross-flow direction and is referred to as lift.

$$C_L = \frac{F_L}{\frac{1}{2}\rho U^2 D} \tag{2.4}$$

Lift force unlike drag has no mean value however, its amplitude has observed to be greater than drag force amplitude [5]. Additionally, by comparing the oscillating drag and lift it is clear that due to nature of vortex shedding in each cycle drag component has frequency twice that of lift [1]. Lift coefficient response to Re variation is included in figure 2.3 as well.

2.1.3 Cylinders With One Degree of Freedom

This study is focusing on sub-critical region due the fact that vortex shedding is strong and highly periodic in this region. Interaction of vortices and structure could lead to

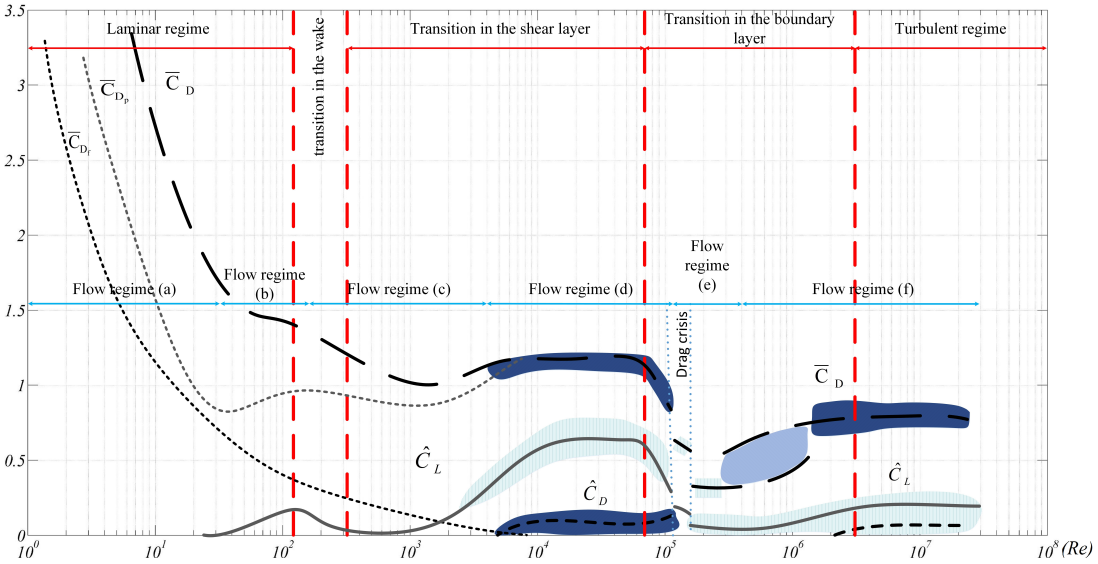

Figure 2.3: Variation of hydrodynamic coefficients as a function of Re for a circular cylinder. As well as, flow regime and boundary layer in respective Re. $\overline{C}_D$ is mean drag($\overline{C}_{D_p}$ and $\overline{C}_{D_f}$ is drag force due to pressure and friction, respectively.), $\hat{C}_D$ and $\hat{C}_L$ are fluctuating drag and lift respectively. Adopted from [1, 6]

strong vibration of the body if it is not constrained in all directions. Such a oscillatory response is known as Vortex Induced Vibration (VIV). Figure 2.4 includes a typical amplitude (a) and frequency response (b) of a cylinder undergoing VIV at different velocities [7]. Free stream velocity (U) is commonly reported in non-dimensional form using system natural frequency in the fluid medium f_n and it is called *reduced velocity* (U_r) [8].

$$U_r = \frac{U}{f_n D} \tag{2.5}$$

The vortex shedding frequency follows the similar trend of a fixed cylinder ($St = 0.2$) and increases with increase of reduced velocity (Strouhal rule). However, as f_s grows larger it coincides with natural frequency of the system, response amplitude is amplified, similar to a resonance response. At this point shedding frequency inter-locks with structure natural frequency ($f_s = f_n$) and becomes independent from reduced velocity until very high U_r when it follows Strouhal rule again. Such a behaviour is known as the *Synchronisation* and this region of reduced velocity, during which structure undergoes high amplitude oscillation, is referred to as *Lock-in range* [9]. It should be noted that since the frequency of drag force is twice of that of lift force, stream-wise lock-in occurs earlier than cross-flow [10].

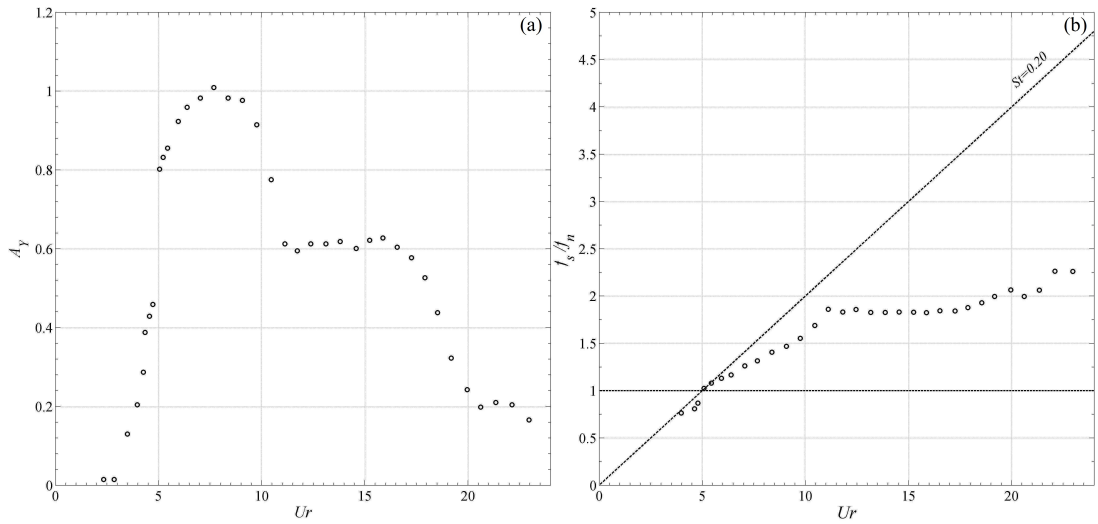

Figure 2.4: Typical VIV (a) amplitude and (b) frequency of a single cylinder where $m^* = 1.2$ and $\xi = 0.01$. Adopted from [7]

Mass Ratio

The width of lock-in range significantly depends on the cylinder mass and fluid in which it is oscillating [11]. As the cylinder vibrates it accelerates the fluid surrounding it which imposes higher force and causes the cylinder to appear heavier than its dry mass. If the fluid medium is air the added fluid mass can be neglected, however, for heavy fluids such as water, it is important to consider the fluid added mass per unit length which is a function of cylinder submerged area and the fluid density. It can be calculated using the following expression:

$$m_a = \frac{\pi}{4} C_a \rho_w D^2 \tag{2.6}$$

Here, C_a is the *added mass coefficient* that can be obtained using potential flow calculation or by forced VIV experiments. The value of this coefficient for a circular cylinder is commonly considered as unit [1, 12]. Ratio of cylinder dry mass to displaced water is defined as *mass ratio* (m^*).

Williamson et al. [9] carried out an extensive observation on the mass ratio effect on VIV response of a single cylinder which revealed that as the mass ratio decreases the

width of lock-in increases. Additionally, they observed that at a very low mass ratio, very high amplitudes could occur. Therefore, they divided VIV response of a single cylinder into three branches; i) *initial branch* which is for systems with both low or high mass ratios at low reduced velocities; ii) *lower branch* which similar to previous branch could be achieved by both systems at medium to high reduced velocities; iii) *upper branch* which was only observed for low mass ratio systems at medium velocities. Govardhan and Williamson [13, 14] observed during their experiments that if the mass ratio was brought down enough, lock-in range could be infinite, meaning that cylinder could stay in synchronisation for a broad range of reduced velocities. In literature, this mass ratio is referred to as a critical mass ratio.

Damping Ratio

In the same manner that mass ratio affect the width of lock-in range, damping can influence maximum response amplitude. In study of VIV two sources of damping exists: i) Structural damping (c) and ii) fluid-added damping and in general is considered to be proportional to cylinder velocity.

The structural viscous damping is commonly reported in non-dimensional form as *damping ratio* (ξ),

$$\xi = \frac{c}{c_r} \tag{2.7}$$

where c_r is critical damping which is proportional to square root of structural stiffness and its dry mass$\left(2\sqrt{km}\right)$. Also, fluid added damping is induced by cylinder motion in the fluid thus it is proportional to mean drag force [1].

Blevins and Coughran [15] observed in their experimental investigation that reduction in the damping ratio significantly increases cylinder maximum response amplitude. Moreover, it was noted that increase in oscillation amplitude influences mean drag coefficient of the cylinder which was observed by Sarpkaya [16] and Vandiver [17] to be proportional to cross-flow response amplitude.

Since the early work of Bishop and Hassan [18] there has been numerous studies on the VIV of a single cylinder especially with a focus on the effect of mass and damping

ratio which comprehensive summary of them can be found in review papers such as Williamson and Govardhan [19], Williamson et al. [9] and Sarpkaya [20].

2.1.4 Systems With Two Degrees of Freedom

In VIV study many researchers have focused on the systems with 1DOF specifically in cross-flow since response in this direction can reach a larger amplitude ([15, 21]) and assumed their findings could be extended to the other direction. However, early works of Moe and Wu [22] and Sarpkaya [23] showed that allowing a cylinder to oscillate in both directions (cross-flow and stream-wise) would significantly increase the cross-flow response amplitude. Govardhan and Williamson [24] reported that this increase is negligible for $m^* > 6$ and adding another degree of freedom for mass ratios smaller than that (the category most of offshore structures fall into) influences behaviour of the system.

Such observations were made by Jauvtis and Williamson [25] as well. They compared two systems with $m^* = 2.6$ and 7 when they were allowed to oscillate in cross-flow only and when they had 2DOF and observed that for $m^* = 7$ cross-flow amplitudes were almost identical. On the other hand, the response of the system with smaller mass ratio displayed a larger maximum amplitude which occurred at a higher reduced velocity. Figure 2.5 shows a comparison between two systems with high and low mass ratio where they are free to oscillate in both directions.

Maximum response amplitude in systems with 2DOF has repeatedly occurred at a higher reduced velocity in comparison with similar systems which are allowed to oscillate only in cross-flow. Srinil and Zanganeh [26] has correlated this phenomenon with geometrical non-linearity of spring system in their model test, however, as it will be observed in chapter3, this deflection occurred in the experiments of this study as well which suggest that cylinder wake should be searched for the source of non-linearity rather than structure.

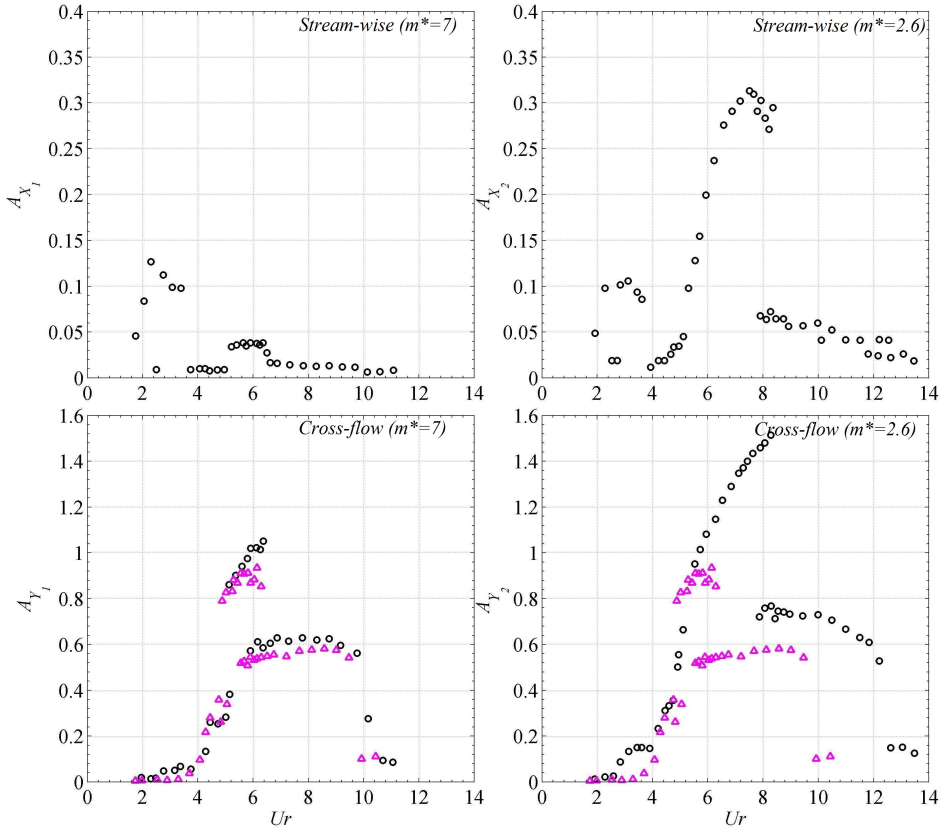

Figure 2.5: Amplitude response of a single cylinder at different mass ratios with one (△) and two degree(s) (○) of freedom. Adapted from [25].

2.1.5 Mathematical Modelling of VIV Phenomenon

Complexity of VIV phenomenon is due to the interaction between oscillating structure and passing fluid which is governed by multiple parameters. Understanding such a phenomenon is challenging with the limited information provided by studies as mentioned earlier. Nevertheless, many attempts have been made to propose a mathematical model to simulate VIV response of a single cylinder [8].

A common notion in literature is to simulate the structural response with a simple equation of motion which has the wake force on the right-hand side as the excitation term. Additionally, the self-exciting and self-limiting nature of fluid force could be simulated by a wake oscillator and be coupled with the structural motion equation. The wake oscillator model is often represented by *van der Pal* or *Rayleigh* equations. Such models are known as *empirical models* due to existing empirical coefficients in the models. Empirical coefficients are usually determined through calibration of these

models against experimental results.

Facchinetti et al. [27] conducted an extensive study on simulation of fluid force on a single rigid cylinder with van der Pal wake oscillator and the structure with a simple mass-damping system. Moreover, they focused on the coupling between two equations (wake oscillator and equation of motion). They considered three different couplings which were proportional to cylinder displacement, speed and acceleration and observed that acceleration coupling yielded the most agreeable simulation with experiment.

However, their study was limited to a system that was assumed to be constrained to oscillate only in cross-flow whereas in real engineering applications structures are often free to oscillate in other directions as well. Thus, Zanganeh [28] tried to extend this model to a system with freedom to oscillate in stream-wise and cross-flow directions. Moreover, he suggested replacing a duffing oscillator to simulate the structural vibration. He demonstrated that empirical coefficients could be determined as a function of mass and/or damping so that the need for calibration of the model against experimental results would not be immediate.

2.2 Wake Interference

In more general settings, when a bluff body is placed immediately in the wake of another body, fluid-structure interaction of both structures transform drastically. In recent years researchers have moved forward from studying the flow regime around an isolated cylinder to multiple cylinders placed nearby [29]. In this section, the focus will be on the simplest arrangement where only two cylinders are considered which is the focus of this study.

The arrangement of two cylinders could be divided into three categories. i) Side by side, where two cylinders are placed in proximity but are not immersed in each other wake. ii) Tandem, where two cylinders are in-line, and one is fully submerged in the wake of the leading cylinder. iii)Staggered, where trailing cylinders is entirely or partially immersed in the wake of the leading body. The spacing between two cylinders significantly impacts the flow regime around them and their interaction with each other. For

first two arrangements this space is reported as centre-to-centre distance between two cylinders (T/D and L/D respectively) (figure 2.6a,b) while for staggered arrangement both could be reported or centre-to-centre spacing (pitch ratio P/D) plus angle of incident between two cylinders could be reported (figure 2.6c).

Regardless of the arrangement, the fluid-induced vibration of a pair of cylinders has been studied through experimental investigation, numerically (CFD) and mathematical modelling. In the following, it is attempted to classify wake -interference based on the flow regime around two cylinders.

2.2.1 Staggered Arrangement

One of the most influential studies on the wake interference is Zdravkovich [29]. He attempted to categorise a cluster of pipes based on the flow pattern around them through a series of experiments. For a pair of cylinders four flow regimes were identified (figure 2.7):

- **Proximity interference**: none of the cylinders is immersed in the wake of the other, but they are close to each other enough to influence their wake. It was observed that if two cylinders placed closely together regardless of their arrangement act as a single body and shape a solo vortex street. It is for $T/D < 1.2$ for side by side and $L/D < 1.8$ for tandem arrangement.

- **Wake interference**: one cylinder is completely, or partially is immersed in the

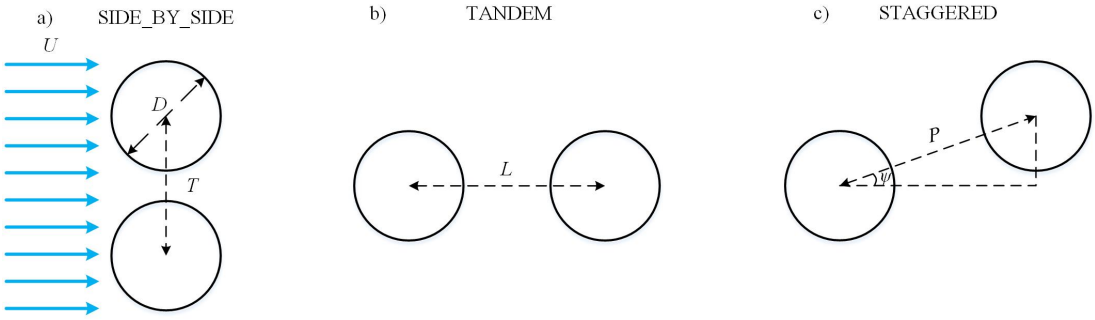

Figure 2.6: Three possible arrangements of a pair of cylinders in close proximity. (a) Side-by-side, (b) Tandem and (c) Staggered.

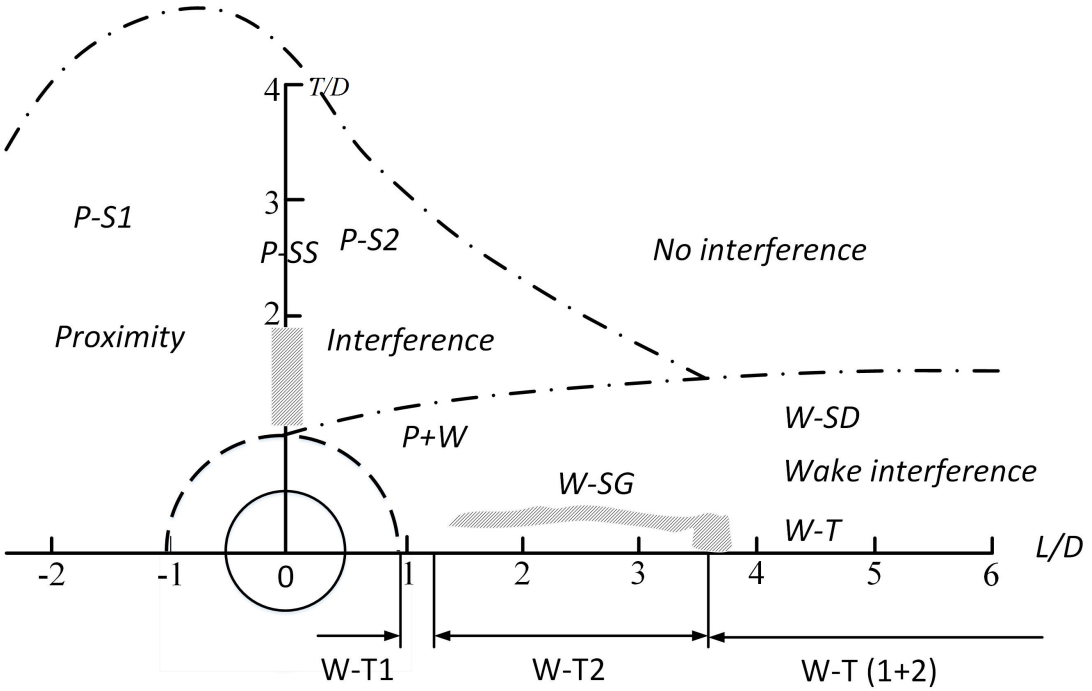

Figure 2.7: Interaction of two fixed rigid cylinders as a function of the distance between them. Four main regions are shown: Proximity interference, Wake interference, the combination of these two and no interference. Adopted from [29].

wake of the other one. Tandem arrangement which is the focus of this study is a particular case of this arrangement.

- **Combination of these two**

- **No-interference regime**: In this regime, two cylinders are distanced from each other enough that the interference is negligible thus the flow around cylinders is similar to that of an isolated cylinder.

Sumner et al. [30] focused his study on the Wake Interference area and extended this classification. He divided the flow pattern around two staggered cylinders into three categories:

- **Single bluff body**: this flow pattern was observed when two cylinders were placed in contact with each other or at very small distances with a large incidence angle between them. It was similar to that of a single body which means a shear layer separated from each cylinder is combined then rolls up in the immediate

wake behind two cylinders and forms a single vortex street.

- **Small-incident-angle flow pattern**: This flow pattern was observed when $0^{\circ} < \psi < 30^{\circ}$ (2.6 C) and can be divided into three groups. i) At small pitch ratios and incidence angles, the upstream shear layers reattached on the trailing cylinder. ii) As ψ grew large the reattachment could not be maintained so the shear layer was deflected into the gap between two cylinders and rolled up which results in separation on the trailing cylinder. iii) While ψ was still small at the large pitch ratios the deflected shear layers in the gap could form a fully developed Kármán vortex street which was referred to as *vortex buffeting* flow pattern.

- **Large-incident-angle flow pattern**: in the large incidence angle both cylinders were observed to develop a separate vortex street. The most common flow pattern was *Synchronised Vortex Shedding* where both vortex streets were synchronised and formed two adjacent anti-phase streets.

Hydrodynamic Coefficients

The alteration of flow pattern around two cylinders in the wake interference region has a significant influence on pressure gradients around both cylinders in comparison with an isolated cylinder. Transformation of the pressure gradients results into different hydrodynamic coefficients for both cylinders.

Zdravkovich [29] showed how lift and drag coefficients vary for two staggered cylinders as well as their Strouhal number, (figure 2.8). He observed that for large incidence angle $\psi > 40$, leading cylinder experienced a lift force pushing it away from trailing body. On the contrary, if two cylinders were close to each other, at a small incidence angle they experienced a lift force towards each other. Moreover, the lift force became stronger as two cylinders came closer together regardless of the incidence angle between them. Additionally, based on his observation, drag force increased with increase of ψ until it reached the value of an isolated cylinder ($C_D = 1.2$).

Sumner et al. [31] also conducted an experiment on two identical fixed staggered cylinders in sub-critical Re. They focused on aerodynamic forces and Strouhal number for both cylinders in different arrangement and tried to classify them based on pitch ratio

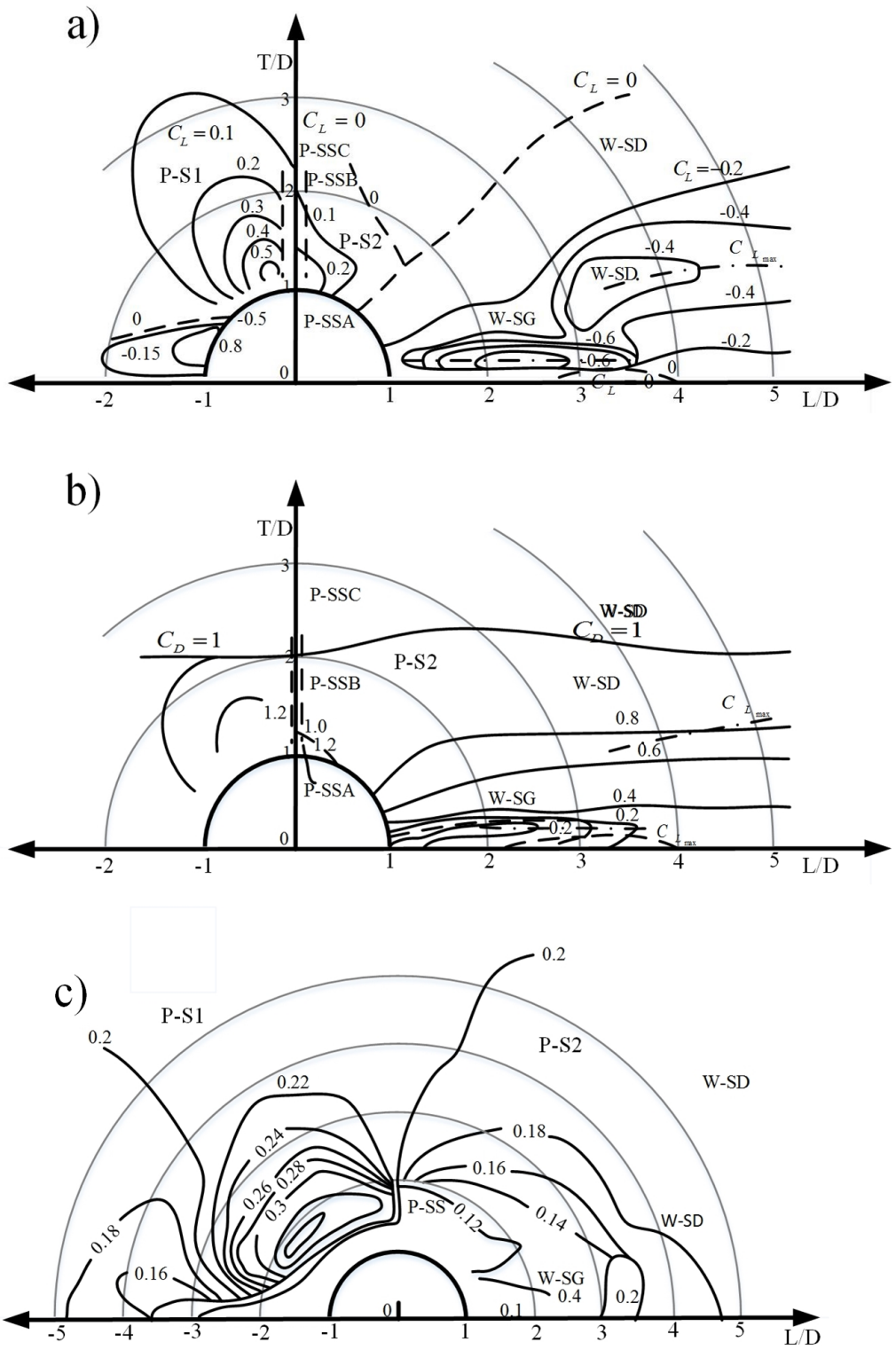

Figure 2.8: Variation of hydrodynamic coefficients and Strouhal number around two fixed rigid cylinders as a function of spacings. Adopted from [29]

and incidence angle. They studied the cylinders in three groups of closely, moderately and widely spaced while changed the incidence angle. In the first group, aerodynamic forces on both cylinders were notably sensitive to variations in the incidence angle. Moreover, they observed significant values of Strouhal number in the second group. A pair of cylinders in the third group behaved similarly to a single cylinder, although at small angles the lift force acting on the second cylinder was at its highest value towards out of the upstream wake.

Response Amplitude

The response of two staggered cylinders, flexibly mounted, was observed by Huang and Herfjord [32] and they noted that the mean lift force on the trailing cylinder was non zero towards the wake centre line, although it reduced to zero as the system experienced lock-in. Additionally, Huang and Sworn [33] conducted their experiment on a pair of non-identical staggered cylinders. In this study, two cylinders had different diameters. The experiment revealed that stream-wise response amplitude was usually a quarter to half of that in cross-flow. Furthermore, trajectories of the cylinders motion were the classic figure of eight. Authors also observed some low-frequency components in the drag. However, they could not find any explanation for them.
Despite the great works conducted to provide a better understanding of interaction between two staggered cylinders, this topic has not received sufficient attention and most of the work done is experimental study on fixed pairs.

2.2.2 Side-by-Side Arrangement

A particular case of proximity interference is the side-by-side arrangement. Sumner et al. [34] conducted an experiment in sub-critical Re for two and three side-by-side cylinders at spacings $1 \leq T/D \leq 6$. They observed three flow patterns: i) single-bluff body at small spacings, ii) biased flow toward one cylinder at intermediate spacings and iii) synchronised vortex shedding at large spacings. Interestingly, Zdravkovich [29] made an observation in synchronised vortex shedding regime which drew this conclusion: " the two vortex streets are couple and mirror each other. The vortex shedding

is synchronised, both in phase and frequency ”

Moreover, Sumner et al. [34] measured St behind both cylinders and compared their measurements with those obtained by other researchers at higher Re and observed that St was independent from Re for side-by-side arrangement.

Bearman and Wadcock [35] also conducted an experiment in this arrangement and measured the base pressure and flow regime around cylinders. Their measurements showed that there was a “repulsive force ” between two cylinders at close distances. They also discovered that change in base pressure was due to wake interference between two cylinder rather than separation of boundary layer.

Moreover, Williamson [36] conducted a similar experiment and observed that vortex synchronisation could occur either in phase or anti-phase. He noted that one large vortex street was formed for in-phase synchronisation whereas for anti-phase synchronisation two separate streets were observed. In latter, two simultaneously formed vortices were washed downstream while swirling around each other and he referred to them as “binary vortex ”. Additionally, his observations approved that two cylinders formed a single vortex street similar to single-bluff body flow regime at small spacings .

Most of the studies focused on this arrangement, similar to staggered, are experiments on fixed cylinders and sufficed to observe the flow regime around two bodies. Due to complexity of flow regime, there are few number of attempts to develop a model for FIV of such an arrangement.

2.3 FIV of Two Cylinders in Tandem Arrangement

Wake interference regime has received more attention since the interaction between upstream wake, and trailing cylinder makes this regime more complex and exciting. Tandem is the most common arrangement in this regime where two cylinders are in-line with each other ($\psi = 0$) and trailing cylinder is completely immersed in the upstream wake. Either of cylinders can be fixed or free and that makes several scenarios as below.

2.3.1 Fixed-Fixed

Igarashi [37] considered two fixed identical cylinders in tandem and confirmed that flow pattern behind them depends on the gap between two cylinders as well as Re. His experimental investigation included very small spacing of $1.1D$ to moderate $5D$ at which he tried to identify different flow regimes by varying Re from 8.7×10^3 to 5.4×10^4. He showed that the base pressure around the leading cylinder is proportional to spacing when the shear layers had the opportunity to roll up and form vortices. Additionally, he observed that, immediately after formation of the first vortex behind the leading cylinder, pressure distribution would be similar to that of a single cylinder.

Zhou and Yiu [38] carried out a similar experiment and discovered that based on Re, flow pattern around two tandem cylinders could be divided into three categories as a function of L. i) "*Extended-body regime* " where two cylinders were extremely close to each other and behaved like a single cylinder. In this regime, the shear layer separated from the surface of leading cylinder, however, could not roll up in the gap so passed over the second cylinder and generated a vortex in the wake of trailing body. There was no separation on the surface of trailing cylinder in this regime (figure 2.9a). ii) "*Reattachment regime* " could be observed in moderate spacings. Shear layers separated from the surface of leading cylinder still could not roll behind it but reattached on the surface of trailing cylinder where partially moved towards the front stagnation point and the shear layer separating from the surface of trailing cylinder [39]. This region could be subdivided into two smaller groups based on the position of reattachment points. When the gap is relatively small, reattachment points are located on the lee-side of trailing cylinder (figure 2.9b), however, as the trailing cylinder shifts further downstream, the reattachment points relocate to upstream half of the cylinder (figure 2.9c). Alam et al. [40] also observed the reattachment of upstream shear layers on trailing cylinder where each split into two layers later; one separated forwards, toward the upstream cylinder at a smaller angle and the other one moved downstream and created the downstream shear layer ($L/D < 3$). It is argued that as the second cylinder moves downstream reattachment position of the upstream shear layer moved forward. Moreover, based on their study pressure diagram reached its peak near separation point. iii) "*Co-shedding*

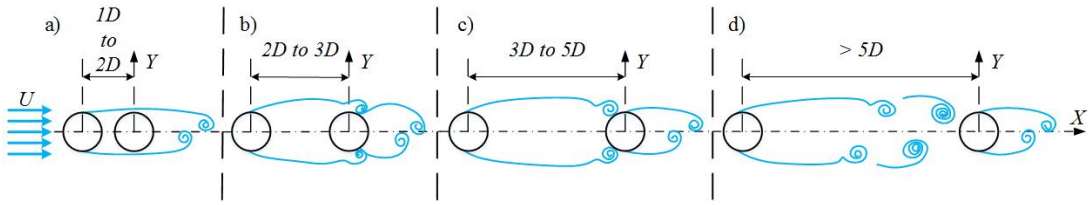

Figure 2.9: Flow regime around two identical cylinders in tandem at various spacing. Adopted from [38].

region " when the gap grew sufficiently large, shear layers detached from leading cylinder had enough space to roll up and form vortices. In this flow regime, both cylinders can develop their own vortex street hence it is named Co-shedding region (figure 2.9d). Alam et al. [40], Kitagawa and Ohta [41] observed that pressure fluctuation was larger on leeward surfaces of both cylinders in contact with the vortices. Furthermore, it was noted that vortex generation itself resulted in an increase of pressure coefficient. It should be pointed out that boundaries to each flow regime are susceptible to Re [42].

Critical Spacing

The transition from *Reattachment* to *Co-shedding regime* is usually indicated by a sudden jump in values of properties such as drag and lift coefficient, base pressure and Strouhal number [29, 31]. The boundary between Reattachment regime and the Co-shedding region is referred to as critical spacing in literature [29, 37, 41, 42, 43]. All these studies observed this transaction between $3 < L/D \leq 4$.

Hydrodynamic Coefficients

The striking feature of hydrodynamic coefficients of two cylinders in tandem is a jump that occurs at critical spacings as mentioned before. Alam et al. [40] observed that drag coefficient is a function of spacing as well as Re. They suggested referring to critical spacing as drag inversion at which drag value of trailing cylinder switches from negative to positive.

Zdravkovich [29] observed that drag coefficient increased after separation; hence he connected the drag inversion to separation phenomenon and explained that when there is no separation in extended body regime C_{D_2} is smaller than C_{D_1}. Additionally, he

observed that wider wake resulted into higher drag force.

Strouhal Number

Strouhal number experiences the same sudden jump after critical spacing [44]. Strouhal number decreases by the increase of spacing in two regions of Extended-body regime and Reattachment. In Co-shedding region Strouhal number increases until it reaches the value similar to that of a single cylinder.

Xu and Zhou [42] conducted an extensive study on St over a wide range of spacings $(1 \leq L/D \leq 15)$ and Reynolds numbers $\left(800 \leq Re \leq 4.2 \times 10^4\right)$. Their measurements behind both cylinders suggested that both structures were shedding vortices at the same frequency. It was discussed that St is a function of L/D and Re. Moreover, they observed that St was extremely sensitive to spacing for $L/D < 2$ and was inversely proportional to spacing. It slowly decreased until spacing reached the critical value at which the leading cylinder started to shed vortices. Additionally, They showed that St increased after critical spacing until it reached the value of 0.21 of an isolated cylinder. However, Igarashi [37] observed that Strouhal number can be independent of Re and then be proportional to spacing after critical spacing.

Based on the numerical studies of Kitagawa and Ohta [41] the speed of travelling vortices was suggested to be considered as a function of Strouhal number and spacing:

$$U_s = \frac{2\pi}{\kappa} St \frac{L}{D} \tag{2.8}$$

where $\kappa = 1.6\dfrac{L}{D} + 1.5$.

2.3.2 Fixed-Free

So far the studies that focused on two fixed cylinders in tandem arrangement were considered, however, if the trailing cylinder were to be switched to a flexibly mounted one, the flow regime will transform drastically [45]. Yang et al. [46] tried to classify flow patterns around two cylinders in tandem. They conducted the experience both

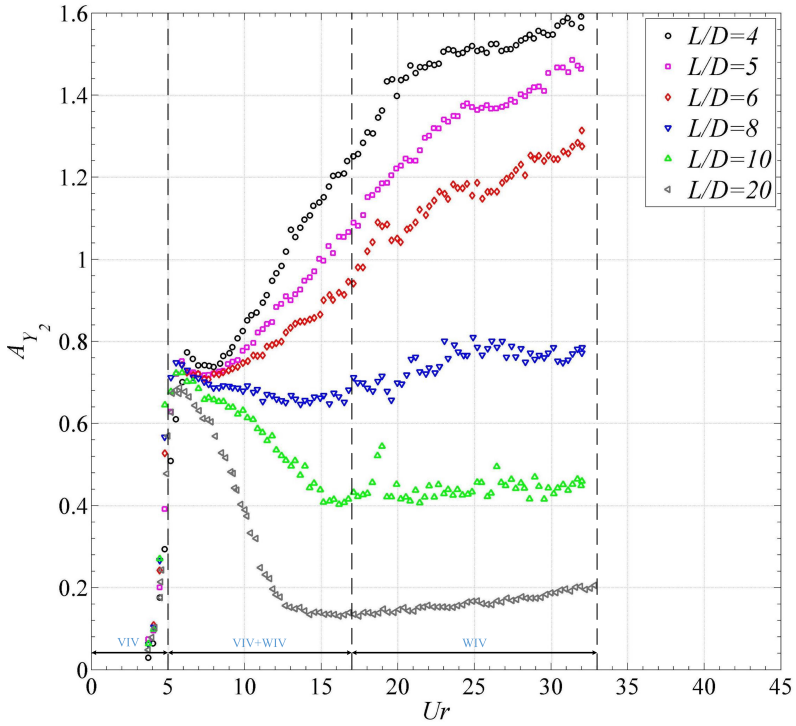

Figure 2.10: Minimum safe initial separation between two cylinders with various supporting rod length to avoid collision at different flow velocities,[47]

for fixed and forced vibrating cylinders. For forced vibration experiment, they chose $L/D = 2$ where flow pattern changed for two stationary cylinders and forced both of them to vibrate in-phase. This part of the experiment showed two different steady flow patterns with high and low frequencies. Next, authors conducted three other types of experiment (out-phase, leading cylinder oscillating only, trailing cylinder oscillating only). It was observed that type of vibration affected the flow pattern to some extends but all the patterns resembled same two patterns from in-phase vibration.

Assi et al. [47] conducted an extensive experiment investigation to observe the effect of spacing on a flexibly mounted trailing cylinder. They discovered that trailing cylinder was behaving independently after $L = 20D$ (figure 2.10). Trailing cylinder at spacings less than $20D$ had a galloping like behaviour. They discussed that response of the trailing cylinder consisted of three regions depending on Re. Cylinder response was similar to an isolated cylinder at low Re (VIV region). As Re rose, the effect of upstream wake increased which establishes the second region where cylinder response was a combination of VIV and wake induced vibration (VIV+WIV region). In the third section, vortices from the cylinder itself did not excite it, nevertheless, response amplitude of

the cylinder had increased due to vortices coming from the leading cylinder (pure WIV region). Furthermore, they observed that harmonic response for motion and fluid was valid.

These were few studies on two cylinders in tandem where trailing cylinder was allowed to oscillate in one or both directions. Based on observations most of the work in this category has been experimental and attempts to simulate such a system numerically or mathematically is rare or non-existing.

2.3.3 Free-Free

Studies on the tandem arrangement where both cylinders were flexibly mounted are limited and mostly have used CFD technique. Though, Re in these studies is very low, around 100 to 200. Papaioannou et al. [48] obtained the amplitude and the drag force on a pair of cylinders in both directions at different spacings (Two spacings below and one above the critical value). They observed that for the trailing cylinder:

- Lock- in range moves to lower U_r as the spacing increase.
- Spacing and length of the lock-in range have a inverse relationship.
- Graph of trailing cylinder response amplitude has at least two peaks. One corresponds to the reduced velocity at which upstream cylinder peak occurs, the second one is cylinder maximum VIV amplitude.
- After vortices formation in the gap between two cylinders, the effect of the trailing cylinder on the leading one is negligible.

Similar numerical study was done by Prasanth and Mittal [49] with heavier cylinders ($m^* = 10$) at spacing of $L/D = 5.5$. Lock-in and hysteresis were observed for both cylinders. Contrary to Assi et al. [50] where downstream cylinder response increased with velocity, in both of these studies the amplitude reduced at higher Re.

Another numerical study on two oscillating cylinders in tandem by Lin et al. [51] which was conducted in poiseuille flow at a low mass ratio. They measured the Strouhal number and maximum amplitude against spacing. It was observed that the influence

of spacing reduced after the critical spacing. Amplitude of oscillation for both structures was observed to be larger than that of a single cylinder.

In all studies mentioned above, the measurements of downstream oscillation amplitudes demonstrated that trailing cylinder underwent vibrations with larger amplitudes, in both directions, in comparison with an isolated cylinder. However, it was not the case in experimental observations.

Huang and Herfjord [32] conducted an experiment on two rigid identical cylinders with 2DOF where in some cases they observed that the leading cylinder had a larger oscillations. They also measured hydrodynamic forces on both cylinders in tandem and staggered arrangement and showed that the effect of reduced velocity significantly affects amplitude and frequency of vibration. They initially observed that variation of reduced velocity did not affect the motion trajectory of either of cylinders which was in contrast with observations on a single cylinder [52]. While experts like Zdravkovich [29] claimed that the effect of trailing cylinder on the leading is insignificant after $4D$ for fixed cylinders, Huang and Herfjord [32] claimed that for a system of two free cylinders this threshold reduces to $3D$.

Behaviour of non-identical cylinders were observed in the experimental study by Huang and Sworn [33]. He conducted his experiment of two cylinders with different mass ratios in tandem and observed that trailing cylinder had a chaotic Fo8 trajectory in comparison with its leading counterpart. In the motion spectrum of trailing cylinder some low-frequency component were found in stream-wise response which their source was unknown.

Shiau and T. Y. Yang [53] is to our knowledge one of few modelling attempts to simulate such an array of cylinders. They tried to use a pair of Rayleigh wake oscillator to model forces from upstream and downstream wakes. This configuration has received the least attention from researcher given the complexity of interaction between structures and their wake. The experimental study is very limited.

2.4 Conclusion

This chapter was a brief review of past studies on FIV of a single and two cylinders in the close proximity. This topic has been approached using different methodologies that can be classified into three groups: experimental investigations, numerical studies (CFD) and mathematical modelling.

- It was discussed that the study of a bluff body in a fluid stream has always been of interest by engineers due to its broad applications. Additionally, it was discussed how separation on the surface of a cylinder causes an asymmetric pressure distribution around it.

- The separated shear layer then folds behind the cylinder and forms a vortex. Moreover, it was explained how Re and St control vortex shedding process. Then, effective parameters in VIV response of a cylinder were discussed, it was observed that structural constraints could influence mechanism and amplitude of VIV.

- It was demonstrated that placing a secondary bluff body can alter the flow regime around both structures drastically. The flow around two cylinders is significantly dependent on the spacing between them. Configuration of these bodies was categorised into three groups of side-by-side, tandem and more general case, staggered.

- Also, few studies on two cylinders in small distances have been discussed, many of which on the flow pattern around two cylinders in different configurations. All these studies chose the experimental method to look at wake interference and limited their work to fixed cylinders.

- It was observed that there is a drag inversion in downstream at the spacing after which the leading cylinder started to form a full vortex street, and it was referred to as *critical spacing*. VIV of the leading cylinder is similar to that of an isolated body after critical spacing.

- Galloping behaviour was observed in some studies conducted on an oscillating cylinder in tandem of a fixed cylinder, where the response amplitude of the trailing

cylinder was investigated in small spacings, trailing cylinder response amplitude grew larger as reduced velocity increased, similar to that of the galloping response. Furthermore, the response of the cylinder became akin to an isolated body as spacing reached the large value of $20D$.

- It was mentioned that response of the oscillating cylinder in wake could be divided into three regions; i) the first region where response was induced by cylinder vortex shedding, ii) the second region where it was induced by a combination of VIV and wake instability, iii) the third region where response was purely induced by the wake. Nevertheless, there is lack of numerical and mathematical simulation for such a configuration.

- It was observed that change from fixed-free to free-free structure had a significant effect on critical spacing. Moreover, trailing cylinder has a different response in comparison with fixed-free configuration or an isolated cylinder. The past researches on this configuration were heavily driven by numerical studies at low Re, lacking research under other methodologies such as mathematical modelling at higher Re.

Such an absence inspired this research. the Present work investigates two oscillating cylinders in tandem configuration at relatively high Re. To this end, an experimental approach is adopted first to better understand the physics of wake interference between cylinders and the governing parameters. Next, taking an analytical method, a mathematical method is developed and validated against the experiments.

Chapter 3

Experimental Studies

3.1 Objectives & Methodology

All experiments in this research have been conducted in facilities of Kelvin Hydrodynamics Lab at the University of Strathclyde. The towing tank is $76m$ long and $4.6m$ wide with the water depth that could be set from 0.5 to $2.3m$ which was set to approximately $1.4m$ for these experiments. The rig supporting two cylinders was securely mounted on a carriage located above the water tank (figure3.1).The carriage is self-propelled with the maximum speed of $4m/s$. Re for this experiment ranged between 7.79×10^3 to 10^5 which falls into sub-critical region.

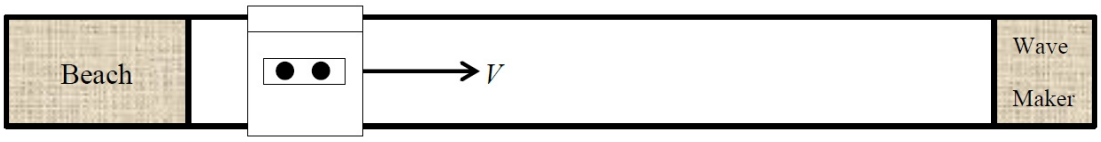

Figure 3.1: Kelvin Hydrodynamic Laboratory tank view from above

3.1.1 Apparatus selection

The experiment rig is designed in a way that the second cylinder can be slid along the carriage to be fixed at several locations relative to the first cylinder. To provide structural support for each cylinder three methods have been repeatedly used in the literature.

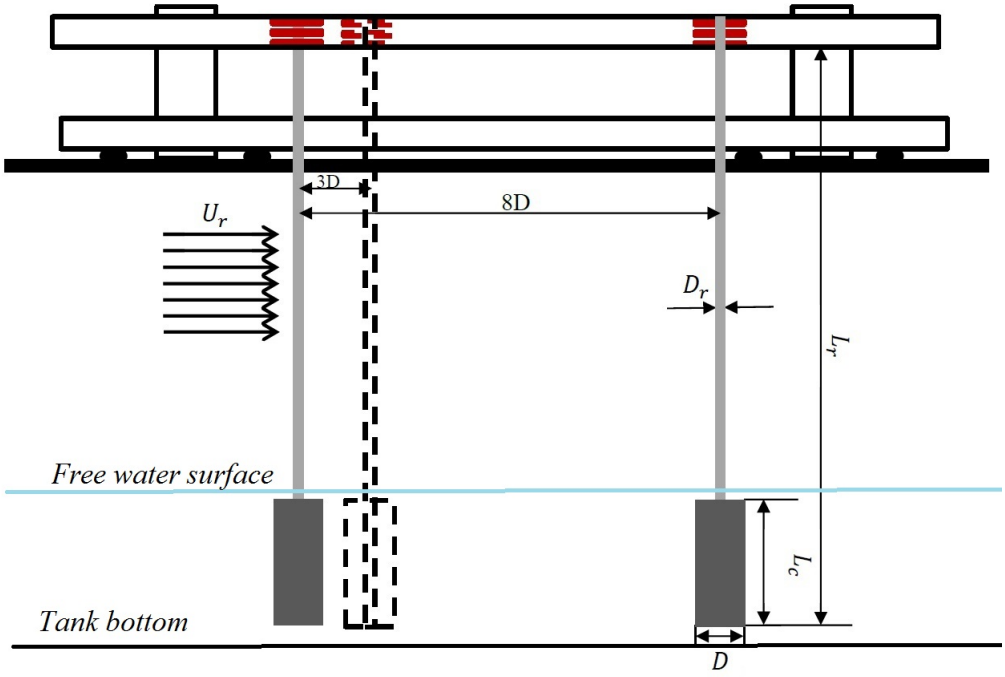

Figure 3.2: Illustration of the rig used in the experimental investigation

The design chose for this experiment was to hang each cylinder by an aluminium rod which was rigidly attached to the rig utilising two clamps at the top (spaced $400mm$ and $200mm$ apart from each other for different experiments so that they create a rigid connection between the rods and the rig). This supporting method provides equal damping and mass ratio in both directions, stream-wise and cross-flow, as well as equal natural frequency. Figure3.2 is a schematic of the experiment rig set-up. Supporting rods allow cylinders to oscillate in both stream-wise and cross-flow directions. Additionally, they are designed in a way that they have minimal deflection under drag force to prevent two cylinders from colliding into each other in small spacings.

Two alternative designs to this test rig were considered as well. One was adopted by Srinil et al. [54] which is called pendulum design here, the other was employed by Assi et al. [50] in which two leaf springs (flexure) were used to support the experiment cylinder.

Pendulum design consists of a long and light *rigid* pole constrained at the top in a manner that allows the pole to rotate around axis in cross-flow and stream-wise direction. Additionally, the pole is connected to four pre-tensioned springs in two directions so that it returns to its equilibrium position. This set-up allows control on stiffness

and damping of the system however does not provide an equal structural damping in all directions as cylinder goes through VIV motion. Furthermore, while this set-up has been used in literature for VIV test of an isolated cylinder, adopting this design is not easy for two cylinders in tandem. To place two cylinders in-line the structure of rig should be altered so it either cannot accommodate any springs between two cylinders which results in unequal structural damping and stiffness or is limited in how close two structures can be placed.

Using flexure as support is not as popular in literature as pendulum design but has been used in several studies. This method has an advantage that allows movements in one direction and is rigid in the other and cylinder remains vertical which is excellent for VIV test in one direction. However assembling the rig is complicated since stiffness of flexure is susceptible to the method used for attaching the plate to rest of the structure and stiffness of one plate could be different from the one on the opposite side. Moreover, It is limited in size of the motion that can be accommodated relative to length of flexure, and has difficulty of stacking two large flexures to create 2D VIV. In author's opinion this method is an acceptable alternative to a flexible pole when extra caution is invested during manufacturing of test apparatus. Moreover, the attached cylinder would have a vertical displacement that should be considered as well during test design and post-processing.

In this stage, both cylinders are chosen to be identical with diameter of $D = 0.1m$ and aspect ratio of 10.1. This ratio is high enough to put sample cylinders in the slender category. Additionally, each cylinder was hanged $20mm$ above the tank's bottom and below the free water surface, so that flow of fluid over and under the cylinders was prevented, therefore the flow could be considered two dimensional without any end-plates. External surfaces of cylinders were machined prior to the experiment and considered hydrodynamically smooth. To determine natural frequency of the system and its damping ratio free decay test was conducted both in air and water at least twice for both cylinders.

3.1.2 Methodology

Four sets of experiment were carried out throughout this research, in two separate occasions. First, a single cylinder was tested in order to observe the VIV response of the structure. Additionally, the performance of the experiment apparatus was examined through validation against previous works available in the literature. Second, two identical cylinders were placed in the tank and towed at several reduced velocities so that the effect of velocity variation on VIV and interaction of a cylinder pair in tandem could be observed. During this experiment trailing cylinder's location was changed relative to the leading structure. Each velocity was repeated for eight different spacings to examine the changes in two cylinders' interaction due to variation in the gap between cylinders. Two other sets of experiments were additionally conducted as a parametric study to confirm how cylinders would respond in a more general condition where two systems are not identical. These experiments could also provide more in-depth detail on physics of multiple structures interaction. To do so, two cylinders were kept the same while the natural frequency of each system was changed by extending the supporting rod (one clamp was moved higher, the lower clamp was brought closer to upper clamp on each rod in turn, figure 3.3). Three different spacing were examined and two cylinders changed place after each set of tests completion (Length of the supporting rod to the leading cylinder were extended first then brought back to its original length, then second supporting rod was extended). The third experiment was conducted at 15% difference in natural frequency and fourth set was conducted at 33% difference which was as high as possible on these rods.

The test with two cylinders in tandem started with two structures initially placed at the furthest desirable distance and then brought closer together after completion of each test to observe the effect of spacing. After placing the cylinders at desired spacing, the rig was secured to make sure the gap does not change during the run. The carriage was towing the rig along the tank at different speeds to obtain a complete response graph for both cylinders undergoing FIV. Spacings for the second experiment include gaps of 20,15,10,8, 5, 4, 3.5 and 3 times the cylinder diameter. Due to design limitation, two cylinders would collide if the distance between two structures became any smaller as

they did at the reduced velocity of 10 for $L/D = 3$. During third experiment spacings of $4D, 8D$ and$12D$ were considered. Furthermore, fourth experiment included $6D, 10D$ and$14D$.

Movement of each cylinder was tracked by *Qualisys* optical tracking system in all 6DOF (Figure3.4). These cameras recorded the motion of four tracking balls (Figure3.5) attached to each rod. Five Qualisys cameras were positioned in a way that at each moment three balls from each cylinder were visible to the system. Then this data was converted into coordination points by *Spike2* software at the sampling rate of $137Hz$.

3.2 Design

3.2.1 Static Analysis

As mentioned earlier it was necessary for experiment apparatus to be as rigid as possible while maintaining a low natural frequency. It was important to have a firm structure so that supporting rod deviation was maintained as small as possible so that firstly, the system could still be considered linear, secondly, two cylinders could be brought together as close as possible. Thirdly, cylinders remain close to vertical.

Based on materials available in the market, a relatively thin cross section with a diameter of $D_r = {}^3/_4"(0.01905m)$ was selected for supporting rod. In order to maintain a low natural frequency, the length of supporting rod (L_r) must have been chosen meticulously. As the length of the towing tank was limited, the low natural frequency could enable us to achieve high reduced velocity without approaching carriage speed

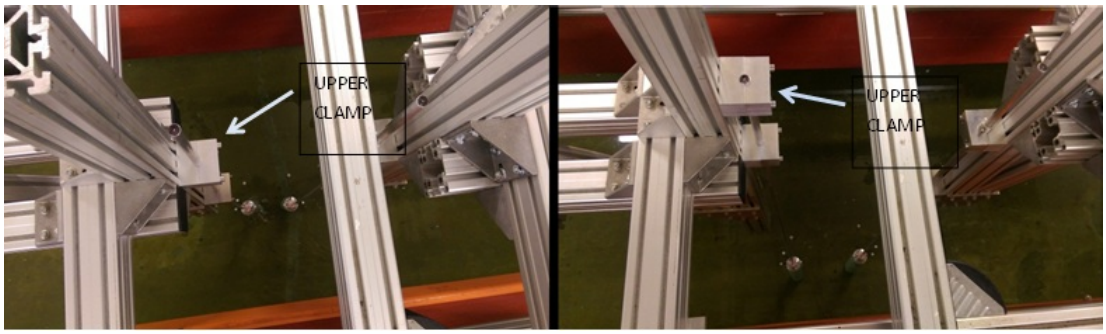

Figure 3.3: Comparison between the first and second experiment set-up. The picture at left shows the first set-up with original rod length. The picture on the right shows the second set-up where leading cylinder has a longer rod and lower natural frequency.

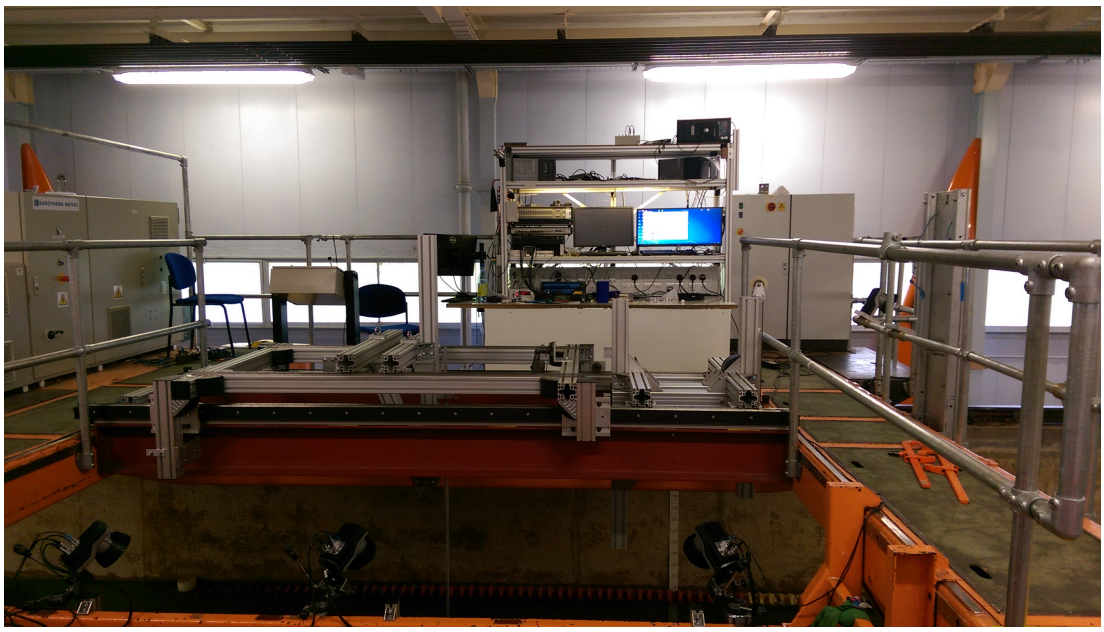

Figure 3.4: Qualisys system: three tracking cameras out of five plus recording PC

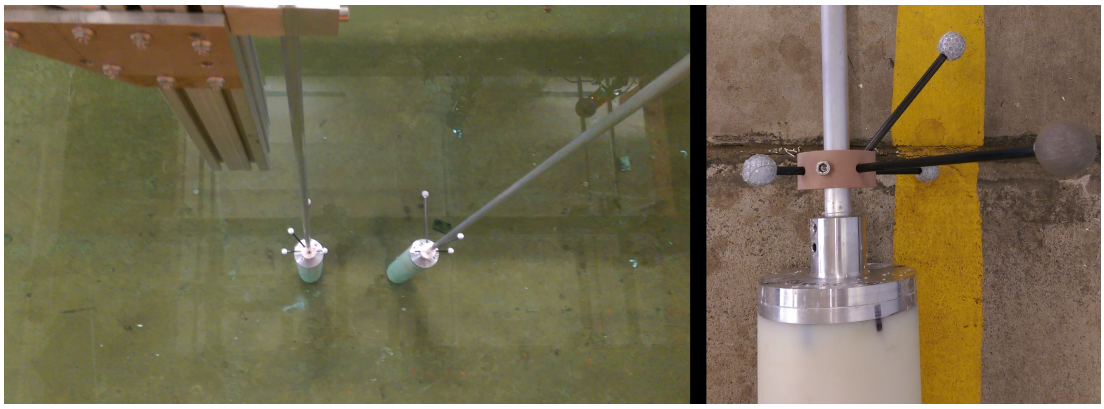

Figure 3.5: On the left, Qualisys tracking balls on top of both cylinders. on the right, close up of tracking balls mounted on top of a cylinder using a collar

limits. Based on the previous experiment done by Srinil et al. [54] it was provided that natural frequency of the system in the air should be around $0.5Hz$. Replacing these two initial assumptions in the equation 3.1 provided by Rao [55] enables us to calculate the supporting rod's length.

$$\omega_n = (\beta_n L_r)^2 \sqrt{\frac{EI}{\rho A L_r}} \tag{3.1}$$

where $\beta_n L_r$ for a cantilever beam vibrating at its nth mode can be defined as $\beta_n L_r = (2n-1)\pi/2$.

However, at this stage, it was important to examine maximum bending stress of sup-

porting rods and amend this design so that the supporting rod stress stays in the elastic area at all time throughout the test. Moreover, the second criteria of high stiffness should be satisfied as well. Table 3.1 includes maximum displacement of leading cylinder supporting rod with the length of $L_r = 1.8m$ at different towing speeds. The drag coefficient is considered of an isolated cylinder regardless of its VIV behaviour (respond amplitude due to VIV was added later as a constant displacement in severe case of $A_{Y_1} = 1.5D$).

Maximum rod deflection was then calculated under this assumption that cylinders motion induced by VIV maintains the highest amplitude experienced in other experiments available in the literature ($A_X = 0.5D, A_Y = 1.5D$) regardless of reduced velocity. Additionally, maximum bending stress at the top of the rod was calculated, considering maximum deflection and not solely drag induced deflection. Moreover, Furthest point downstream which indicates the location of the closest point on the leading cylinder to its trailing counterpart was identified; it is calculated by using supporting rod's slope under drag force plus $0.5D$ displacement due to in-line VIV motion. This point shows how close two cylinders may get during a test, which is necessary to establish the clearance between two cylinders. Considering similar approach to calculate maximum displacement of the trailing cylinder yields minimum distance between two cylinders during the test so that the minimum initial gap (L) between two cylinders could be identified.

Table 3.1: Bending moment and deflection of an aluminium rod with length of $L_r = 1.8m$ and Diameter of $D_r = 0.01905m$ due to static drag force at various flow velocities.

U_r	$V(m/s)$	Drag (N/m)	Rod Deflection(m)	Deflection angle (Degrees)	Maximum Deflection(m)	Maximum Stress(Pa)	Furthest Point(m)
1	0.061332	0.248266539	0.001532792	0.029601809	0.165007119	33.47123582	0.174388132
2	0.122664	0.993066155	0.006131168	0.118407237	0.165113873	33.49289059	0.175840822
2.25	0.137997	1.256849353	0.007759759	0.149859159	0.165182365	33.506784	0.176378056
2.5	0.15333	1.551665867	0.00957995	0.185011308	0.165277873	33.52615752	0.17699236
2.75	0.168663	1.8775157	0.011591739	0.223863682	0.165406676	33.55228474	0.17768818
3	0.183996	2.234398849	0.013795128	0.266416283	0.165575679	33.5865666	0.178470334
4	0.245328	3.972264621	0.024524671	0.473628947	0.166812648	33.83748227	0.182569926
4.5	0.275994	5.02739741	0.031039037	0.599436636	0.167894079	34.0568476	0.185284858
5	0.30666	6.20666347	0.038319799	0.74004523	0.169391284	34.36055138	0.188510308
5.25	0.321993	6.842846475	0.042247579	0.815899866	0.170322805	34.54950787	0.190330687
5.5	0.337326	7.510062798	0.046366957	0.895454729	0.171391058	34.76619999	0.192298133
5.75	0.352659	8.208312439	0.050677934	0.978709817	0.172607222	35.01289549	0.194419029
6	0.367992	8.937595396	0.055180511	1.065665131	0.173982438	35.29185429	0.196699633
6.25	0.383325	9.697911671	0.059874686	1.156320672	0.175527713	35.60530902	0.199146034
6.5	0.398658	10.48926126	0.064760461	1.250676439	0.177253822	35.95544533	0.201764112

7	0.429324	12.1650604	0.075106806	1.450488651	0.181289912	36.77415517	0.207537572
8	0.490656	15.88905848	0.098098686	1.894515789	0.191959246	38.93839986	0.221372744
9	0.551988	20.10958964	0.124156149	2.397746546	0.206493945	41.8867232	0.238473427
10	0.61332	24.82665388	0.153279197	2.960180921	0.225209929	45.68320854	0.259017
11	0.674652	30.04025119	0.185467828	3.581818914	0.248240438	50.35488338	0.283096663
12	0.735984	35.75038158	0.220722043	4.262660526	0.275577975	55.90022678	0.310738923
13	0.797316	41.95704505	0.259041843	5.002705756	0.30712811	62.30008406	0.341924357
14	0.858648	48.6602416	0.300427226	5.801954605	0.34275577	69.52705587	0.376606285
15	0.91998	55.85997123	0.344878193	6.660407072	0.382316581	77.5518564	0.414724966
16	0.981312	63.55623393	0.392394744	7.578063157	0.42567433	86.34685535	0.456217093
17	1.042644	71.74902971	0.442976879	8.554922861	0.4727087	95.88764672	0.501021452
18	1.103976	80.43835857	0.496624598	9.590986183	0.523317295	106.1534596	0.549081856
19	1.165308	89.6242205	0.5533379	10.68625312	0.577414783	117.1269849	0.600348348
20	1.22664	99.30661551	0.613116787	11.84072368	0.634930858	128.7939609	0.654777381

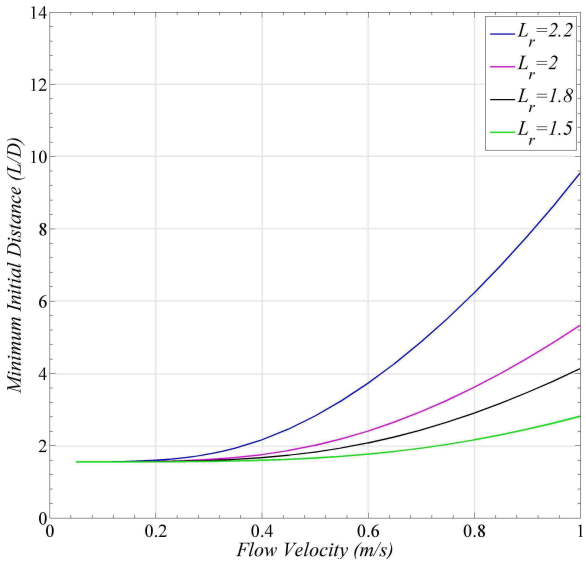

Figure 3.6: Minimum safe initial separation between two cylinders with various supporting rod length to avoid collision at different flow velocities

Initial design suggested that $L_r = 2.5m$ yields a very low natural frequency, however, this length failed to satisfy stiffness criteria, as figure 3.6 shows with this rod length cylinders would collide together at all spacings smaller than $5D$. Therefore, three shorter lengths of $2, 1.8$ and $1.5m$ were examined in order to find a length that satisfies both criteria. Figure 3.6 was produced using data from table 3.2 and similar tables which can be found in appendix A for cylinders with different rod length.

Table 3.2 includes drag force, maximum deflection and maximum bending stress for trailing cylinder supporting rod similar to its leading counterpart, as well as furthest point which is lowest point of trailing cylinder on its *upstream half* (measuring reference is centre of the cylinder at its original position). It should be noted that based on the experiment data produced by OKAJIMA [56] mean drag coefficient for stationary downstream cylinder is approximately $C_{D_2} = 0.4$ for all spacings larger than $2D$ due to shielding effect from leading cylinder. Moreover, Assi et al. [47] showed that WIV amplitude of a cylinder oscillating in the wake of another identical fixed cylinder is less than $1.5D$ for all spacings greater than $4D$, thus it was possible to take a similar approach to leading supporting rod for analysing trailing one.

It is clear that spacing less than $3D$ is not achievable by this design however, it is evident from figure 3.6 that a rod with length of $L_r = 1.5m$ could provide a good stiffness for our system. On the other hand, system's natural frequency would be too high at

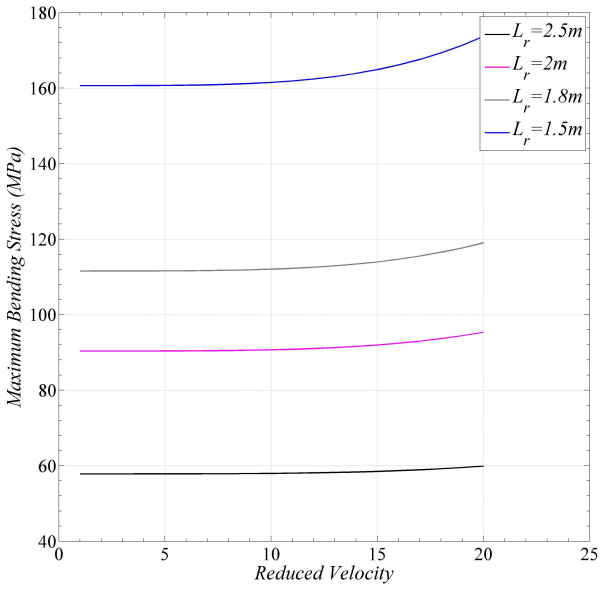

Figure 3.7: Maximum bending stress of supporting rod with various lengths due to hydrodynamic drag force and maximum VIV response

$f_n = 0.749$ which is higher than desirable value. The $1.8m$ long rod was the best option for this design as it provides desirable stiffness while maintaining low natural frequency. Next step was to examine if the maximum stress of a rod with this length would be under aluminium maximum tensile stress. Figure 3.7 shows the bending moment of rods with different lengths due to deflection calculated in table 3.1, A. Maximum tensile stress af aluminium is $276MPa$ which is much higher than the stress that would be experienced by any of prospect supporting rods.

All natural frequencies were calculated under this assumption that the weight of each cylinder is $20Kg$. Mass ratio of the whole system then can be calculated using equation 3.2 which yields 2.362. Here M is mass of rod-cylinder system and m_a is displaced water by cylinder. This mass ratio was selected considering that offshore structures are slender and have a very low mass ratio. Moreover, it has been reported in literature that structures with very low mass ratio show galloping like response rather than typical VIV motion however mass ratio of our system was high enough to be out of such a category $m^* = 2.36$.

$$m^* = \frac{M}{m_a} \tag{3.2}$$

3.2.2 Dynamic Analysis

Natural frequency

After test apparatus assembly, multiple free decay tests were conducted on both cylinders in cross-flow and stream-wise directions so that natural frequency and structural damping of both cylinders could be calculated. Additionally these tests confirmed that both structures were identical and had similar structural property in all directions. Figure 3.8 shows the time history for four of these tests in air, each test was done independently. Natural frequency of a cylinder after determining diameter and length of the supporting rod was calculated $f_n = 0.5592Hz$.

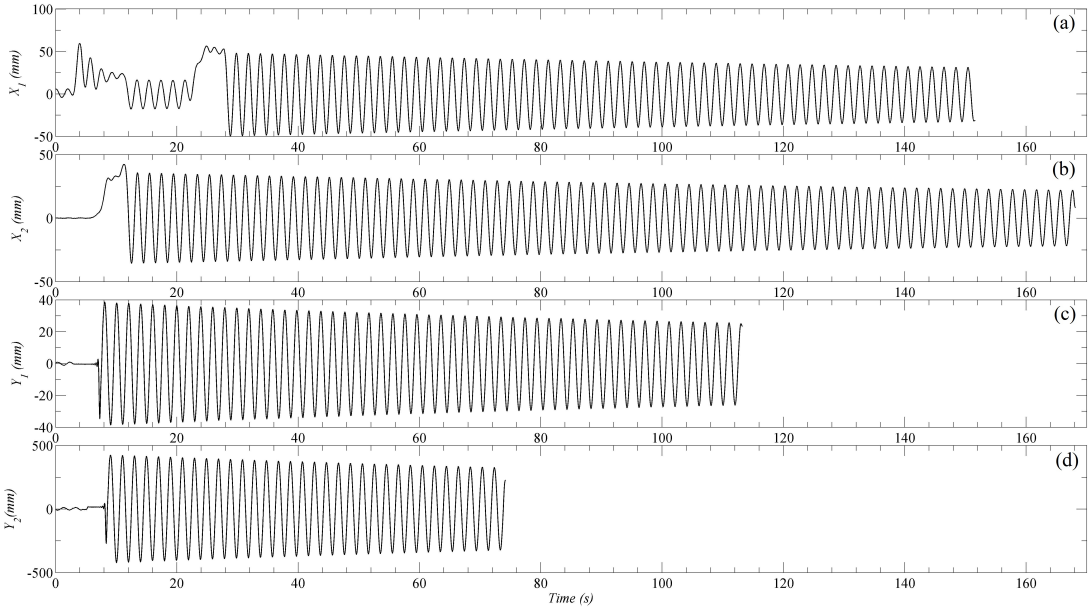

Figure 3.8: Time history of free decay test in air for both cylinders, (a) first cylinder in stream-wise direction, (b) second cylinder in stream-wise direction, (c) first cylinder in cross-flow direction, (d) second cylinder in cross-flow direction.

Table 3.2: Bending moment and deflection of an aluminium rod with length of $L_r = 2.5m$ and Diameter of $D_r = 0.01905m$ due to static drag force at various flow velocities.

U_r	$V(m/s)$	Drag(N/m)	Rod Deflection(m)	Deflection Angle(Degrees)	Maximum Deflection(m)	Stress (Pa)	Furthest point(m)	Clearance(m)
1	0.0333336	0.024444836	0.000371048	0.004096083	0.550000125	57.83581316	-0.109749785	0.20269537
2	0.0666672	0.097779342	0.001484193	0.016384332	0.550002003	57.83601058	-0.108999138	0.207181479
2.25	0.0750006	0.12375198	0.001878432	0.020736421	0.550003208	57.83613731	-0.108733284	0.20877031
2.5	0.083334	0.152780222	0.002319051	0.025600519	0.550004889	57.83631411	-0.108436153	0.210546061
2.75	0.0916674	0.184864069	0.002806052	0.030976628	0.550007158	57.83655271	-0.108107745	0.212508734
3	0.1000008	0.22000352	0.003339434	0.036864748	0.550010138	57.83686606	-0.107748061	0.214658328
4	0.1333344	0.391117369	0.005936771	0.065537329	0.55003204	57.83916922	-0.105996552	0.225125917
4.5	0.1500012	0.49500792	0.007513726	0.082945682	0.550051321	57.84119674	-0.104933137	0.231481239
5	0.166668	0.611120889	0.009276205	0.102402077	0.55007822	57.84402529	-0.103744613	0.238584245
5.25	0.1750014	0.67376078	0.010227016	0.11289829	0.550095075	57.84579774	-0.103103436	0.24241613
5.5	0.1833348	0.739456276	0.011224208	0.123906513	0.550114518	57.84784225	-0.102430982	0.246434937
5.75	0.1916682	0.808207376	0.012267781	0.135426746	0.5501368	57.85018532	-0.101727251	0.250640664
6	0.2000016	0.88001408	0.013357735	0.14745899	0.550162184	57.85285466	-0.100992243	0.255033313
6.25	0.208335	0.954876389	0.01449407	0.160003245	0.550190947	57.85587921	-0.100225958	0.259612883
6.5	0.2166684	1.032794302	0.015676787	0.17305951	0.550223374	57.85928915	-0.099428396	0.264379375

7	0.2333352	1.197796942	0.018181362	0.20070807	0.550300429	57.86739189	-0.097739442	0.274473121
8	0.2666688	1.564469476	0.023747085	0.262149316	0.55051242	57.88968399	-0.09398621	0.296903668
9	0.3000024	1.98003168	0.030054905	0.331782728	0.550820567	57.92208757	-0.089732546	0.322324955
10	0.333336	2.444483556	0.03710482	0.409608307	0.551250186	57.96726457	-0.084978452	0.350736981
11	0.3666696	2.957825102	0.044896833	0.495626051	0.551829435	58.02817609	-0.079723927	0.382139747
12	0.4000032	3.52005632	0.053430941	0.589835962	0.552589238	58.10807387	-0.073968971	0.416533253
13	0.4333368	4.131177209	0.062707147	0.692238038	0.553563173	58.21048899	-0.067713585	0.453917498
14	0.4666704	4.791187769	0.072725448	0.802832281	0.554787338	58.33921735	-0.060957767	0.494292483
15	0.500004	5.500088	0.083485846	0.92161869	0.556300177	58.49830137	-0.053701518	0.537658207
16	0.5333376	6.257877903	0.09498834	1.048597265	0.558142262	58.69200772	-0.045944838	0.584014672
17	0.5666712	7.064557476	0.107232931	1.183768006	0.560356049	58.92480067	-0.037687727	0.633361875
18	0.6000048	7.920126721	0.120219618	1.327130914	0.562985574	59.20131103	-0.028930186	0.685699819
19	0.6333384	8.824585636	0.133948402	1.478685987	0.566076121	59.52630054	-0.019672213	0.741028502
20	0.666672	9.777934223	0.148419282	1.638433227	0.569673839	59.90462225	-0.00991381	0.799347924

To determine the natural frequency of each cylinder in water both cylinders were placed in the tank separately and underwent a similar decay test in both directions. Due to increase in viscous resistance of fluid medium, damping raised and natural frequency of the system reduced. Figure 3.9 includes four sample time history for both cylinders in two directions. It should be noted that each test was repeated several times to ensure repeatability of tests and accuracy in calculations. Figure 3.10 also shows a sample time history for the other two sets of experiment where rod length was extended to 2.2 and $2.8m$.

Each time history was analysed using Fast Fourier Transfer (FFT) and the dominant frequency component was detected from time history power spectrum (principle and Matlab code would be discussed in the following section). Figure 3.11 includes power spectrum obtained from 4 time histories in figure 3.10 and 3.11. All power spectrum have a dominant peak which is identical in both in-line and cross-flow directions. This figure confirms that the test apparatus possessed identical structural property in all directions, as the natural frequency of the system is equal in both directions. Extending the length of supporting rod resulted in a reduction in the natural frequency of the system that is observable by comparing left and right figures.

Damping

Structural damping of experiment apparatus can be calculated from free decay test results as well. The logarithmic decrement method has been widely used in the literature to calculate damping ratio of a system with viscous damping. In this approach N number of free decay oscillation is selected (from oscillation i to $i+N$) if the amplitude of response is known X_i,X_{i+n} then logarithmic decrement can be calculated from equation 3.3 and then the damping ratio (ξ) is simply calculated by using equation 3.4 [57].

$$\delta = \frac{1}{N} ln\ (\frac{X_i}{X_{i+n}}) \tag{3.3}$$

$$\xi = \frac{\delta}{\sqrt{4\pi^2 + \delta^2}} \tag{3.4}$$

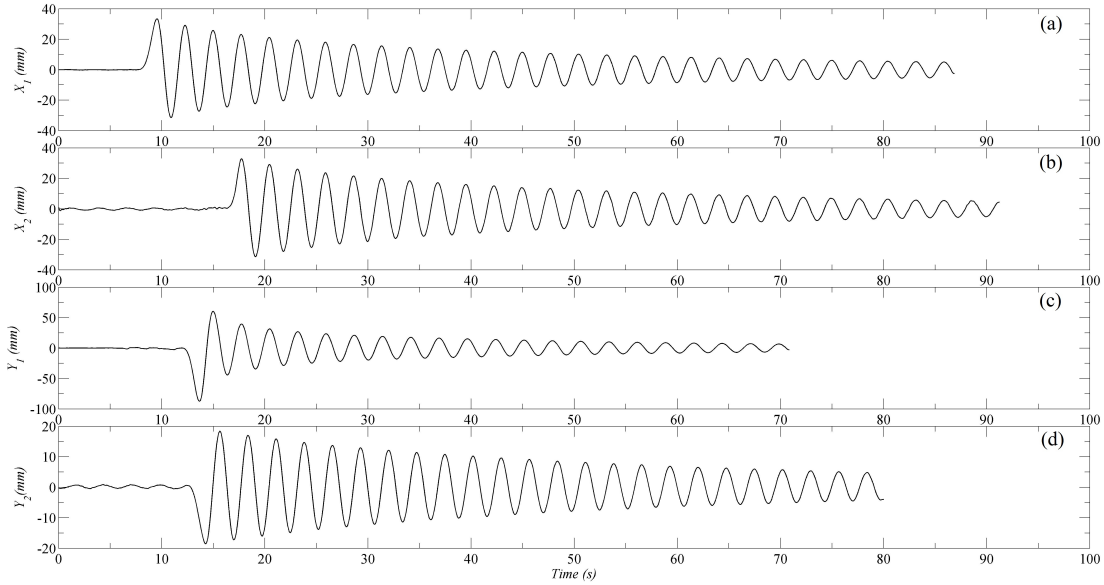

Figure 3.9: Time history of free decay test in water ($L_r = 1.8m$) for both cylinders, (a) first cylinder in stream-wise direction, (b) second cylinder in stream-wise direction, (c) first cylinder in cross-flow direction, (d) second cylinder in cross-flow direction.

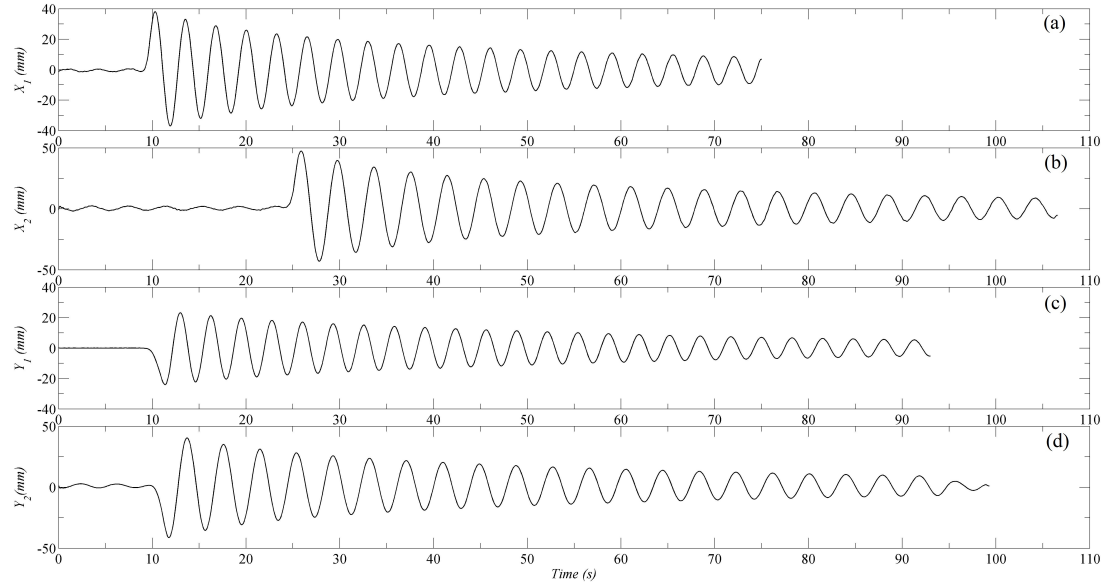

Figure 3.10: Time history of free decay test in water for both cylinders, (a) cylinder with $L_r = 2.2m$in stream-wise direction, (b) cylinder with ($L_r = 2.8m$) in stream-wise direction, (c) cylinder with ($L_r = 2.2m$) in cross-flow direction, (d) cylinder with ($L_r = 2.8m$) in cross-flow direction.

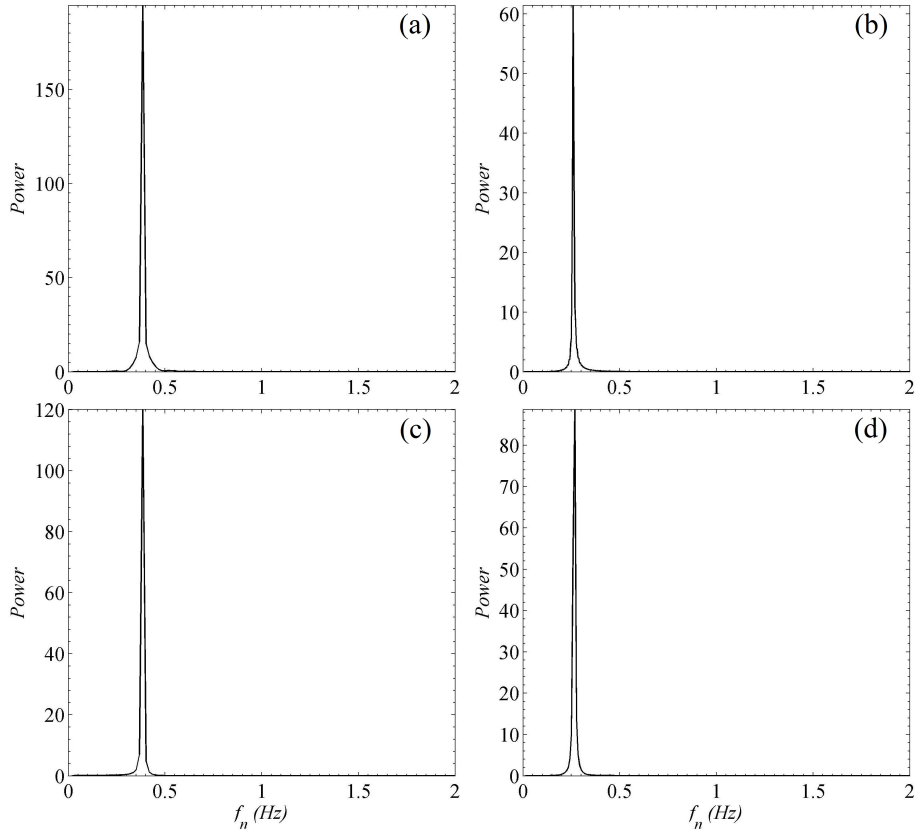

Figure 3.11: Time history's power spectrum of free decay test in water for both cylinders, (a) cylinder with $L_r = 1.8m$ in stream-wise direction, (b) cylinder with ($L_r = 2.2m$) in stream-wise direction, (c) cylinder with ($L_r = 1.8m$) in cross-flow direction, (d) cylinder with $L_r = 2.2m$ in cross-flow direction.

A minimum of 20 oscillations was considered for damping calculations to eliminate the effect of drag force. These oscillations were chosen from different parts of the time history, beginning, end and the whole timeline, and the average among three of them was reported as the ratio. The following table contains the natural frequencies and damping ratios of all cylinders used in this research.

	Air				Water			
	Cross-flow		In-line		Cross-flow		In-line	
Cylinder	$f_n(Hz)$	ξ	$f_n(Hz)$	ξ	$f_n(Hz)$	ξ	$f_n(Hz)$	ξ
Leading($L_r = 1.8$)	0.505	0.007	0.506	0.007	0.367	0.015	0.367	0.011
Trailing($L_r = 1.8$)	0.506	0.008	0.506	0.006	0.365	0.014	0.366	0.011
$L_r = 2.2$	—	—	—	—	0.318	0.010	0.317	0.011
$L_r = 2.8$	—	—	—	—	0.267	0.008	0.259	0.008

Table 3.3: Free decay results on different supporting rods in air as well as water

Structural stiffness

Structural stiffness was important in this research to determine the hydrodynamic forces acting on the cylinders. Stiffness of the rod was calculated using static loading. A piece of string was attached to the end of a hung rod at one end and connected to a free weight at the other end by help of a pulley. Using this displacement, measured by Qualisys, stiffness of the rod can be obtained from equation 3.5. This test was repeated 11 times during which the free weight were increased by increments of $100gr$ each time, ranging from 0.1 to $1.1kg$. If all these loading are drawn against their induced displacement will create a line for linear structures of which slope is structural stiffness. Figure 3.12 shows the displacement of supporting rod end under loading. Slope of this straight line is 247.69 $\frac{N}{m}$. This stiffness yields a natural frequency ($\omega_n = \sqrt{\frac{k}{M}}$) of $0.526Hz$ which is 3% above measurements in free decay tests.

$$k = \frac{3EI}{L_r^3} \tag{3.5}$$

3.3 Post processing

After collecting data from experiments, all raw time histories should be processed to be prepared similar to figure 3.8- 3.10. In this regard, the noise recorded during the test

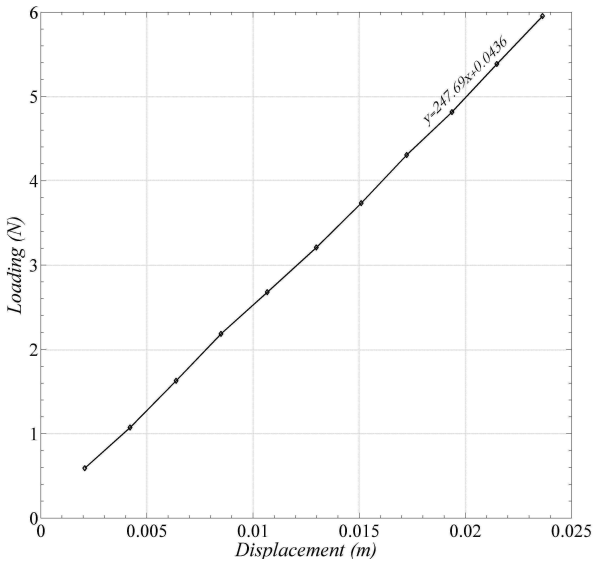

Figure 3.12: Supporting rod's stiffness acquire by loading the rod with free weight with increments of $100gr$.

due to vibration of carriage or similar external sources should be filtered out with the help of digital filters. Moreover, it will be observed in section 3.5 that motion response of both cylinders at very high speeds consist of several frequency components that are required to be cautiously separated so that a better understanding of governing hydrodynamics is obtained. This objective was met by using FFT as well as digital filtering. In this section, both methods are discussed, and Matlab codes will be shared for future references.

3.3.1 Digital filter design

The digital filter used in this study is *Butterworth*. Butterworth is an infinite impulse response filter that acts as a gate and stops motions with frequencies above or below a certain threshold. Filters can be categorised based on which side of the threshold are allowed to pass. Four categories of filters are low pass, high pass, band pass and band stop. It is important to know that digital filters reduce the magnitude of stopped frequencies gradually, and it is not a clear line between passed and stopped frequencies. However, as the order of the filter increases, the cut between allowed and stopped frequencies becomes sharper. On the other hand, as the filter's order increases, it creates a ripple through the allowed bandwidth, which means the stoppage of desirable fre-

quency and entrance of noise. Therefore, it is recommended that filter to be designed with the lowest order possible while cutting frequency is adequately distanced from desirable frequencies so that the filter does not carve into acceptable response.

It has been discussed earlier that natural frequency of the system was $0.376Hz$. Additionally, it has been reported in the literature that VIV frequency can reach up to 2.5 times of the cylinder's natural frequency, [58, 59], i.e. $0.9175Hz$ for this experiment. Thus for digital filter design, the cut-off frequency of $1Hz$ was chosen to filter high-frequency noise. However, it is the cut-off frequency in the time domain (analogue); therefore it is necessary to find the corresponding digital frequency using frequency warping [60]. The cut-off frequency can be obtained using equation 3.6. Considering that the sampling ratio for Spike2 software was fixed to be $T_s = 1/137s$, expression 3.7 creates a low pass Butterworth filter of 12th order in Matlab with the analogue cut-off frequency of $1Hz$.

$$\omega_d = \frac{2}{T_s} tan(\frac{\omega_a T_s}{2}) \tag{3.6}$$

$$[b, a] = butter(12, 2\pi/137, ' low') \tag{3.7}$$

Additionally, digital filter output has a phase difference with original data, which must be eliminated by filtering the data with the same filter twice, forward and backwards (or using "filfilt" command in Matlab).

3.3.2 Fast Fourier Transform

FFT transforms a time domain response to its frequency components so that more in-depth studies could be conducted on the response motion. FFT is an algorithm to compute *Discrete Fourier Transform* (DFT) which creates frequency domain signal samples. If there are N number of frequency sample data points of a certain signal (x), it is possible to determine the Fourier series coefficient using equation 3.8, [61], where $X(k)$ contains the DFT coefficients.

$$X(k) = \sum_{n=0}^{N-1} x(n) e^{-j\frac{2\pi kn}{N}}, \quad k = 0, 1, \cdots, N-1 \tag{3.8}$$

In FFT algorithm the number of data points must be equal to a power of two, in other words, there should be 2^m samples where m is a positive integer and if not available, the remaining of data sequence will be considered zero to produce enough samples. Since each FFT coefficient calculated from equation 3.8 is a complex number, its magnitude can be plotted against its corresponding frequency calculated from equation3.9.

$$f = \frac{k}{2^m T_s} \tag{3.9}$$

Following is the code that has been used in Matlab to calculate the power spectrum and the corresponding frequency. Where fw is frequency index, and X-power is its amplitude in the signal spectrum.

```
m=length(Signal-sample);
n=pow2(nextpow2(m));
X=fft(Signal-sample,n);
fw=1/T_{s}*(0:n/2)/n;
xf1=2*abs(X)/n;
X-power=xf1.*xf1;
```

Additionally, inverse fast Fourier transform could be used to map frequency domain signal sample back into time domain signal. Further in section 3.5 this method will be used to separate conventional VIV motion from other FIV.

3.4 Test Validation & Repeatability

A single cylinder was placed in the tank initially and tested to be compared with existing result in literature to verify the accuracy and performance of experiment apparatus. Also, the same experiment was repeated ten months later to examine the reproducibility of the test. Additionally, a random speed at a random spacing was chosen and repeated several times so that repeatability of test could be evaluated.

3.4.1 Single Cylinder's Test

The first single cylinder test was carried out in March 2015. Data acquired from Qualisys and Spike2 were filtered using low pass filter discussed in section 3.3.1 to be separated from high-frequency noise. Root mean square(RMS) of cylinder motion response, after it reaches steady state, was calculated in two directions, cross-flow and stream-wise. Then, these data was compared to previous experiments for the sake of evaluating the performance of experimental equipment. Figure 3.13 shows RMS of response amplitude for this experiment and two others against the corresponding reduced velocity.

A smaller value of maximum amplitude in the experiments by Srinil et al. [54] and Blevins and Coughran [58] is due to higher damping in the other two experiments (0.05 and 0.02 respectively). Also, the difference in mass ratio resulted into different lock-in range width, where the mass ratio is 1.75 in [54] experiment and for [58] it is 2.8.

The initial lock-in range in the stream-wise direction (caused by coinciding in-line oscillation frequency and system natural frequency) was not captured due to high-velocity starting point. Due to low mass-damping ($m^*\xi$) three branches of excitation can be observed based on the Govardhan and Williamson [7] study. The initial branch approximately starts at U_r =2 to 6 then upper branch can be observed from U_r =8 to 10 and finally lower branch which starts at U_r =11.

3.4.2 Test Repeatability& Reproducibility

Repeatability and reproducibility are two concepts that describe the accuracy of measurements during an experiment. According to ISO 5725 - 2:1994, repeatability is described as probability to produce same results in multiple experiments that possess the repeatability condition criteria:

- Measurement procedures are the same.
- Same measurement instruments are used for identical test items.
- Tests are conducted under same environmental condition (such as temperature) at the same facilities.

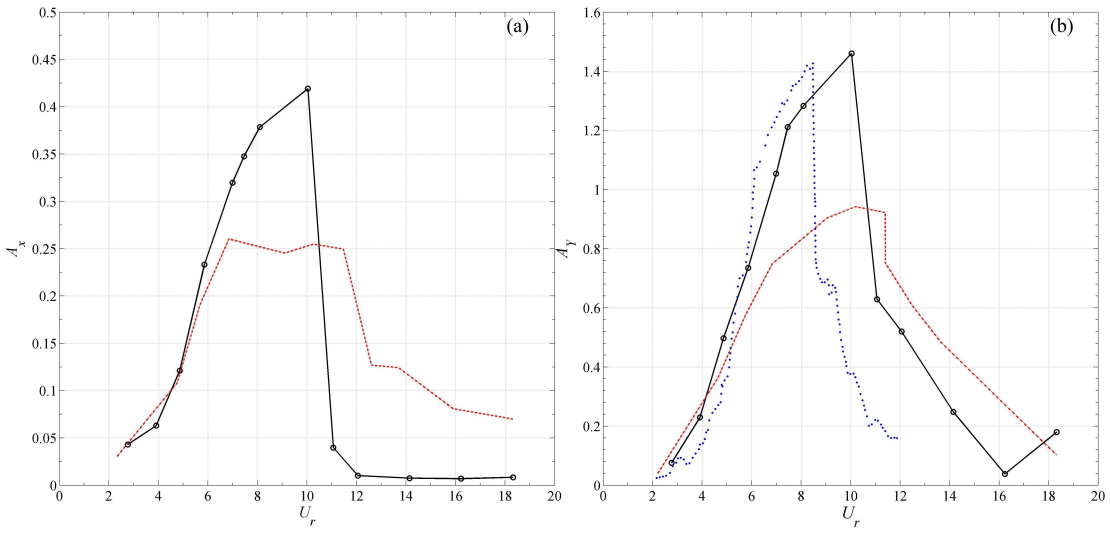

Figure 3.13: A comparison between results obtained from single cylinder test (black solid line) and Srinil et al. [54] (red -·- line) and Blevins and Coughran [58](blue ··· line)

- Tests are conducted over a short period by the same operator.

Reproducibility has similar definition where reproducibility condition is determined as:

- Measurement procedures are the same.
- Measurements are conducted on identical test items.
- Tests are conducted at different facilities and/or by different operators and/or with different equipment and/or at a different time.

Repeatability

It should be noted that due to the complexity of experimental procedure it was not possible to replicate the test completely. However, operators tried at best to keep the experimental condition identical. For instance, carriage speed was kept constant up to two decimal points.

Isolated cylinder experiment was repeated at a fixed speed four times to calculate the test repeatability. Carriage speed was fixed at 0.36 m/s which is equal to reduced velocity of 9 and amplitude response in stream-wise and cross-flow directions were recorded with identical equipment. Each test was conducted within five minutes period

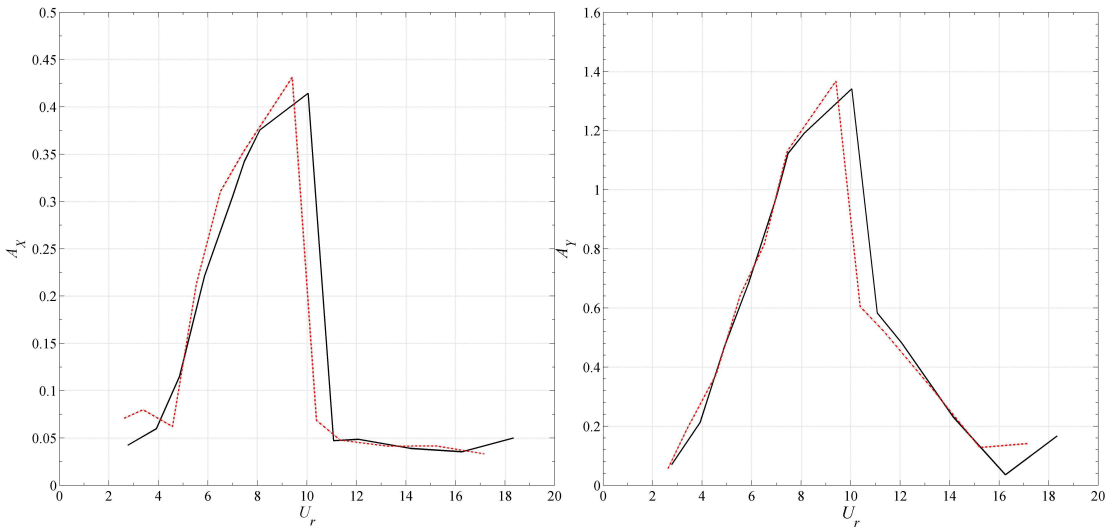

Figure 3.14: Single cylinder experiment was conducted twice, ten months apart. First experiment (solid black line) was conducted March 2015 and the second test was carried on January 2016 (red -·- line).

after the end of the previous test. Table 3.4 is containing measured amplitudes in mm for each test.

	Trial 1	Trial 2	Trial 3	Trial 4
X_1	24.9587	26.1641	26.1324	22.8603
Y_1	105.499	102.17	106.31	104.434

Table 3.4: Amplitude response (mm) obtained from four repetitions of isolated cylinder test at velocity of 0.36 m/s ($U_r = 9$).

If n repetition of an identical test is conducted in repeatability condition, the repeatability variance can be calculated from following equation.

$$s_r{}^2 = \frac{1}{n-1} \sum X_i - \bar{X} \tag{3.10}$$

Thus average variance for repeatability of this test is $2.8131mm$, using this value repeatability of the test with 95% probability (assuming the results are normally distributed)can be calculated from equation 3.11 which yields $r = 4.6490$.

$$r = 1.96\ s_r\sqrt{2} \tag{3.11}$$

	$U_r = 2$	$U_r = 3$	$U_r = 4$	$U_r = 5$	$U_r = 6$	$U_r = 7$	$U_r = 8$	$U_r = 10$	$U_r = 11$	$U_r = 12$	$U_r = 14$	$U_r = 16$	$U_r = 18$
	Trial 1												
X_1	6.61	3.43	4.70	9.19	17.00	17.02	30.83	19.31	0.10	1.62	1.34	2.01	3.42
Y_1	1.00	6.50	17.49	38.57	54.63	84.49	96.17	106.89	45.73	38.46	21.65	2.06	12.32
	Trial 2												
X_1	6.26	5.54	5.18	4.79	16.98	25.23	21.83	27.22	3.04	0.58	0.93	0.93	2.09
Y_1	0.05	5.04	15.86	31.08	53.33	67.83	91.47	109.33	49.06	41.363	27.0382	12.28	9.081

Table 3.5: Amplitude response (mm) obtained from two sets of isolated cylinder test with six-month gap in between them.

Reproducibility

The probability of test reproducibility was examined through replication of full isolated cylinder experiment in the same facility with identical observer and equipment but with a six-months interval between the two experiments. Figure 3.14 includes the results from both experiments which confirms overall agreement between two experiments.
Measured oscillation amplitudes in millimetres are shown in the table 3.5. Repeatability probability between experiments (s_L) can be obtained from data in table 3.5 using a similar expression as equation 3.10. Then, reproducibility probability can be calculated from equation 3.12.

$$S_R{}^2 = s_r{}^2 + s_L{}^2 \tag{3.12}$$

Average variance for reproducibility of isolated cylinder test is 17.81880715; therefore reproducibility of the test with 95% probability is $R = 11.70066063$.

3.5 Results & Discussion

In this section, the results from other three sets of experience will be introduced and discussed. furthermore, the author will attempt to explain the excitation mechanism of trailing cylinder.

3.5.1 Identical cylinders

In first set-up of two cylinders in tandem, both structures had identical supporting rods and cylinders so all structural properties were the same. Two cylinders were placed at the largest targeted spacing $20D$ and then brought closer together after each test till they collided at $L = 3D$ as it was predicted in figure 3.6 at the reduced velocity of $U_r = 10$ when the leading cylinder was at its maximum oscillation. It should be noted that maximum deflection experienced by supporting rods was by the downstream body which was approximately 0.501 degrees.
Figure 3.15 shows RMS of response amplitude for all spacings versus reduced velocity. In the leading cylinder the initial lock-in range in stream-wise can be observed for

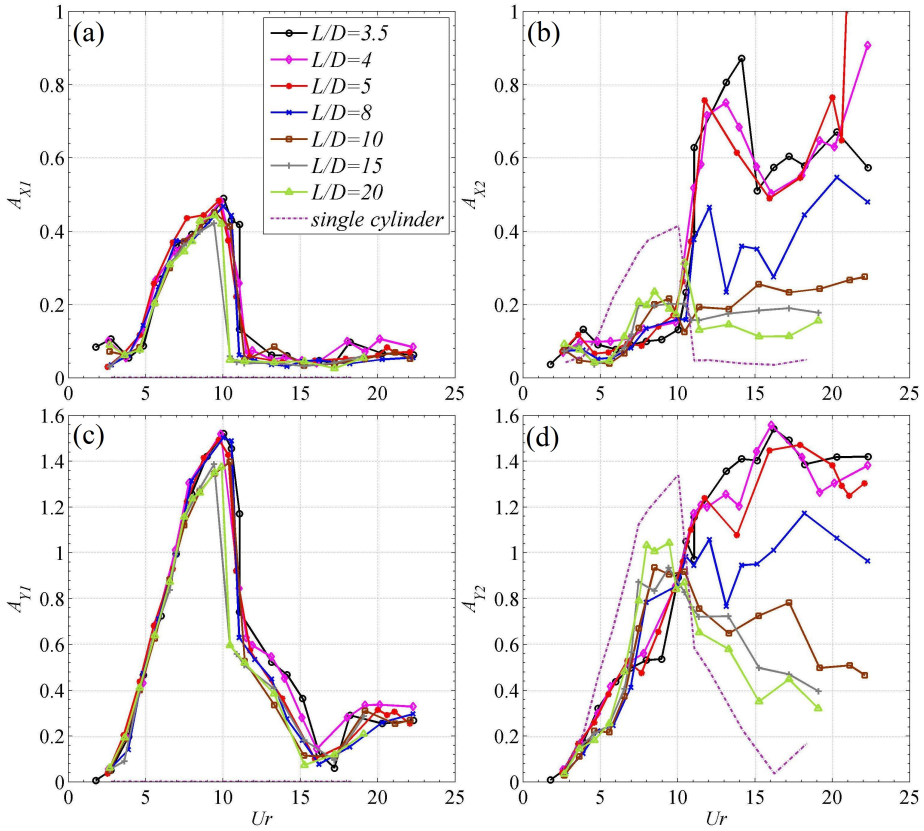

Figure 3.15: Amplitude response of all spacings in first experiment set-up against reduced velocity.(a)Leading cylinder's stream-wise response amplitude,(c)Leading cylinder's cross-flow response amplitude, (b)Trailing cylinder's stream-wise response amplitude, (d)Trailing cylinder's cross-flow response amplitude

spacings of $3.5D$ and $4D$ and as the spacing increase, it can be seen again at spacings of $10D$ and $20D$. The in-line lock-in range shifted to higher reduced velocities as two bodies placed closer together. As Xu and Zhou [42] observed in their study when two cylinders are placed within proximity the shear layers do not have enough space to roll up behind the leading cylinder. However, when Reynolds number increases, separation happens earlier on the face of the cylinder, thus shear layers have enough time to turn into vortices. It may explain why lock-in range is shifting to higher Re in smaller gaps. Papaioannou et al. [48] also claimed that when the leading cylinder starts to generate vortices, it acts similar to an isolated cylinder. Nevertheless, when Re is high enough for leading cylinder to undergo lock-in range, the wake behind the leading cylinder is fully developed thus spacing has no effect on the lock-in range. The response of the leading cylinder in cross-flow is higher than that of stream-wise similar to a single cylinder.

On the other hand, trailing cylinder response is completely affected by the presence of the other body thus the effect of spacing is more significant. Behaviour of the trailing cylinder should be interpreted considering two important facts. First, the flow velocity passing the trailing cylinder is less than that in the free stream due to leading cylinder shielding effect. Second, vortices washed from upstream cylinder buffet trailing cylinder. It appears that at small spacings trailing cylinder has the same maximum amplitude in cross-flow direction as that of the leading body. Nonetheless, the maximum oscillation amplitude occurs at a higher reduced velocity due to shielding effect. As the trailing cylinder moves further away from the first one, vortices lose a fraction of their energy travelling downstream due to viscous friction, so the buffeting force on the trailing cylinder subsides significantly. It can be observed that due to such a reduction the response amplitude reduces as the gap grows. Observing response graph of larger spacings ($\frac{L}{D}$>5) reveals that the forces exerted on trailing cylinder by coming vortices have a greater share in cylinder response in comparison to hydrodynamic forces from the wake of the cylinder. The increase in spacing means a reduction of force from vortices, due to viscous resistant, and an increase of flow velocity in the gap. However, the effect of latter was not observable until the largest spacing where response amplitude started to increase after constant reduction in smaller spacings.

Stream-wise response graph for trailing cylinder shows four peaks regardless of the distance between two cylinders. The first peak can be observed at the same U_r as that of the leading cylinder. The second peak happens between reduced velocities of 8 to 10 where the leading cylinder experiences the largest oscillations. This peak becomes dominant as the gap increases which indicates that the cylinder response is evolving towards that of a single cylinder. The third peak happens between $U_r = 10$ to 15 which is the most dominant for small and moderate spacings and appears to be the main lock-in range. The width of this lock-in range has an inverse relationship with the size of the gap and disappears as the gap increases. The last peak happens at around reduced velocity of 20 which appears to receive no influence from changing the spacing until large spacings at which it gradually disappears.

Furthermore, the cross-flow response of the trailing cylinder (figure 3.15 d) presents three distinct peaks. Considering the reduced velocity at which each peak happens as

well as the effect of spacing on them, could lead to a conclusion about the excitation mechanism of each peak. The first peak happens at $U_r = 5$ to 10 which is during leading cylinders lock-in range. Change in spacing does not have any effect on the reduced velocity at which the first peak occurs, however, the magnitude of the peak changes by spacing. The value of this peak has a direct relation with the gap size. As it can be observed in the figure 3.15 the peak is at its highest value at the spacing of $20D$ where the cylinder response is similar to that of an isolated cylinder the most.

The second peak occurs at the same reduced velocity as that in the stream-wise direction, and the variation in the magnitude of these peaks, caused by change in spacing, is similar as well which suggests that lock-in phenomenon in stream-wise direction is affecting the cross-flow response which is contrary to the case of a single cylinder. Finally, this peak slowly disappears as the spacing increases further. The third peak, which is the most dominant and is exclusive to cross flow response of the trailing cylinder, occurs at very high reduced velocities. Nevertheless, the peak loses its dominance from spacing of $8D$ onwards and gradually transforms to a sudden increase of response at very high velocities for an isolated cylinder.

The frequency content of transverse oscillation has a dominant frequency in all cases. Figure 3.16 compares the cross-flow oscillation frequency normalised to natural frequency in water, against reduced velocity for both cylinders. It is evident that trailing cylinder followed leading cylinder where it was in lock-in range and despite shielding effect it oscillated with the same frequency. After the leading cylinder exit the lock-in range, trailing cylinder vibrated at a lower frequency which is due to lower flow velocity in the wake. However, it is in contrast with what Xu and Zhou [42] and Kitagawa and Ohta [41] observed in their experiments on two identical fixed cylinders in tandem with two identical shedding frequencies. Results of their experiments showed that both cylinders have similar Strouhal numbers regardless of Re. Moreover, the leading cylinders shedding frequency graph display a significantly larger jump compare to its downstream counterpart which can be a sign of change in its wake regime, but more investigation with flow visualisation techniques is required.

On the other hand as the gap between two cylinders increases, vortices detached from leading cylinder are not strong enough to keep the following structure excited at the

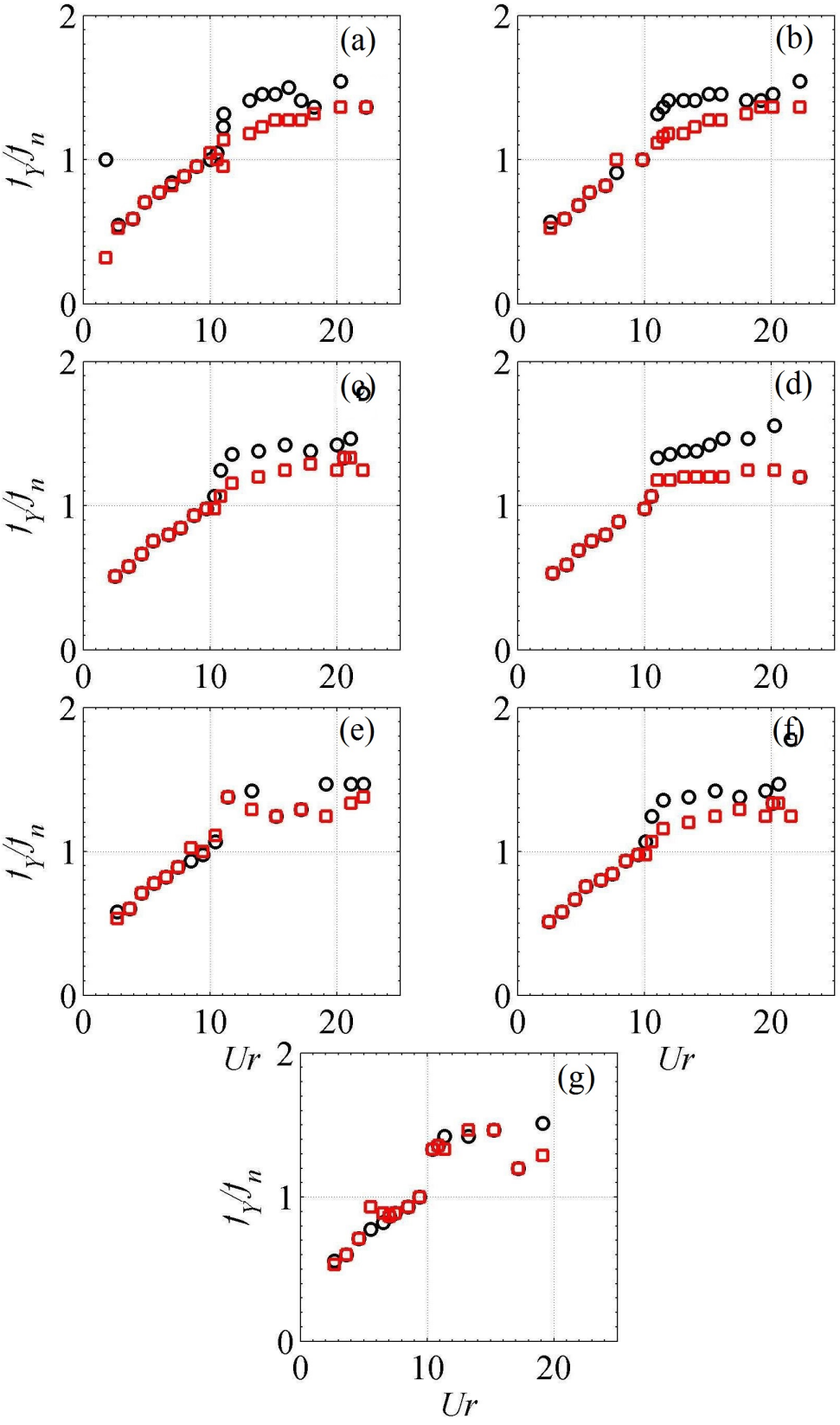

Figure 3.16: Comparison between frequency response of leading (○) and trailing (□) cylinder in cross-flow direction at various spacings. L/D = (a)3.5, (b)4, (c)5, (d)8, (e)10, (f)15, (g)20.

same frequency as the first cylinder after its lock-in range. Thereby, VIV response of downstream cylinder becomes dominant, and its frequency differs from its leading counterpart. However, since the velocity in the gap is less than that of the free stream, trailing cylinders oscillation frequency is lower in comparison with its upstream counterpart, although both have the same natural frequency. It can be observed in Figures 3.16 e, f and g, that oscillation frequency of the trailing cylinder moves towards that of the leading as the gap between two cylinders grows.

In-line oscillation frequency for either of cylinders does not follow an isolated cylinders graph (figure 3.17). Very low frequencies are dominant in relatively high reduced velocities while for reduced velocities on the initial branch the in-line frequency is twice as of that for transverse as Bearman [62] observed in his study. The domination of low frequency in power spectrum of stream-wise response is observed by Huang and Sworn [33] as well.

By considering the frequency spectrum of both cylinders in cross-flow and stream-wise directions, it is observed that the in-line responses of both cylinders are a collection of motions with different frequencies. Figure 3.18 shows an example of such a test where the gap is $4D$, and reduced velocity is approximately 12. It is observed that although the dominant stream-wise frequency is not twice of that in cross-flow, a distinct peak still can be located at that particular frequency. The time history of this test is also shown in figure 3.19. It is clear that response of both cylinders in in-line direction consists of two frequency components, one very low frequency with relatively large amplitude and one high frequency with smaller oscillation amplitude, especially for the trailing cylinder. This motion can be seen in oscillation path of downstream cylinders. If the amplitude of each cylinder in cross-flow was drawn against its amplitude in stream-wise direction, it yields a trajectory of its oscillation in the test. Figure 3.20 shows trajectories for all runs during which $L/D = 4$. It is evident that trajectory of trailing cylinder is different from what Dahl et al. [52] observed during their experiment on a single cylinder. Leading cylinder's trajectory is similar to Dahl et al. [52] observation at all reduced velocities and resembles the figure of number eight in English. Hence it is called *figure of eight* (fo8) trajectory in the literature. However, trailing cylinder's trajectory maintained fo8 up to around $U_r = 10$ then a secondary

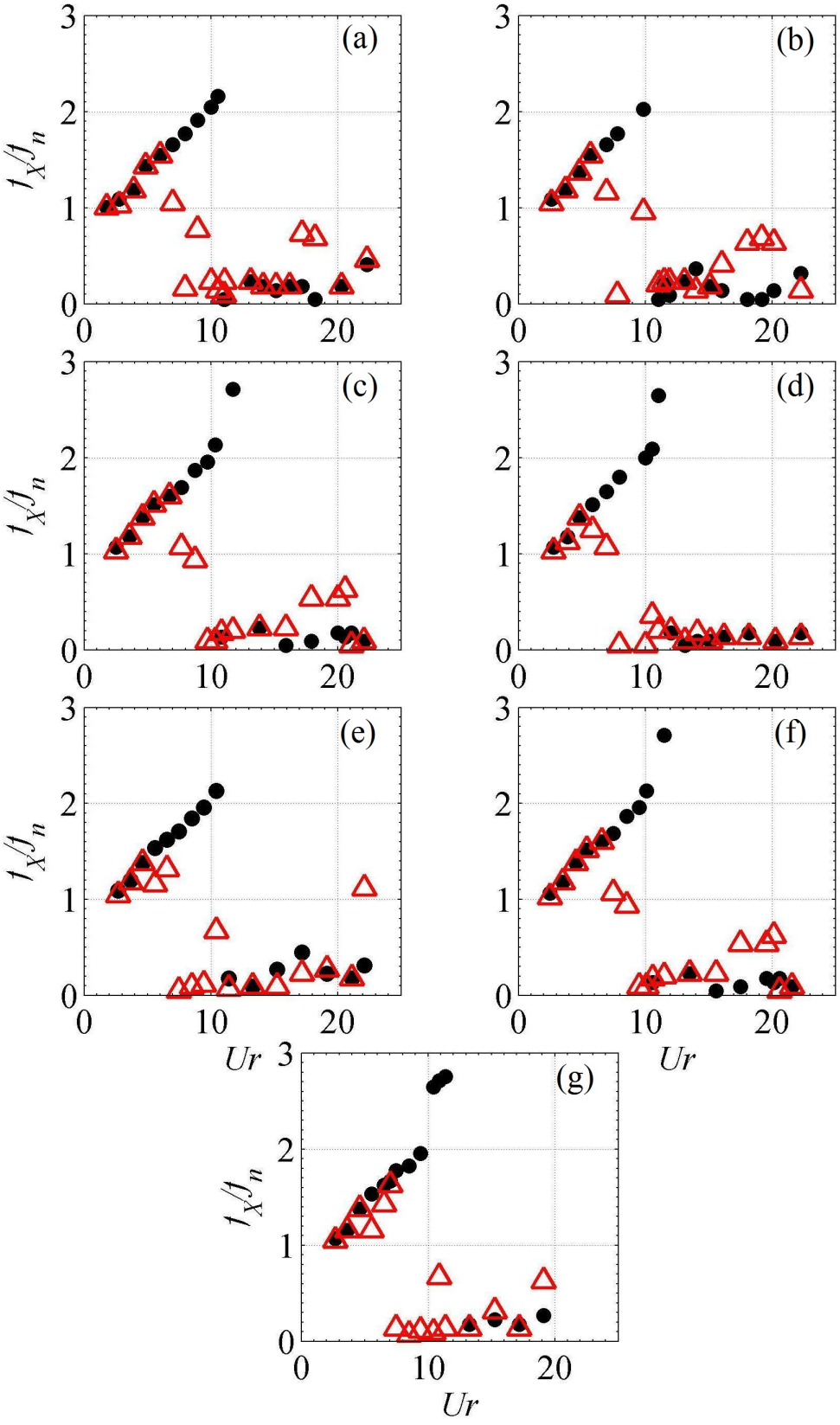

Figure 3.17: Comparison between frequency response of leading (●) and trailing (△) cylinder in stream-wise direction at various spacings. L/D = (a)3.5, (b)4, (c)5, (d)8, (e)10, (f)15, (g)20.

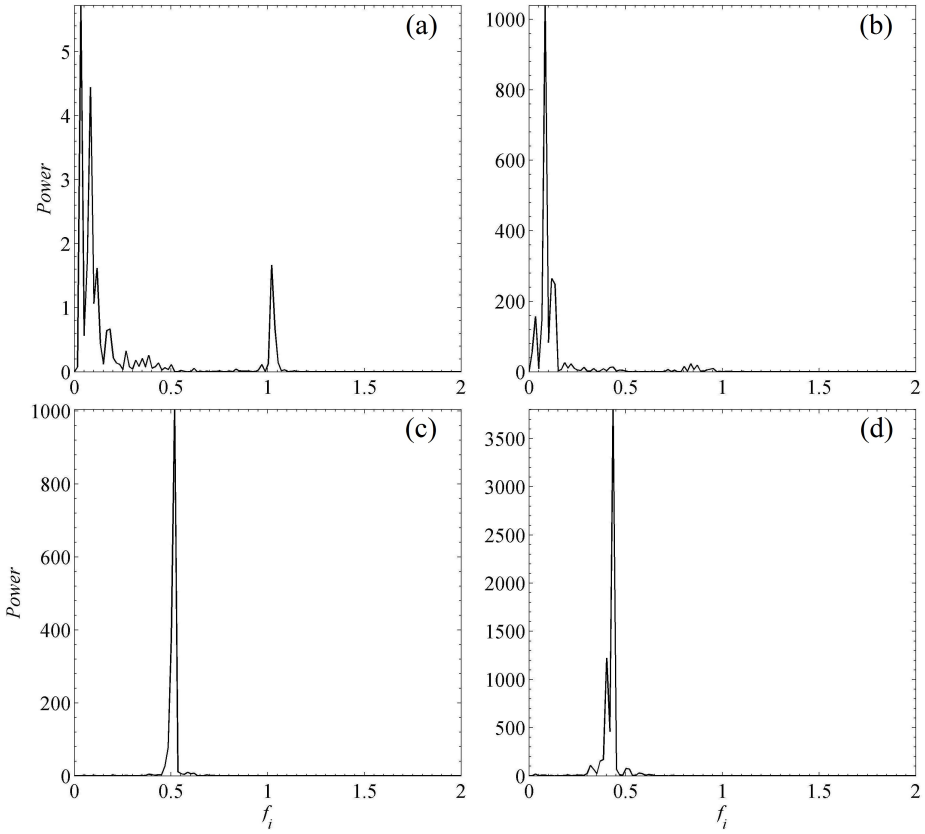

Figure 3.18: Power spectrum sample of a test with U_r =12 and L/D =4. (a)Leading cylinder's stream-wise response frequency,(c)Leading cylinder's cross-flow response frequency, (b)Trailing cylinder's stream-wise response frequency, (d)Trailing cylinder's cross-flow response frequency

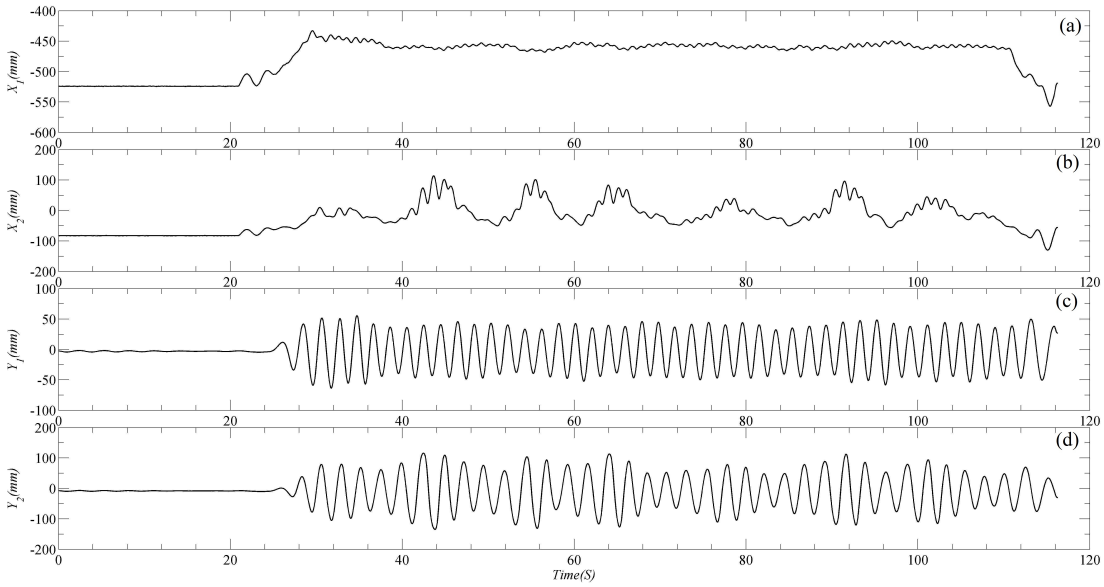

Figure 3.19: Time history of a test with U_r =12 and L/D =4. (a)Leading cylinder's stream-wise response amplitude, (b)Trailing cylinder's stream-wise response amplitude, (c)Leading cylinder's cross-flow response amplitude, (d)Trailing cylinder's cross-flow response amplitude.

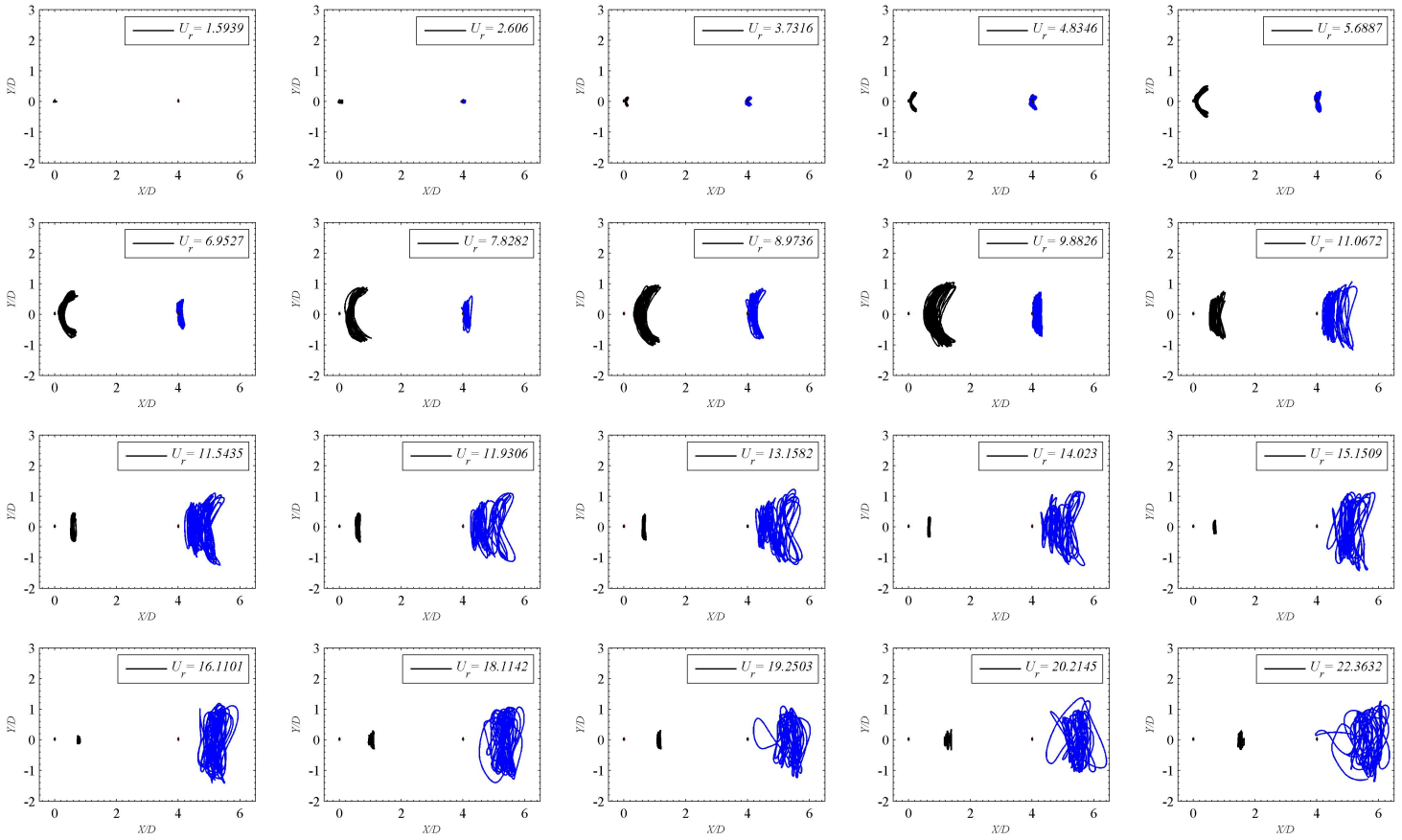

Figure 3.20: Oscillation trajectories for $L/D = 4$ $\left(\frac{f_{n_1}}{f_{n_2}} = 1\right)$; leading cylinder at (0,0) and trailing cylinder at (0,4)

motion appears in the stream-wise direction which disrupted cylinder's movement. An observer could identify and associate these movements with low-frequency motions in figure 3.19.

Such observations can bring up a hypothesis on multiple motions involved in the trailing cylinder's response specifically in stream-wise direction. Considering power spectrums from all tests reveals that multiple peaks appear in stream-wise trailing cylinder spectrum after $U_r = 11$, it is approximately the speed after which leading cylinder exits lock-in range and generates relatively weaker vortices. From this reduced velocity onward vortices detached from the leading cylinder cannot excite the structure in wake anymore; nevertheless, they interrupt its VIV motion (note the difference between single cylinder's trajectory by Dahl et al. [52]and trailing cylinder in this study). Upstream vortices do not have significant effect on trailing cylinder in cross-flow direction due to its strong motion in this direction. On the other hand, since response amplitude is subtle in stream-wise direction, vortices can significantly affect trailing cylinder motion in this direction.

In order to reach a better understanding of this phenomenon, an attempt was made to separate VIV response from other frequency components and their corresponding oscillation amplitude in drag direction using Fourier transform. It is established that in VIV, drag excitation frequency is always twice as the lift. Since shedding frequency in cross flow direction always has a strong and dominant component, it is possible to double this value and assume that it is approximately the stream-wise VIV frequency. The methodology is to perform FFT on the stream-wise response of each cylinder and separate the frequency bandwidth of $0.3345Hz$ (which is 10 point of FFT sampling on each side of the targeted frequency. The size of bandwidth was selected by try and error between 10,20,30 and 50 points.) around the frequency equal to twice the value of cross-flow frequency to accommodate possible discrepancy in exact values of the in-line oscillation frequency. Therefore, there will be two matrices; one containing frequency components of VIV and the other including frequency components of in-line movements of two cylinders towards each other. Then, by performing inverse FFT on each matrix separately the new oscillation time history can be obtained. These two new time histories could be used to calculate RMS of oscillation amplitude.

Figure 3.21 shows the motion frequency of the VIV response of both cylinders in drag and lift directions. It is evident that the frequency of two cylinders in stream-wise direction is almost identical except for a small interval between reduced velocities of 10 to 16, the period during which trailing cylinder goes throw a lock-in like response. However, the author cannot propose an explanation for such behaviour at the moment. Nevertheless, it is clear that two cylinders have a significant effect on each other in stream-wise direction comparing to cross-flow. The difference between frequencies of two cylinders in this direction disappears as the gap grows large and it is clear that two cylinders have almost identical response frequencies.

The different nature of two motion responses are clearer if RMS of both time histories, obtained by inverse FFT of two frequency component groups, are compared together. Figure 3.22 shows amplitudes of VIV and wake induced vibrations in two directions. Comparing stream-wise amplitude responses (figure 3.22 a and b) reveals that motion induced by the turbulent wake of the leading cylinder makes up a larger part of the cylinder oscillation. On the contrary, vibration of the cylinder in cross-flow (figure 3.22 c, d) is mostly induced by vortices detached from it.

3.5.2 Two identical cylinder with 15% difference in Natural frequency

In the next two experiments, an attempt was made to assess the effect of natural frequency on the response of the trailing cylinder. Results of these experiments helped to shed light on the role of each exciting mechanisms and showed which one has a more significant effect on the trailing cylinder's oscillation.

Initially, the supporting rod of leading cylinder was extended (from $1.8m$ to $2.2m$) and test was carried out at spacings $L/D = 4$, 8, 12. Then the carriage direction was reverse so the cylinder with lower natural frequency becomes the trailing one and same procedure was repeated for this set-up likewise. Figure 3.23 includes RMS of response amplitude at different reduced velocities where leading cylinder has a lower natural frequency. It should be noted that reduced velocity in all figures is calculated using initial natural frequency (reference) of systems, where $L_r = 1.8m$, so that comparison between all set-ups is possible.

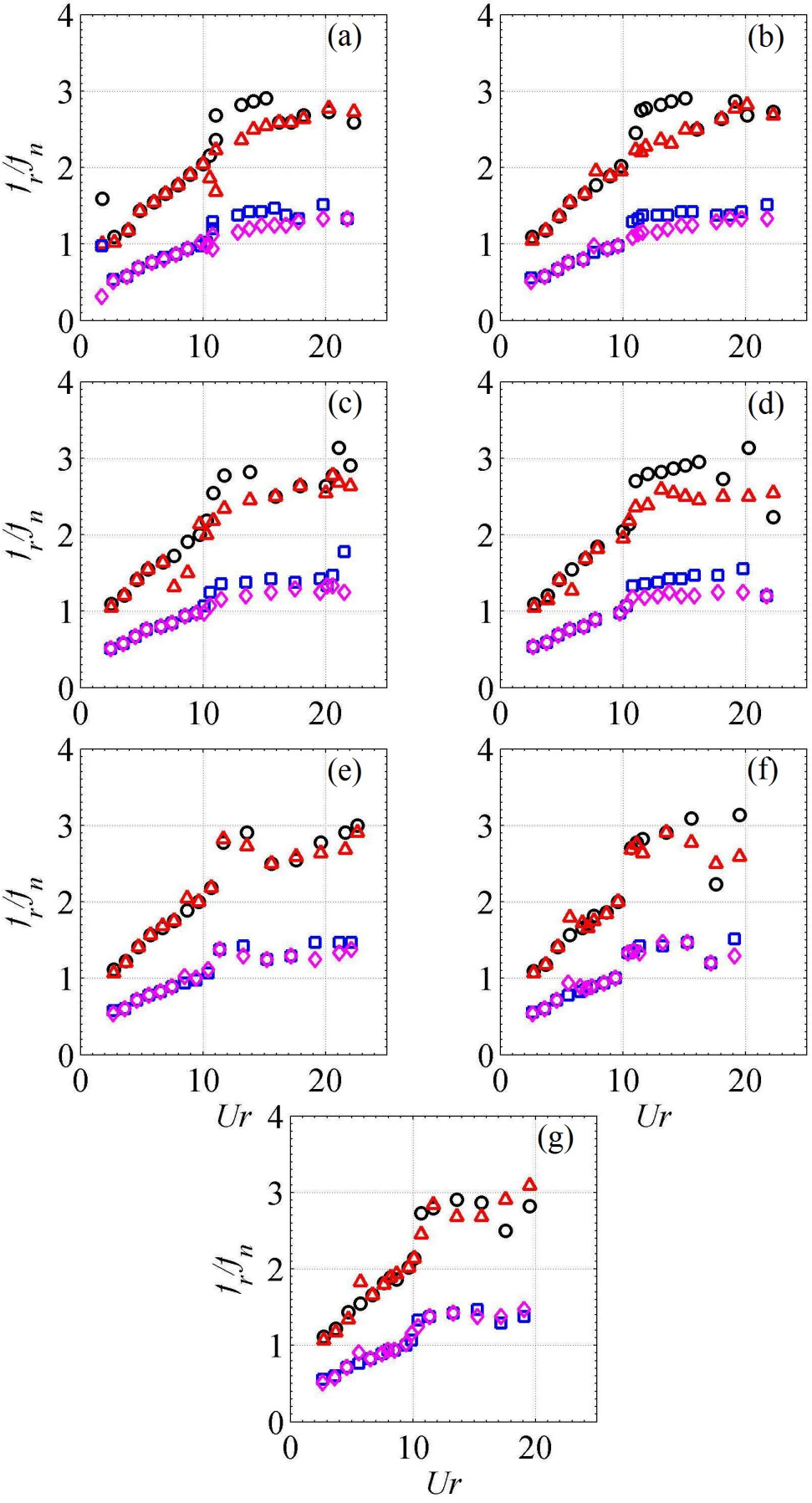

Figure 3.21: Comparison between response frequency of leading (○) and trailing (△) cylinder in stream-wise direction and leading (□) and trailing (♢) cylinder in cross-flow direction at various spacings. L/D = (a)3.5, (b)4, (c)5, (d)8, (e)10, (f)15, (g)20.

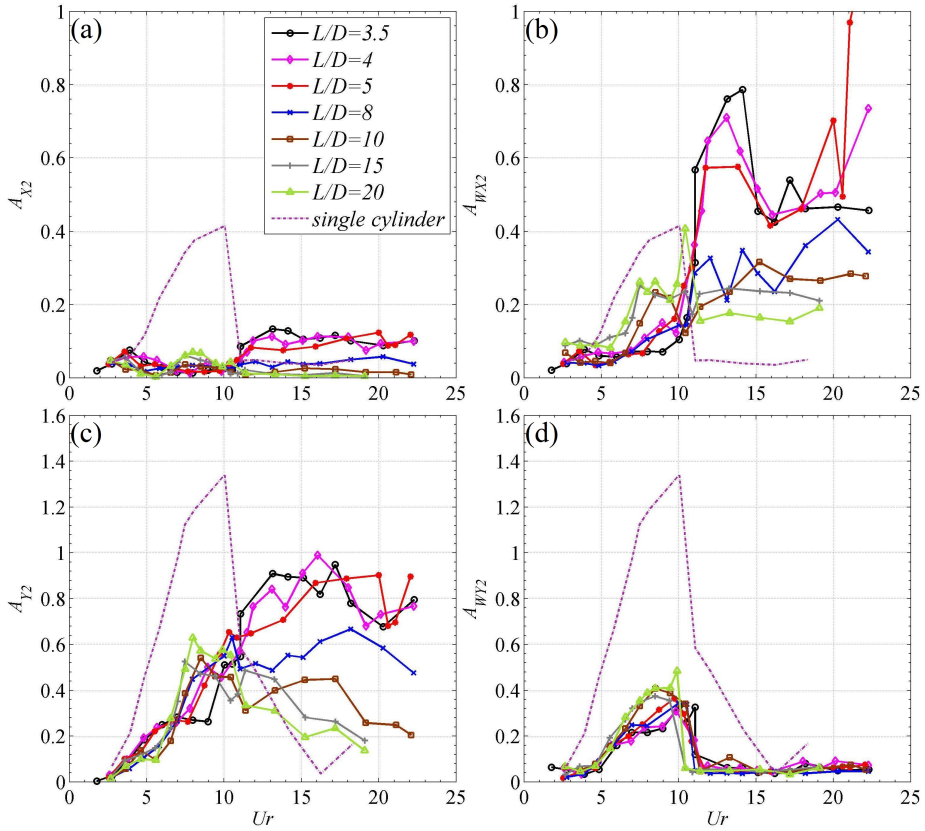

Figure 3.22: RMS amplitude response of downstream cylinder due to VIV and wake force. Stream-wise response amplitude due to (a) VIV and (b) the wake force. Cross-flow amplitude response due to (c) VIV and (d) the wake force

The maximum response amplitude of the first cylinder is slightly lower than its counterpart in earlier set up which is due to increase in damping and mass ratio. Leading cylinder is not affected by the trailing structure, similar to original set up. On the other hand, trailing cylinder's response is significantly different from the original set-up. The distinct peaks in trailing cylinder response cannot be observed anymore which could be explained by the difference between vortices frequency and cylinder natural frequency. Although buffeting vortices in the wake of leading cylinder increase the energy and intensity of the trailing cylinder response, however, the resonance-like phenomenon cannot be observed. Additionally, it can be observed that trailing cylinder behaves similarly to what Assi et al. [47] discovered in their study where leading body was fixed, and the trailing cylinder response could be described as galloping. Moreover, spacing has a significant effect on the trailing cylinder where an increase in spacing results in reduction of oscillation amplitude. However, this reduction is more dramatic than what

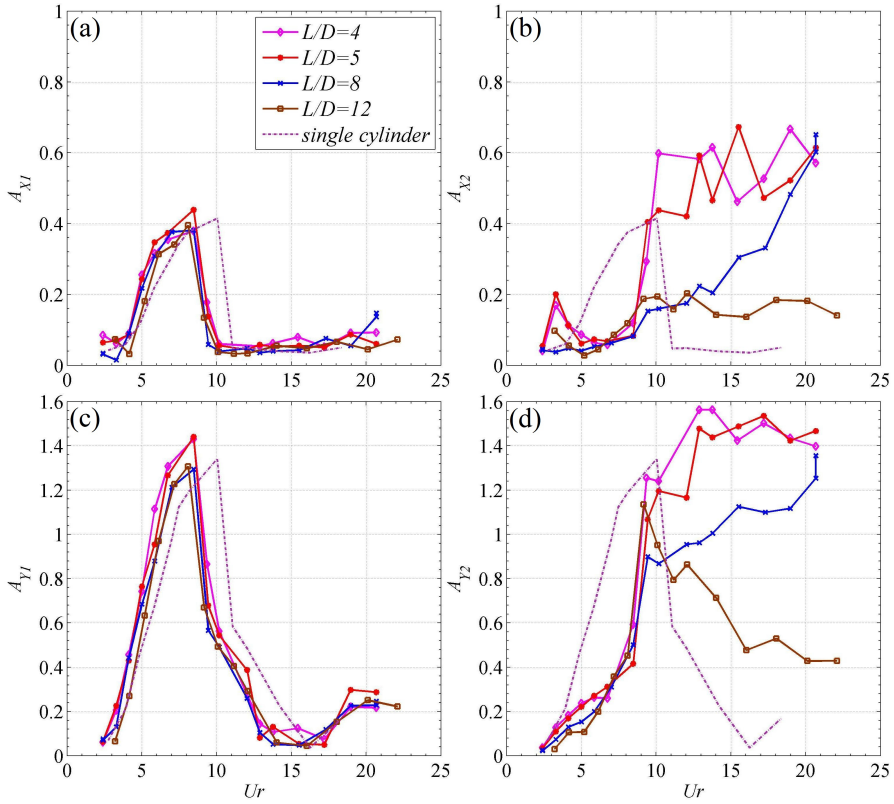

Figure 3.23: Amplitude response of all spacings in second experiment set-up against reduced velocity where $\frac{f_{n_1}}{f_{n_2}} = 0.8657$. (a)Leading cylinder's stream-wise response amplitude,(c)Leading cylinder's cross-flow response amplitude, (b)Trailing cylinder's stream-wise response amplitude, (d)Trailing cylinder's cross-flow response amplitude

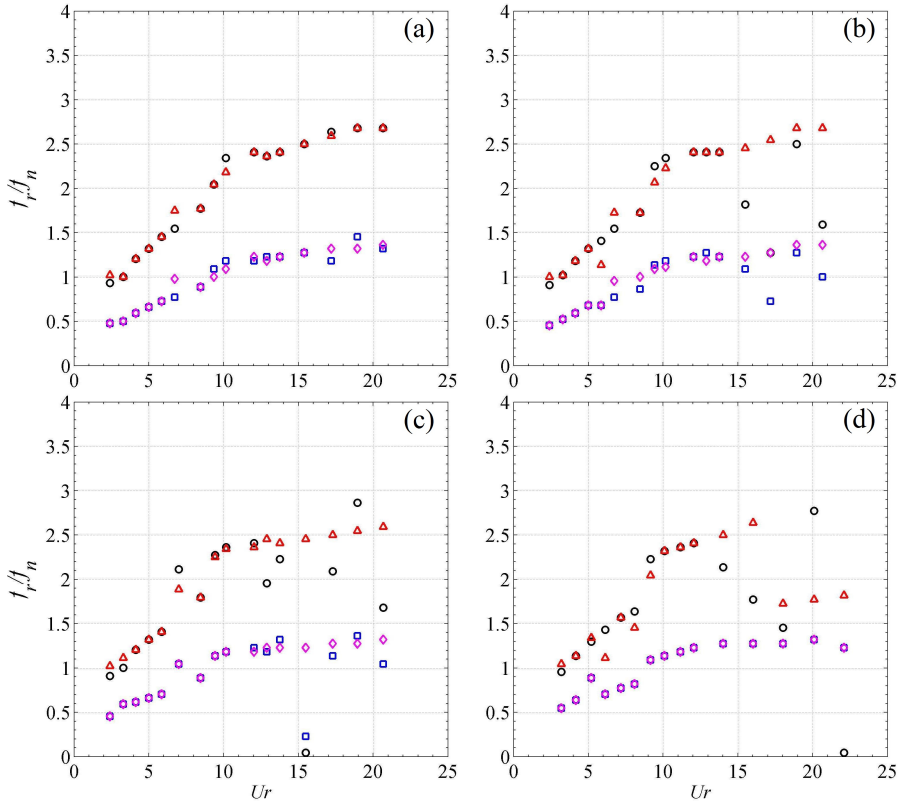

Figure 3.24: Comparison between VIV response frequency of leading (○) and trailing (△) cylinder in stream-wise direction and leading (□) and trailing (♢) cylinder in cross-flow direction at various spacings where $\frac{f_{n_1}}{f_{n_2}} = 0.8657$. L/D = (a)4, (b)5, (c)8, (d)12.

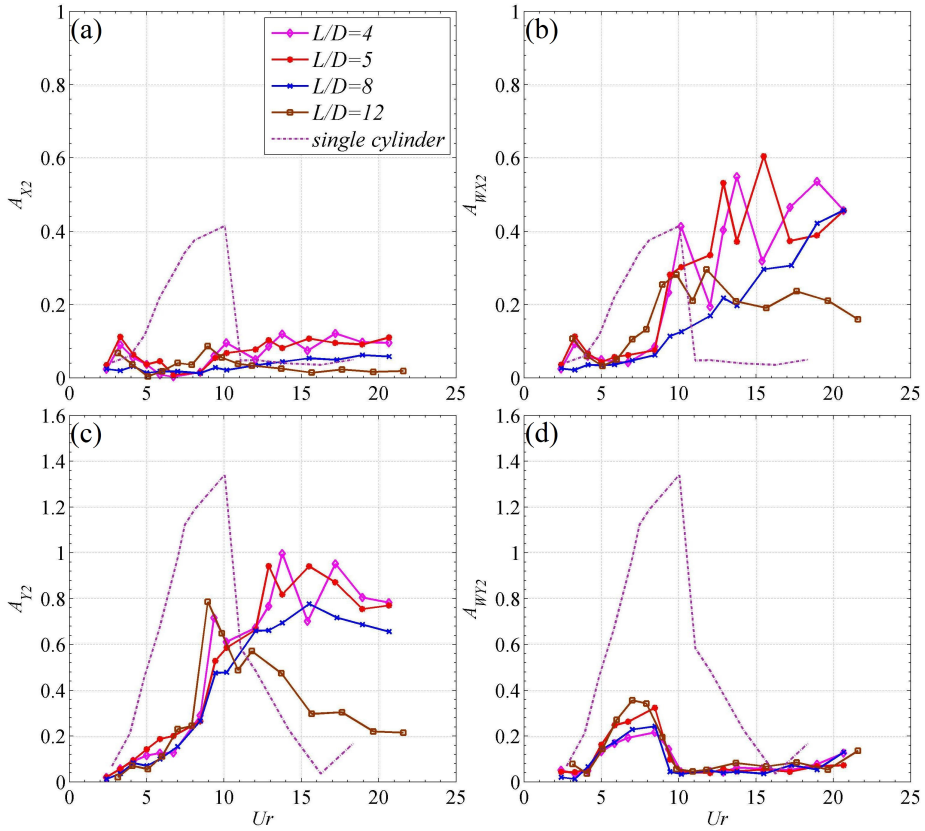

Figure 3.25: Response amplitude of downstream cylinder due to VIV and wake force. Stream-wise amplitude response due to (a) VIV, (b) wake force. Cross-flow response amplitude due to (c) VIV, (d) wake force where $\frac{f_{n_1}}{f_{n_2}} = 0.8657$

was observed in the first set-up. The spacing of $12D$ has a much smaller amplitude than that of $15D$ in the first set-up. On the other hand increase of amplitude that was observed at $20D$ in the first experiment can be seen here at $12D$.

Frequency spectrum has the similar multi-peak behaviour in stream-wise direction as that of first experiment. Therefore, it is possible to separate motions induced by VIV from those evoked by the upstream turbulant wake. It is possible to follow the same procedure, using FFT, as the first experiment. Figure 3.24 compares the response frequency of both cylinders in cross-flow and steam-wise directions. Spacing does not affect the shedding frequency, similar to previous test. Moreover, leading cylinder dictates the oscillation frequency of the trailing body similarly, however after lock-in range of the first cylinder no jump in frequency of the second cylinder, similar to the first experiment, can be observed.

Comparing the result obtained by inverse FFT from two different matrices containing

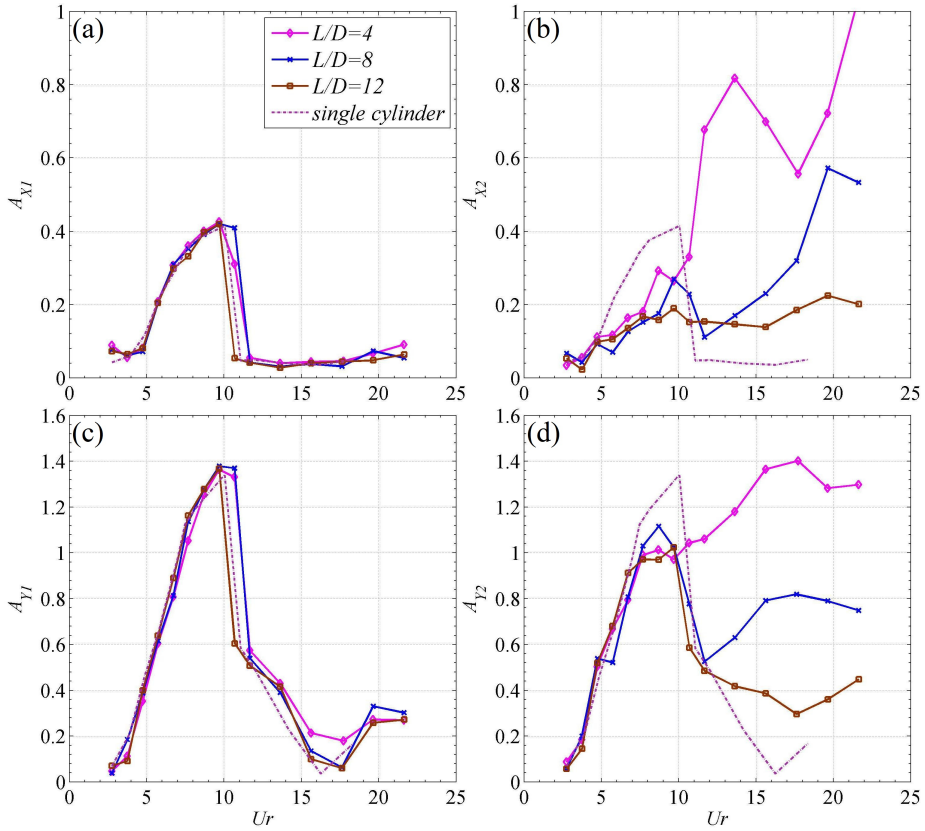

Figure 3.26: Amplitude response of all spacings in second experiment set-up against reduced velocity where $\frac{f_{n_1}}{f_{n_2}} = 1.1552$. (a)Leading cylinder's stream-wise response amplitude,(c)Leading cylinder's cross-flow response amplitude, (b)Trailing cylinder's stream-wise response amplitude, (d)Trailing cylinder's cross-flow response amplitude

high and low frequency components, confirms the observation on VIV and wake induced motions in the previous experiment. Figure 3.25 shows the contribution of two components. Trailing cylinder response in cross-flow direction is highly dependent on motions with higher frequency components which is due to VIV motion. However, the vortices of the leading cylinder cannot excite the trailing cylinder significantly in comparison with its effect on the cylinder in stream-wise direction. Low-frequency motion in stream-wise direction made up the main part of trailing cylinder motion. It starts exactly after the end of lock-in range for leading cylinder when the wake is not as well developed and strong as it was during lock-in.

Furthermore, to confirm if the leading cylinder can always dictate the motion frequency of the trailing structure, two cylinders switched places so that natural frequency ratio becomes $\frac{f_{n_1}}{f_{n_2}} = 1.1552$ then cylinders were tested at three aforementioned spacings

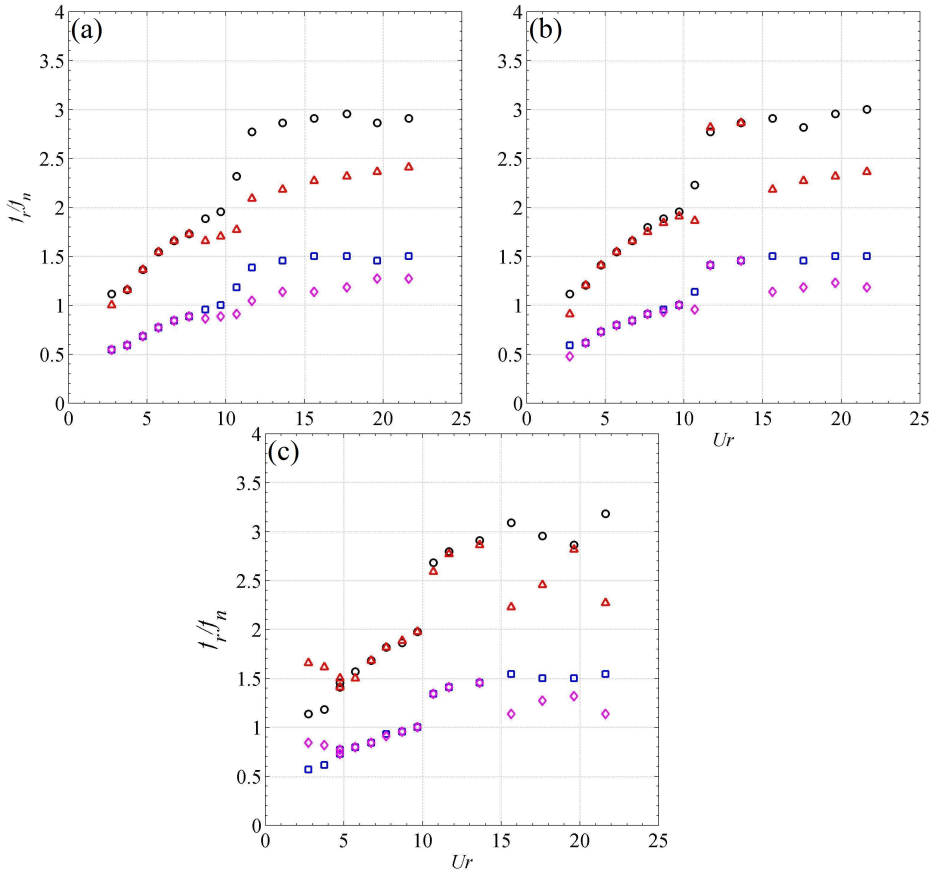

Figure 3.27: Comparison between VIV response frequency of leading (○) and trailing (△) cylinder in stream-wise direction and leading (□) and trailing (♢) cylinder in cross-flow direction at various spacings where $\frac{f_{n_1}}{f_{n_2}} = 1.1552$. $L/D =$ (a)4, (b)8, (c)12.

again. Figure 3.26 shows the response amplitudes of two cylinders at different spacings. It is evident that leading cylinder still vibrates independently from trailing structure. However, it is observed that leading cylinder has a weaker control over trailing body since it has a different natural frequency. The trailing cylinder response in either direction is larger during lock-in range of the leading cylinder and behaves more like a conventional VIV response. The dependence of training cylinder's peak response (cross-flow) on spacing in this range confirms that this similarity is due to weaker influence of the leading cylinder.

Nevertheless, this effect is terminated after lock-in range of the leading cylinder. Figure 3.27 is obtained by separating VIV frequency from low frequency component and demonstrates how response frequency of the trailing cylinder shifts to a lower value than that of the leading cylinder after its lock-in range. Furthermore, this shifts be-

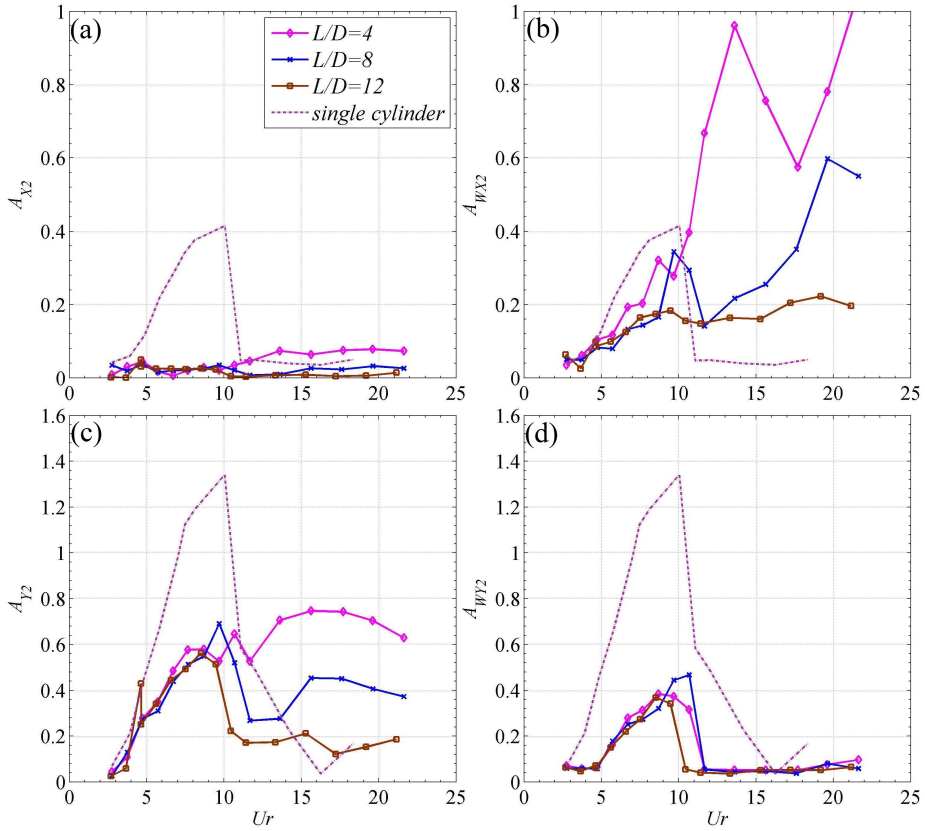

Figure 3.28: Response amplitude of downstream cylinder due to VIV and wake force. Stream-wise amplitude response due to (a) VIV, (b) wake force. Cross-flow response amplitude due to (c) VIV, (d) wake force, where $\frac{f_{n_1}}{f_{n_2}} = 1.1552$

comes smaller as the trailing cylinder moves downstream which can be observed by comparing figure 3.27 c and a.

Plotting amplitudes of motions induced by VIV and wake in figure 3.28 reveals that VIV of the trailing cylinder started in lower reduced velocities in comparison with two previous experiments. This early starts in VIV response plus motions elicited by upstream wake creates a peak in trailing cylinder response graph around $U_r = 8$. Other observations made in figure 3.22 and 3.25 are still valid for this experiment.

3.5.3 Two identical cylinder with 30% difference in Natural frequency

Further investigation on the interference of two tandem cylinders was done by extending the supporting rod even longer to $L_r = 2.8m$. To compensate for the extra weight of the rod cylinder's mass was reduced by $0.5kg$ so the whole system maintained its

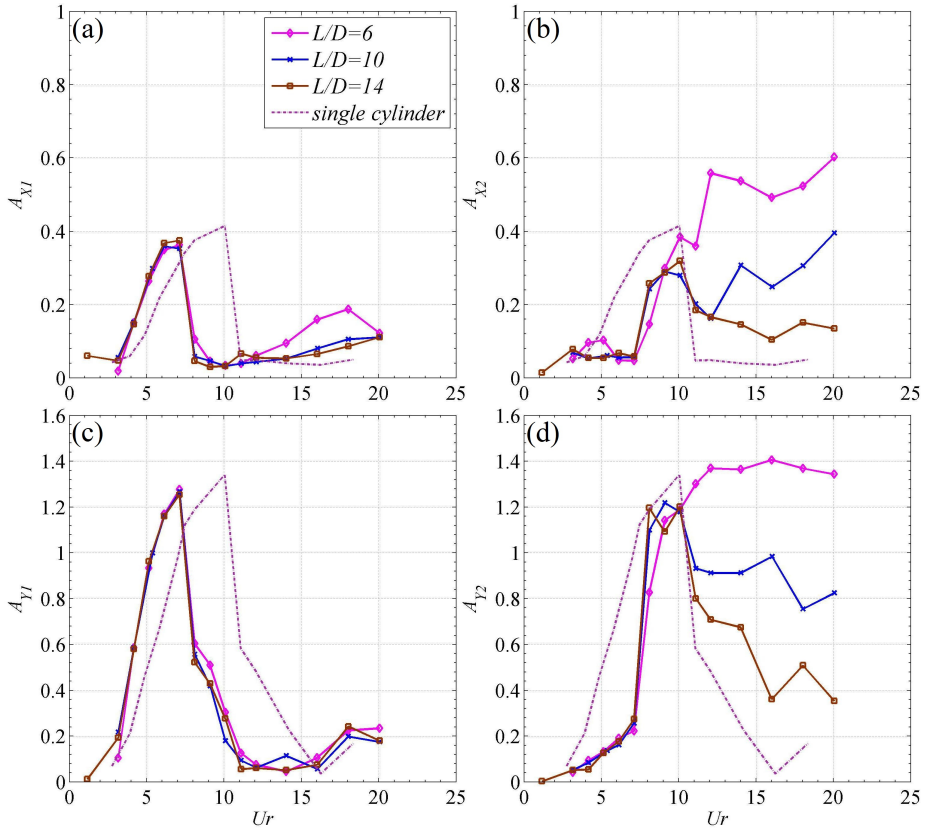

Figure 3.29: Amplitude response of all spacings in second experiment set-up against reduced velocity where $\frac{f_{n_1}}{f_{n_2}} = 0.7166$. (a)Leading cylinder's stream-wise response amplitude,(c)Leading cylinder's cross-flow response amplitude, (b)Trailing cylinder's stream-wise response amplitude, (d)Trailing cylinder's cross-flow response amplitude

mass ratio. The cylinder with longer supporting beam was used first as the leading cylinder then trailing, similar to the previous experiment, at spacings of $6D, 10D$ and $14D$. The initial spacing was chosen at $6D$ to take caution and avoid collision between two cylinders since, the supporting rod was longer and more flexible under the drag force.

Figure 3.29 shows the result of fifth experimental set-up where cylinder with the longer supporting rod was leading and $\frac{f_{n_1}}{f_{n_2}} = 0.7166$. It should be noted that first cylinder lock-in range occurs at a lower reduced velocity comparing to perivious experiments since the natural frequency is lower; it was not significantly clear in figure 3.23 due to the smaller difference between system natural frequency and reference frequency. The length of the lock-in range and value of the maximum amplitude is similar to that of a single cylinder. Furthermore, trailing cylinder amplitude at the small spacing of $6D$

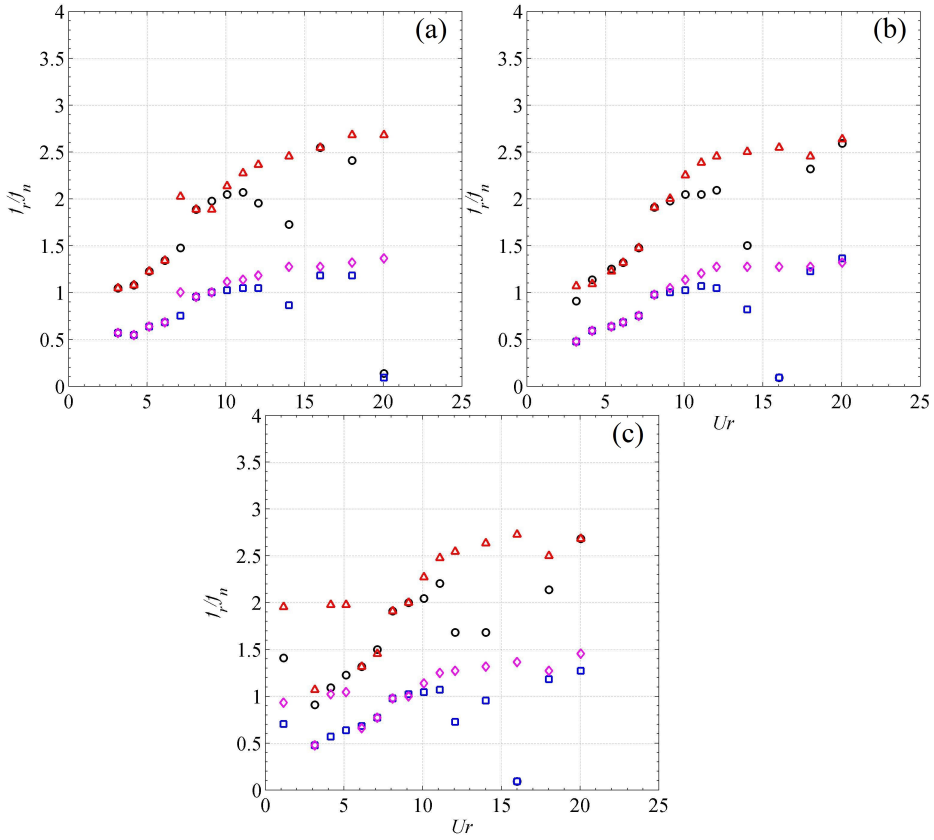

Figure 3.30: Comparison between response frequency of leading (○) and trailing (△) cylinder in stream-wise direction and leading (□) and trailing (♢) cylinder in cross-flow direction at various spacings where $\frac{f_{n_1}}{f_{n_2}} = 0.7166$. L/D = (a)6, (b)10, (c)14.

is similar to galloping behaviour that has been discussed before. However, response of the cylinder during supposed lock-in range of a single cylinder has a large amplitude in all three spacings and shows a small variation in regards to changes in spacing; this is a demonstration of relative independence from the leading cylinder which is due to a large difference in natural frequency. The boldest difference between cylinder response in the spacing of $14D$ and a single cylinder is a late lock-in onset that could be explained by shielding effect from leading cylinder. This dependence is so significant that stream-wise response at $14D$ resembles an isolated cylinder VIV motion where so far response of the trailing cylinder in this direction was always similar to galloping regardless of the gap between two cylinders.

Figure 3.30 shows VIV frequency of two cylinders in all three spacings. This figure is a confirmation of previous observations. It can be determined from the figure that the trailing cylinder follows the leading structure up to $U_r = 10$ when upstream lock-in ter-

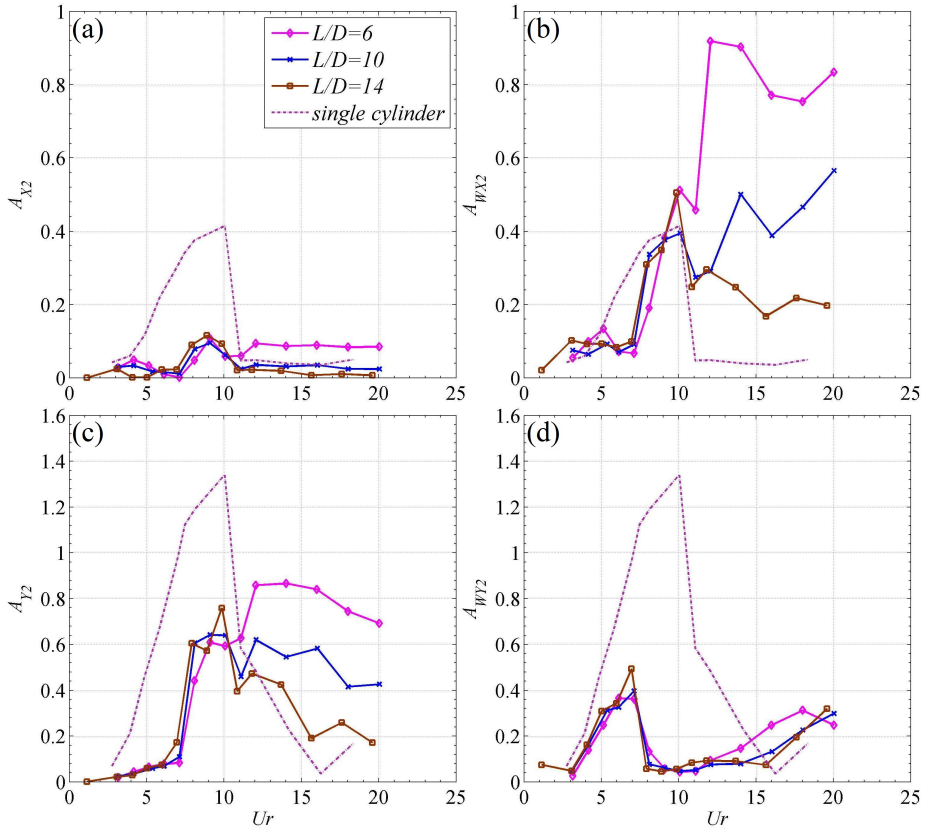

Figure 3.31: Amplitude response of downstream cylinder due to VIV and wake force. Stream-wise amplitude response due to (a) VIV, (b) wake force. Cross-flow amplitude response due to (c) VIV, (d) wake force where $\frac{f_{n_1}}{f_{n_2}} = 0.7166$

minates and then trailing cylinder continues its response at higher frequencies, similar to observations from the second experiment.

Additionally, data obtained from inverse FFT of this experiment shows how the difference between natural frequencies of two structures could not eliminate the interference of leading cylinder with trailing cylinder response. Figure 3.31 shows this data against corresponding reduced velocity. Cross-flow response of the cylinder in this figure shows that although trailing body undergoes VIV in higher U_r, excitation of leading cylinder induces some vibrations with relatively small amplitude in the trailing structure.

Two cylinders switched places for the last set of experiments so that the cylinder with the longer rod became the trailing body and the experiment was carried out in the same three spacings. Figure 3.32 shows the response amplitude of cylinders at these spacings. Similar to previous tests leading cylinder acts alike an isolated one and spacing variation has no significant effect on its response. On the other hand, the response

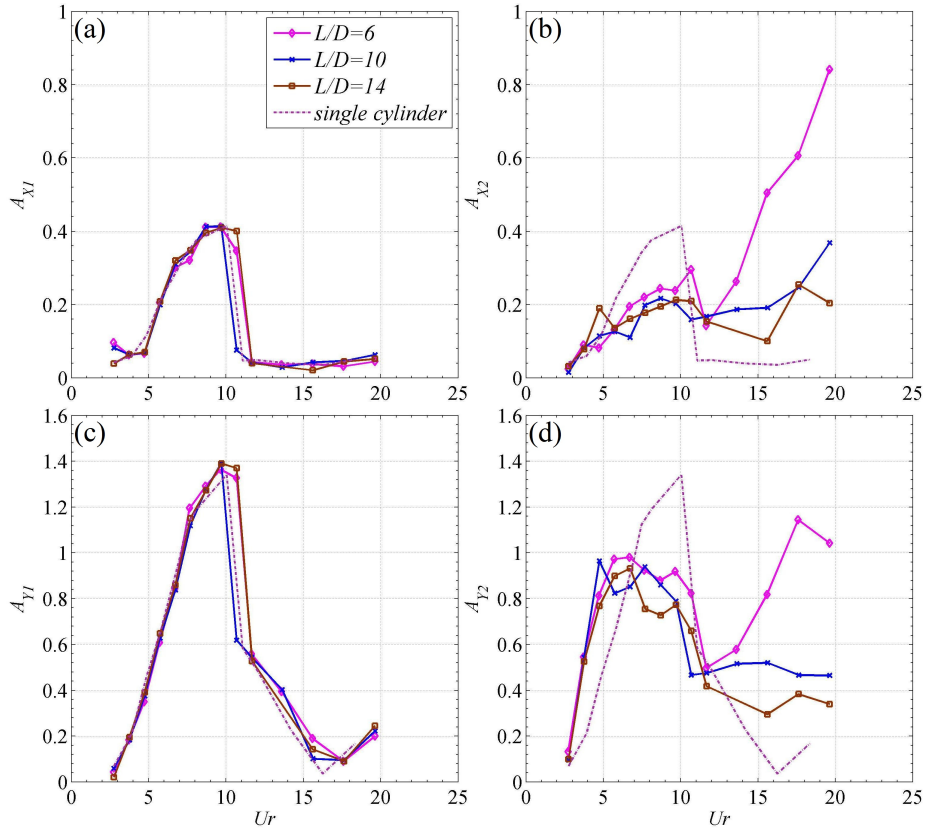

Figure 3.32: Response amplitude of all spacings in second experiment set-up against reduced velocity where $\frac{f_{n_1}}{f_{n_2}} = 1.39556$. (a)Leading cylinder's stream-wise response amplitude,(c)Leading cylinder's cross-flow response amplitude, (b)Trailing cylinder's stream-wise response amplitude, (d)Trailing cylinder's cross-flow response amplitude

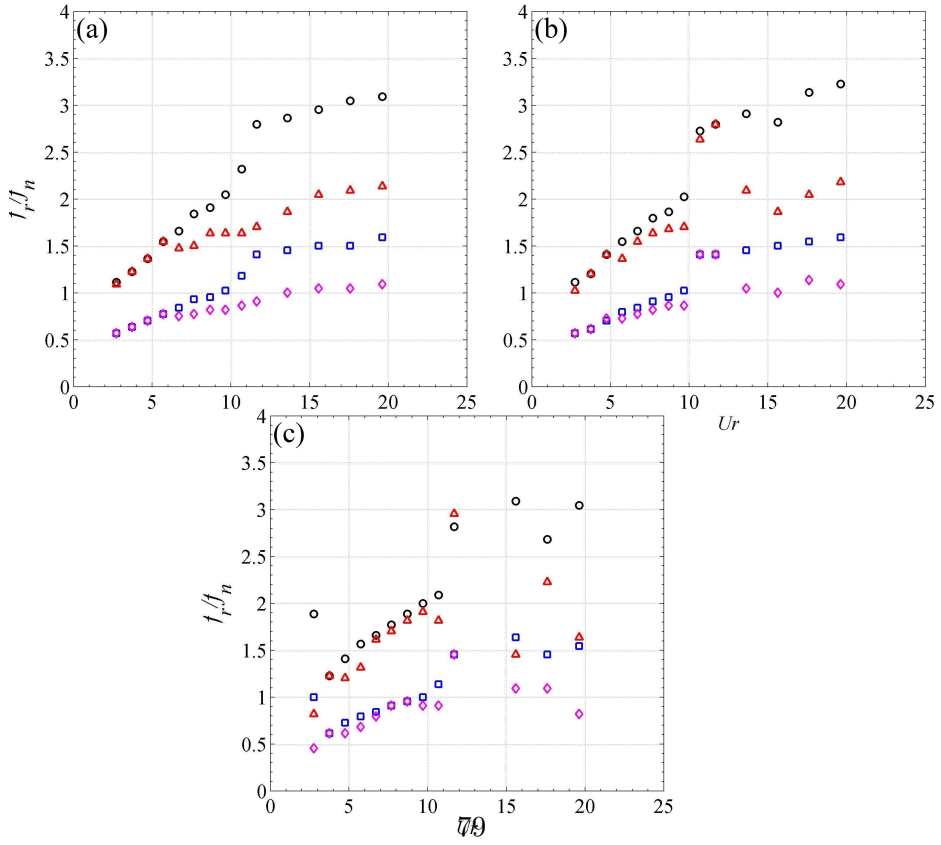

Figure 3.33: Comparison between VIV response frequency of leading (○) and trailing (△) cylinder in stream-wise direction and leading (□) and trailing (♢) cylinder in cross-flow direction at various spacings where $\frac{f_{n_1}}{f_{n_2}} = 1.3955$. $L/D =$ (a)6, (b)10, (c)14.

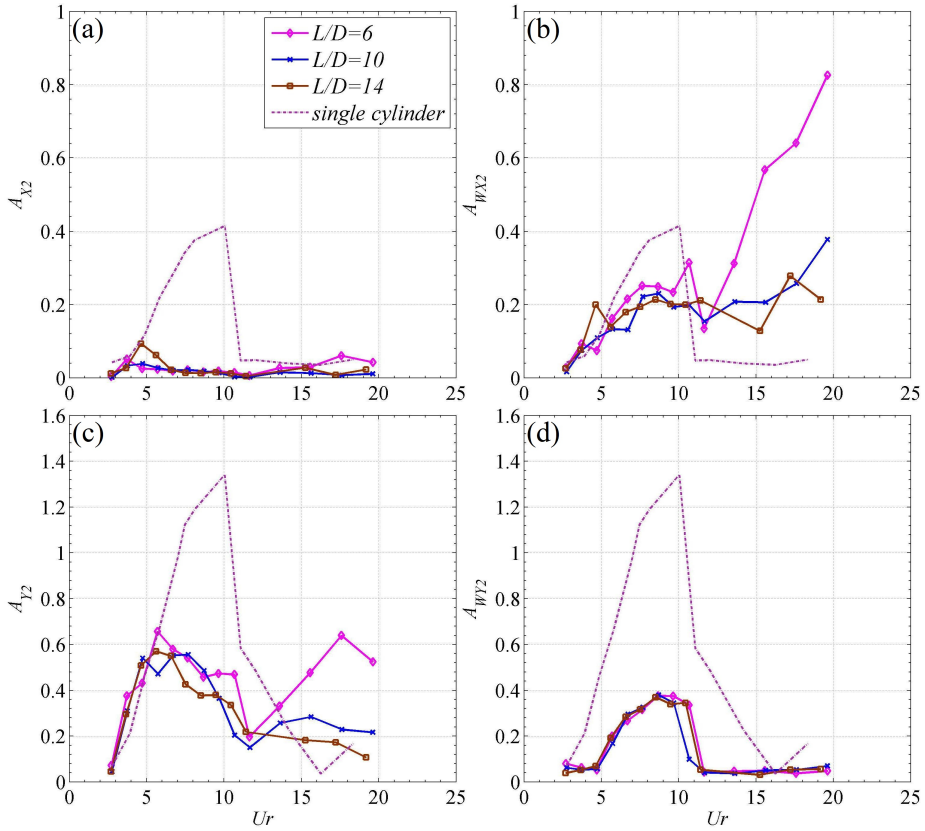

Figure 3.34: Response amplitude of downstream cylinder due to VIV and wake force. Stream-wise response amplitude due to (a) VIV and (b) wake force. Cross-flow amplitude response due to (c) VIV and (d) wake force where $\frac{f_{n_1}}{f_{n_2}} = 1.3955$

of trailing cylinder is very interesting since it is the most similar to an isolated cylinder among all tests conducted in this study. Furthermore, it should be noted that although trailing cylinder natural frequency is lower and consequently its lock-in range should start at a lower reduced velocity than the single cylinder, due to shielding effect of the leading cylinder, its onset somehow is coinciding with that of the leading cylinder. This coincidence was clearer in experiment four. Trailing cylinder response at the moderate spacing of $10D$ does not resemble galloping in comparison to previous set-up or any other moderate spacing tested in this study.

Figure 3.33 includes oscillation frequency of both cylinders in different spacings. Response frequency of this experiment is very similar to figure 3.28. However, it is notable that shift in response amplitude of the trailing cylinder occurs earlier in comparison with previous tests due to the bigger difference between their natural frequency. Nevertheless, frequency response of two structures becomes more similar as gap between

them grow larger alike to what has been observed previously.
A comparison between trailing cylinder's motions induced by VIV and upstream wake is provided in figure 3.34. It is evident that the main part of the cross-flow motion is made up by VIV induced motion. Nonetheless, wake-induced motion is major response of the trailing cylinder in stream-wise direction.

3.6 Conclusion

In order to assess the effect of spacing on the interference of two bluff structures in tandem arrangement, two identical cylinders were placed in-line with a gap between them equal to $20D$, from the centre of one cylinder to the other and towed at different velocities. Then, the distance was reduced to $15D, 10D, 8D, 5D, 4D, 3.5D$ and $3D$ in sequence and the test was repeated at the same velocities.

- It was concluded from this experiment that as the spacing increases the effect of leading cylinder decreases and the response amplitude of trailing cylinders reduces along with it. This reduction was consistent up to the largest spacing when amplitudes of trailing cylinder started to rise.

- It is evident that trailing cylinder behaves more independently as it moves further from leading structure. Such a change in the behaviour of the cylinder suggests that there are two mechanisms of excitation. One is VIV of the trailing cylinder itself which is controlled by flow velocity in the gap (which is smaller than free stream due to shielding effect of the leading cylinder). Two is buffeting vortices generated by leading cylinder and washed downstream towards trailing cylinder.

- In an attempt to separate motions induced by two mechanisms, frequency components associated with two mechanisms were separated employing FFT and dividing each time history into two matrices, one representing VIV response and the other containing the rest of frequency components.

- By comparing the motion obtained from these two matrices, it was revealed that response in cross-flow direction is mainly induced by vortices detached from the

cylinder itself. On the other hand, buffeting vortices from leading cylinder were the main cause of the cylinder stream-wise response.

- Comparing frequency of VIV response at various spacing confirms that the gap between two cylinders has no influence on the VIV motion of the cylinder. Moreover, frequency response of the trailing cylinder is dictated by leading structure up to the reduced velocity that marks the end of leading cylinder's lock-in range, after this velocity trailing cylinder oscillates with a lower frequency which is due to lower flow velocity in the gap.

- A series of experiments were conducted in order to observe the effect of system natural frequency on the trailing cylinder response. In these experiments, two cylinders were kept identical while their natural frequencies were altered by changing the length of their supporting rod. It was observed that two mechanisms of excitation are still valid. Additionally, the frequency of VIV response does not depend on the spacings.

- It can be concluded from these experiments that in real practice structures with higher natural frequency are better to be placed in front so that after lock-in range trailing cylinder can oscillate at a higher frequencies with minimum possibility of coinciding with upstream vortices. It is due to the fact that both cylinders could enter lock-in range simultaneously and exit it at the same time in this arrangement. It means smaller lock-in range for the trailing structure so that it could be more independent from the leading cylinder. If structure with a lower frequency was to be placed in front, during and after lock-in range its response frequency stays fairly constant due to upstream vortices and if velocity in the gap increases, response frequency of trailing cylinder could gradually increase and coincide with upstream response frequency which means wider natural frequency.

- With a comparison between these experiments and experiment with two identical cylinders it can be concluded that due to difference in natural frequency between two cylinders, trailing cylinder does not become excited enough by coming vortices to go through a lock-in phase. Thus, multi-peaks feature that were observable in

response graph of the trailing cylinder in the first experiment did not reoccur in the rest of experiments.

Chapter 4

Mathematical Modelling

4.1 Objective & Methodology

An attempt was made during this study to offer a mathematical model to simulate the structural response of two tandem cylinders. The methodology to achieve this objective was to assume that each cylinder could be simulated by a simple mass and spring system similar to figure 4.1.

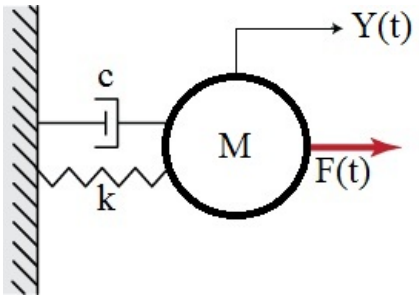

Figure 4.1: Model of an oscillating cylinder as a simple mass, spring and damping system

Here, c is equivalent of viscose damping and fluid added damping ($c = c_s + c_a$) where c_a can be calculated using equation 4.1 where where ω_s is vortex shedding frequency and γ is stall parameter and is a function of mean drag coefficient [1].

$$c_a = \gamma \omega_s \rho D^2 \tag{4.1}$$

Mass (M) is a combination of structural mass (m) and fluid added mass (m_a) which can be calculated from following expression.

$$m_a = \frac{\pi C_a \rho D^2}{4} \tag{4.2}$$

As mention earlier the mass ratio is defined by structural mass (Equation 3.2), however, in some literatures dealing with modelling it is defined with wet mass of the cylinder as in equation 4.3 [63].

$$\mu = \frac{m + m_a}{\rho D^2} \tag{4.3}$$

Additionally, k is the structural stiffness. If the stream direction is assumed to be from top down, fluid's lift force is shown by $F(t)$ which induces $Y(t)$ cylinder motion response. According to such a system, structural response can be model by an equation of motion (equation 4.4). Doted parameters in this equation and through out this chapter represent derivatives with respect to time. Lift (wake) force exerted on the structure is proportional to flow velocity and oscillating lift coefficient of the cylinder and can be obtained from Equation 4.5.

$$M\ddot{Y} + c\dot{Y} + kY = F_Y(t) \tag{4.4}$$

$$F_Y = \frac{1}{2}\rho U^2 D C_L \tag{4.5}$$

Simulation of fluid interaction with structure has been discussed in the literature extensively [26, 27, 64]. It has been remarked in these studies that VIV response is a self-exciting and self-limiting phenomenon, hence two equations have been suggested to simulate oscillating lift coefficient (C_L) of the cylinder, van der Pal (Eq.4.6) and Rayleigh (Eq.4.7) wake oscillators which have such a feature.

$$\ddot{q} + \epsilon\omega_s(q^2 - 1)\dot{q} + \omega_s^2 q = T \tag{4.6}$$

$$\ddot{C_L} - \alpha\omega_s\dot{C_L} + \frac{\lambda}{\omega_s}\dot{C_L}^3 + \omega_s^2 C_L = T \tag{4.7}$$

It should be noted that ω_s is vortex shedding frequency and q is *reduced vortex lift coefficient* which is twice as oscillating lift coefficient over the amplitude of lift coefficient of a stationary cylinder (C_{L_0}). The reference value of C_{L_0} can be considered 0.3 for wide range of Re based on Blevins [1] and Pantazopoulos [65] studies. It is also referred to these equations as empirical models due to two observational coefficients in each equation. α and ϵ are both empirical coefficients that should be determined case by case and tuned against experimental results. Although, some work has been done to determine these variables as a function of mass or/and damping. λ is also related to α in equation 4.7 and it can be obtain from expression 4.8 [66].

$$\lambda = \frac{4\alpha}{3{C_{L_0}}^2} \tag{4.8}$$

In order to couple two equations of motion and wake oscillators, the right hand side of wake oscillators (T) can be defined in such a manner that serve as coupling terms. Facchinetti et al. [27] has done an extensive study on dynamic coupling terms which could be a function of cylinder acceleration, speed or displacement. In this study two coupling terms of acceleration and speed were chosen for van der Pol and Rayleigh respectively in order to be compared together and more accurate coupling term could be identified to simulate the trailing cylinder response as it was observed in section 3.5. Since leading cylinder response observed in previous chapter was similar to that of a single cylinder, therefore, the system of equations to be solved for the leading cylinder would be Eq. 4.9 for van der Pol and 4.10 for Rayleigh wake oscillators.

$$\begin{cases} M\ddot{Y} + (2\xi M\omega_n + \gamma\omega_s\rho D^2)\dot{Y} + kY = \dfrac{1}{4}\rho U^2 D C_{L_0} q \\ \ddot{q} + \epsilon\omega_s(q^2-1)\dot{q} + \omega_s^2 q = b\ddot{Y} \end{cases} \tag{4.9}$$

$$\begin{cases} M\ddot{Y} + (2\xi M\omega_n + \gamma\omega_s\rho D^2)\dot{Y} + kY = \dfrac{1}{2}\rho U^2 D C_L \\ \ddot{C_L} - \alpha\omega_s\dot{C_L} + \dfrac{4}{3}\dfrac{\lambda}{\omega_s C_{L_0}^2}{\dot{C_L}}^3 + \omega_s^2 C_L = b'\dot{Y} \end{cases} \tag{4.10}$$

Here, ξ is reduced structural damping which is defined, $\xi = \frac{c_s}{2M\omega_s}$. Moreover, γ is fluid added damping coefficient which is a function of mean drag coefficient and can be assumed equal to 0.8 in sub-critical region ($300 < Re < 1.5 \times 10^5$) for sake of simplicity[27]. Same principle could be applied to extend these model to simulate stream-wise motion.

4.1.1 Non-dimensional van der Pol equation

In order to apply these models to any set-up regardless of size and dimensions of the structures, it is necessary for equations 4.9 and 4.10 to be in dimensionless form. This is possible by introducing dimensionless time and space coordinate respectively, $\tau = \omega_n t$ and $y = \frac{Y}{D}$. By replacing these dimensionless variables into equation 4.9, it becomes:

$$\begin{cases} MD\omega_n^2\ddot{y} + (2\xi M\omega_n + \gamma\omega_s\rho D^2)D\omega_n\dot{y} + Dky = \frac{1}{4}\rho U^2 DC_{L_0}q \\ \\ \omega_n^2\ddot{q} + \epsilon\omega_s(q^2-1)\omega_n\dot{q} + \omega_s^2 q = bD\omega_n^2\ddot{y} \end{cases} \tag{4.11}$$

Equation of motion can be rearranged through dividing it by $MD\omega_n^2$. Additionally, van der Pol equation can be rearranged by ω_n^2.

$$\begin{cases} \ddot{y} + (2\xi + \frac{\gamma\omega_0\rho D^2}{M})\dot{y} + y = \frac{1}{4}\frac{\rho U^2 C_{L_0}q}{M\omega_n^2} \\ \\ \ddot{q} + \epsilon\omega_0(q^2-1)\dot{q} + \omega_0^2 q = bD\ddot{y} \end{cases} \tag{4.12}$$

implementing equation 4.2 into 4.12 would yield

$$\begin{cases} \ddot{y} + (2\xi + \frac{\gamma}{\mu}\omega_0)\dot{y} + y = \frac{1}{16}\frac{\omega_0^2 C_{L_0}}{\pi^2 St^2\mu}q \\ \\ \ddot{q} + \epsilon\omega_0(q^2-1)\dot{q} + \omega_0^2 q = bD\ddot{y} \end{cases} \tag{4.13}$$

Strouhal number (St) which is a dimensionless number and a function of shedding frequency and free stream velocity, and is defined:

$$St = \frac{f_s D}{U} \tag{4.14}$$

Strouhal number is also a function of Re and roughness and is assumed 0.2 for sub-critical range of Re [1, 65].

Further simplification and assuming $a_L = \frac{1}{16}\frac{\omega_0^2 C_{L_0}}{\pi^2 St^2 \mu}$ and $A = bD$ van der Pol wake oscillator equation becomes:

$$\begin{cases} \ddot{y} + (2\xi + \frac{\gamma}{\mu}\omega_0)\dot{y} + y = a_L q \\ \\ \ddot{q} + \epsilon\omega_0(q^2 - 1)\dot{q} + \omega_0^2 q = A\ddot{y} \end{cases} \tag{4.15}$$

Herein, A is another empirical coefficient that should be determined by tuning the model against appropriate experimental data.

This procedure can be repeated for stream-wise motion equation (equation 4.16).

$$\begin{cases} \ddot{x} + (2\xi + \frac{2\gamma}{\mu}\omega_0)\dot{x} + x = a_D p \\ \\ \ddot{p} + 2\epsilon\omega_0(p^2 - 1)\dot{p} + 4\omega_0^2 p = A\ddot{x} \end{cases} \tag{4.16}$$

It should be noted that as it was observed during chapter 3 and by Bearman [62], stream-wise shedding frequency is twice of that in cross-flow therefore shedding frequency in equation 4.16 should be considered $2\omega_s$. Furthermore, p is *reduced vortex drag coefficient* and similar to reduced vortex lift coefficient is $p = 2\frac{C_D}{C_{D_0}}$. Through out this study it is assumed that $C_{D_0} = 0.2$ [67].

4.1.2 Non-dimensional Rayleigh equation

Similar approach can be adopted for Rayleigh wake oscillator by introducing dimensionless time and coordinate into equation 4.10.

$$\begin{cases} \ddot{y} + (2\xi + \frac{\gamma}{\mu}\omega_0)\dot{y} + y = \frac{1}{8}\frac{\omega_0^2}{\pi^2 St^2 \mu} C_L \\ \\ \omega_n^2 \ddot{C_L} - \alpha\omega_n\omega_s\dot{C_L} + \frac{\lambda\omega_n^3}{\omega_s}\dot{C_L}^3 + \omega_s^2 C_L = \omega_n D b'\dot{y} \end{cases} \tag{4.17}$$

After rearrangement of this equation similarly to Eq.4.11 it becomes:

$$\begin{cases} \ddot{y} + (2\xi + \frac{\gamma}{\mu}\omega_0)\dot{y} + y = a'_L C_L \\ \ddot{C_L} - \alpha\omega_0 \dot{C_L} + \frac{\lambda}{\omega_0}\dot{C_L}^3 + \omega_0^2 C_L = A'\dot{y} \end{cases} \tag{4.18}$$

Herein, $a' = \frac{1}{8}\frac{\omega_0^2}{\pi^2 St^2 \mu}$, A', α and λ are empirical coefficients that are determined through tuning against experimental data.

Additionally, this model can be extended to stream-wise direction by adapting the same approach as equation 4.16 and it reads:

$$\begin{cases} \ddot{x} + (2\xi + \frac{2\gamma}{\mu}\omega_0)\dot{x} + x = a'_D C_D \\ \ddot{C_D} - 2\alpha\omega_0 \dot{C_D} + \frac{\lambda}{2\omega_0}\dot{C_D}^3 + 4\omega_0^2 C_D = A'\dot{x} \end{cases} \tag{4.19}$$

4.1.3 A wake oscillator to describe trailing cylinder

Modelling two cylinders in tandem requires to place another system similar to figure 4.1 in the wake of the first cylinder. Two mechanisms of excitation were observed as contributions to trailing cylinder response in previous chapter (3.5). Oscillation induced by VIV of the trailing cylinder could be model with one of the wake oscillators discussed earlier. Additionally, modifying this model to capture the effect of buffeting upstream vortices on the trailing cylinder is possible through adding a force term to right hand side of the structural motion equation (4.4).

$$M_2\ddot{Y_2} + c_2\dot{Y_2} + k_2 Y_2 = F_{Y_2}(t) + F_{Y_1}(t) \tag{4.20}$$

Shiau and T. Y. Yang [53] suggested that it is possible to assume that vortices conduct the same energy to the trailing cylinder as they do to the leading cylinder before their detachment from it. Therefore, they replaced F_{Y_1} with wake force obtained from equation 4.18 with a time delay to account for the travelling time $(t + t_1)$required by upstream vortices to reach the trailing cylinder. This time delay as suggested by Shiau [66] is a function of spacing between two cylinders (L), spacing between vortices $(\frac{d}{D}$,

which can be assumed fixed at 4.5 for cylinder undergoing lock-in) and shedding frequency and can be calculated from equation 4.21.

$$t_1 = \frac{L}{f_s d} \tag{4.21}$$

Implementing this notion in dimensionless form ($\tau_1 = \frac{2\pi}{\omega_0}\frac{L}{D}\frac{D}{d}$) into equations 4.15 and 4.18 yields mathematical models to describe response of the trailing cylinder. It should be noted that from here on $C_{L_1} = C_L$ and $q_1 = q$.

$$\begin{cases} \ddot{y}_2 + (2\xi_2 + \frac{\gamma_2}{\mu_2}\omega_0)\dot{y}_2 + y_2 = a_{L_2}\Big(q_2 + q_1(\tau_1)\Big) \\ \\ \ddot{q}_2 + \epsilon\omega_0(q_2^2 - 1)\dot{q}_2 + \omega_0^2 q_2 = A\ddot{y}_2 \end{cases} \tag{4.22}$$

$$\begin{cases} \ddot{y}_2 + (2\xi_2 + \frac{\gamma_2}{\mu_2}\omega_0)\dot{y}_2 + y_2 = a'_{L_2}\Big(C_{L_2} + C_{L_1}(\tau_1)\Big) \\ \\ \ddot{C}_{L_2} - \alpha\omega_0\dot{C}_{L_2} + \frac{\lambda_2}{\omega_0}\dot{C}_{L_2}^3 + \omega_0^2 C_{L_2} = A'\dot{y}_2 \end{cases} \tag{4.23}$$

Solving any pairs of equations 4.15 and 4.22 or 4.18 and 4.23 could provide a simulation of the system compromised of two flexibly mounted identical cylinders in tandem.

4.2 Initial Solution

Solution for systems of non-linear differential equations discussed in section 4.1 is possible by making some assumptions about response functions. Since response of a cylinder undergoing VIV is sinusoidal, it is valid to assume that the response function has amplitude of y and frequency of ω [62]. Equation 4.24 is the solution function to describe response of the leading cylinder in cross-flow.

$$y_1 = \boldsymbol{y}_1 e^{i\omega_1 t} \tag{4.24}$$

4.2.1 Solution to 1DOF van der Pol (VDP)

The force inducing a sinusoidal motion should be of the same nature with similar frequency, which its exact value can be calculated by an additional phase difference to the motion frequency. Therefore, four van der Pol unknowns in cross-flow direction would have solutions as described in equation 4.25.

$$\begin{cases} y_1 = \boldsymbol{y}_1 e^{i\omega_1 t} \\ q_1 = \boldsymbol{q}_1 e^{i(\omega_1 t+\phi_1)} \\ y_2 = \boldsymbol{y}_2 e^{i(\omega_1 t+\theta)} \\ q_2 = \boldsymbol{q}_2 e^{i(\omega_1 t+\phi_2)} \end{cases} \tag{4.25}$$

It should be emphasised that as observed in chapter 3 leading cylinder dictates the oscillation response of both cylinders for majority of reduced velocities tested, additionally OKAJIMA [56] and Tsutsui [68] observed in their experiments on two fixed cylinders in tandem arrangement that both cylinders have identical Strouhal number hence it is a valid assumption for these solutions that both cylinders are oscillating with similar frequency. ϕ_1 and ϕ_2 are phase difference between leading cylinder motion and wake force of leading and trailing cylinders respectively in equation 4.25. Moreover, here θ_2 is phase difference between leading and trailing cylinders motion.
Replacing equation 4.25 into van der Pol model for both cylinders would yield:

$$\begin{cases} -\omega^2 y_1 e^{i\omega t} + i(2\xi_1 + \dfrac{\gamma_1}{\mu_1}\omega_0)\omega y_1 e^{i\omega t} + y_1 e^{i\omega t} = a_{L_1} q_1 e^{i(\omega t+\phi_1)} \\ -\omega^2 y_2 e^{i\omega t} + i(2\xi_2 + \dfrac{\gamma_2}{\mu_2}\omega_0)\omega y_2 e^{i(\omega t+\theta)} + y_2 e^{i(\omega t+\theta)} = a_{L_2}\left(q_2 e^{i(\omega t+\phi_2)} + q_1 e^{i\omega(t+t_1)}\right) \\ -\omega^2 q_1 e^{i(\omega t+\phi_1)} + i\varepsilon\omega_0(q_1^2-1)\omega q_1 e^{i(\omega t+\phi_1)} + q_1 e^{i(\omega t+\phi_1)} = -\omega^2 A y_1 e^{i\omega t} \\ -\omega^2 q_2 e^{i(\omega t+\phi_2)} + i\varepsilon\omega_0(q_2^2-1)\omega q_2 e^{i(\omega t+\phi_2)} + q_2 e^{i(\omega t+\phi_2)} = -\omega^2 A y_2 e^{i\omega t} \end{cases} \tag{4.26}$$

Since the trailing cylinder has a direct input from the leading wake oscillator equation, thus the solution should be started from two equations describing leading cylinder. Following equations can be obtained by separating imaginary and real terms of equations

in lines 1 and 3 of expression 4.26:

$$\begin{cases} 1-\omega^2 = a_L \dfrac{q_1}{y_1}\cos\phi_1 \\ (2\xi_1 + \dfrac{\gamma_1}{\mu_1}\omega_0)\omega = a_L \dfrac{q_1}{y_1}\sin\phi_1 \\ (\omega^2-\omega_0^2) = A\omega^2 \dfrac{y_1}{q_1}\cos\phi_1 \\ \epsilon\omega_0(q_1^2-1) = A\omega^2\dfrac{y_1}{q_1}\sin\phi_1 \end{cases} \tag{4.27}$$

There are 4 unknowns in this system of equations that should be determined. ω is the first to be determined which can be calculated from power of six polynomial equation (Equation 4.28)

$$\omega^6 + \left(\left(2\xi_1 + \frac{\gamma_1}{\mu_1}\omega_0\right)^2 - \omega_0^2 + Aa_L - 2\right)\omega^4 + \left(\left(2-(2\xi_1+\frac{\gamma_1}{\mu_1}\omega_0)^2\right)\omega_0^2 - Aa_L + 1\right)\omega^2 - \omega_0^2 = 0 \tag{4.28}$$

Here, ω_0 can be obtain from reduced velocity through expression 4.29

$$\omega_0 = StU_r \tag{4.29}$$

Now that response frequency has been calculated it is possible to obtain wake force (q_1) from following expression.

$$q_1 = \sqrt{\frac{4\left(2\xi_1 + \dfrac{\gamma_1}{\mu_1}\omega_0\right)(\omega^2-\omega_0^2)\omega}{(1-\omega^2)\epsilon\omega_0} + 4} \tag{4.30}$$

The phase difference of ϕ_1 can be calculated from combination of the first two equations of 4.27.

$$\phi_1 = \arctan\left(\frac{2\omega\xi_1}{1-\omega^2}\right) \tag{4.31}$$

Amplitude of oscillation can be obtained from any equations from 4.27.

The system of equations for trailing cylinder can be solved now with the same approach by separating imaginary and real parts from each other, assuming two cylinders oscillate

at similar frequencies.

$$\begin{cases} (1-\omega^2)y_2\cos\theta - \big(2\xi_1 + \dfrac{\gamma_1}{\mu_1}\omega_0\big)\omega y_2\sin\theta = a_L\big(q_2\cos\phi_2 + q_1\cos\omega t_1\big) \\ (1-\omega^2)y_2\sin\theta + \big(2\xi_1 + \dfrac{\gamma_1}{\mu_1}\omega_0\big)\omega y_2\cos\theta = a_L\big(q_2\sin\phi_2 + q_1\sin\omega t_1\big) \\ (\omega_0^2-\omega^2)q_2\cos\phi_2 - \epsilon\omega_0\omega(q_2^2-1)q_2\sin\phi_2 = Ay_2\omega^2\cos\theta \\ (\omega_0^2-\omega^2)q_2\sin\phi_2 + \epsilon\omega_0\omega(q_2^2-1)q_2\cos\phi_2 = Ay_2\omega^2\sin\theta \end{cases} \tag{4.32}$$

It is necessary to follow the same order as for the leading cylinder solution procedure to obtain unknowns in this system of equations. Since frequency can be obtained from equation 4.28 hence wake force is the first unknown to be obtained. Solving this system for q_2 gives a power of twelve polynomial equation which only produces one acceptable answer. Then it is possible to obtain phase difference. ϕ_2 which is the phase difference between downstream wake force and motion response of the leading cylinder can be calculated at this stage.

θ is the phase difference between motion of leading cylinder and its trailing counterpart and can be defined:

$$\tan\theta = \frac{\left(\omega_0^2-\omega^2\right)q_2\sin\phi_2 + \epsilon\omega\omega_0\left(q_2^2-1\right)q_2\cos\phi_2}{\left(\omega_0^2-\omega^2\right)q_2\cos\phi_2 - \epsilon\omega\omega_0\left(q_2^2-1\right)q_2\sin\phi_2} \tag{4.33}$$

At this stage it is possible to calculate the amplitude of trailing cylinder (y_2).

$$y_2 = \frac{\sqrt{\Big(\left(\omega_0^2-\omega^2\right)q_2\cos\phi_2 - \epsilon\omega\omega_0\left(q_2^2-1\right)q_2\sin\phi_2\Big)^2 + \Big(\left(\omega_0^2-\omega^2\right)q_2\sin\phi_2 + \epsilon\omega\omega_0\left(q_2^2-1\right)q_2\cos\phi_2\Big)^2}}{A\omega^2} \tag{4.34}$$

All unknowns in the system 4.26 have been solved now. If two empirical coefficient of A and ϵ are assumed to be 12 and 0.03, based on tuning done against the results from chapter 3, figure 4.2 can be produced for a cylinder with similar structural properties. It can be observed that model under-predicts for leading cylinder, while it produces better results for the trailing cylinder simulation. The source of this rather large gap between results produced by model and obtained from experiment is the fact that this model

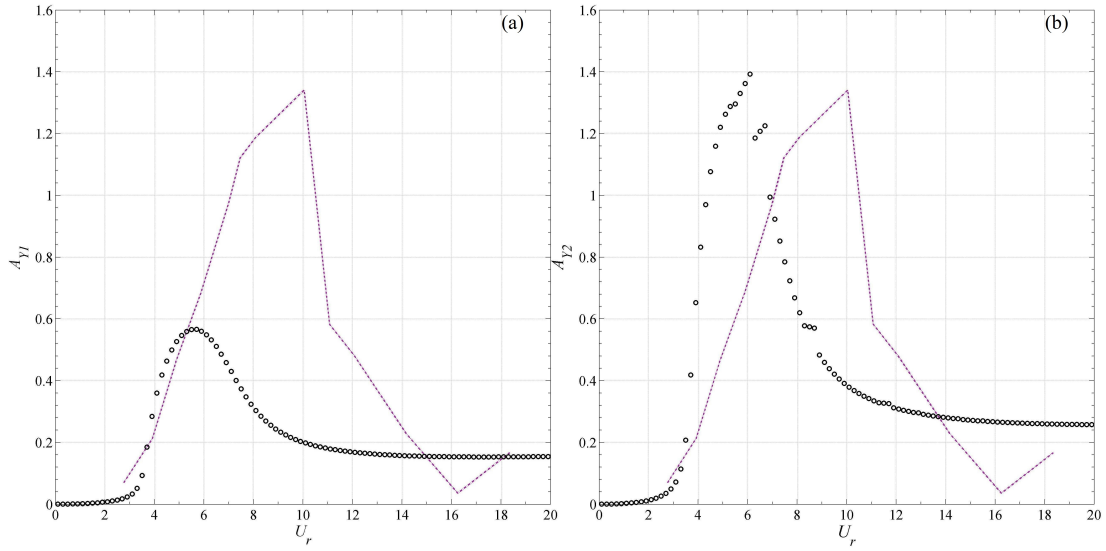

Figure 4.2: Results obtained from VIV experiment conducted by author on a single cylinder (purple -·- line) versus analytical solution of VDP model (○) for (a)leading and (b)trailing cylinders.

is developed solely for cross-flow direction, whereas a cylinder with 2 DOF undergoes oscillations with larger amplitude as Moe and Wu [22] and Sarpkaya [23] observed in their studies.

4.2.2 Solution to 1DOF Rayleigh

As in van der Pol, Rayleigh has two empirical coefficients as well, α and A that should be tuned against experimental data to reduce deviation between the model and practical results. Rayleigh wake oscillator in parallel with a structural motion equation can be solved if similar assumption to van der Pol model can be made. Solution to Rayleigh model can be assumed similar to equation 4.25:

$$\begin{cases} y_1 = y_1 e^{i\omega_1 t} \\ C_{L_1} = C_{L_1} e^{i\omega_1 t + \phi_1} \\ y_2 = y_2 e^{i\omega_1 t + \theta_2} \\ C_{L_2} = C_{L_2} e^{i\omega_1 t + \phi_2} \end{cases} \tag{4.35}$$

It should be emphasised that response frequencies of both cylinders are assumed to be identical. Replacing equation 4.35 into Rayleigh model yields:

$$\begin{cases} -\omega^2 y_1 e^{i\omega t} + i(2\xi_1 + \dfrac{\gamma_1}{\mu_1}\omega_0)\omega y_1 e^{i\omega t} + y_1 e^{i\omega t} = a'_L C_{L_1} e^{i\omega t+\phi_1} \\ -\omega^2 y_2 e^{i\omega t} + i(2\xi_2 + \dfrac{\gamma_2}{\mu_2}\omega_0)\omega y_2 e^{i\omega t+\theta_2} + y_2 e^{i\omega t+\theta_2} = a'_L \left(C_{L_2} e^{i\omega t+\phi_2} + C_{L_1} e^{i\omega(t+t_1)} \right) \\ -\omega^2 C_{L_1} e^{i\omega t+\phi_1} - i\alpha\omega\omega_0 C_{L_1} e^{i\omega t+\phi_1} + i\dfrac{\lambda_1\omega^3}{\omega_0} C_{L_1}^3 e^{i\omega t+\phi_1} + \omega_0^2 C_{L_1} e^{i\omega t+\phi_1} = iA'\omega y_1 e^{i\omega t+\phi_1} \\ -\omega^2 C_{L_2} e^{i\omega t+\phi_2} - i\alpha\omega\omega_0 C_{L_2} e^{i\omega t+\phi_2} + i\dfrac{\lambda_2\omega^3}{\omega_0} C_{L_2}^3 e^{i\omega t+\phi_2} + \omega_0^2 C_{L_2} e^{i\omega t+\phi_2} = iA'\omega y_2 e^{i\omega t+\phi_2} \end{cases} \tag{4.36}$$

Two equations describing leading cylinder should be solved first. Therefore if real and imaginary terms of each equation is separated from each other, four equations of 4.37 would be obtained.

$$\begin{cases} 1 - \omega^2 y_1 = a'_L C_{L_1} \cos\phi_1 \\ (2\xi_1 + \dfrac{\gamma_1}{\mu_1}\omega_0)\omega y_1 = a'_L C_{L_1} \sin\phi_1 \\ (\omega_0^2 - \omega^2) C_{L_1} = A'\omega y_1 \sin\phi_1 \\ \left(\alpha\omega_0 + \dfrac{\lambda_1\omega^2}{\omega_0} C_{L_1}^2 \right) C_{L_1} = A' y_1 \cos\phi_1 \end{cases} \tag{4.37}$$

Four unknowns of this system can be determined by solving 4.37 for ω. Expression 4.38 is an explicit solution for the frequency.

$$-\omega^6 + \left(\omega_0^2 - (2\xi_1 + \frac{\gamma_1}{\mu_1}\omega_0)^2 + 2 \right)\omega^4 + \left(\omega_0^2 \left((2\xi_1 + \frac{\gamma_1}{\mu_1}\omega_0)^2 - 2 \right) - A' a'_L (2\xi_1 + \frac{\gamma_1}{\mu_1}\omega_0) - 1 \right)\omega^2 + \omega_0^2 = 0 \tag{4.38}$$

By knowing the response frequency, wake force on the leading cylinder can be obtained from following equation:

$$C_{L_1} = \sqrt{\left(\frac{\left(\omega_0^2 - \omega^2\right)\left(1 - \omega^2\right)}{\omega^2(2\xi_1 + \dfrac{\gamma_1}{\mu_1}\omega_0)} + \alpha\omega_0 \right) \frac{\omega_0}{\omega^2\lambda}} \tag{4.39}$$

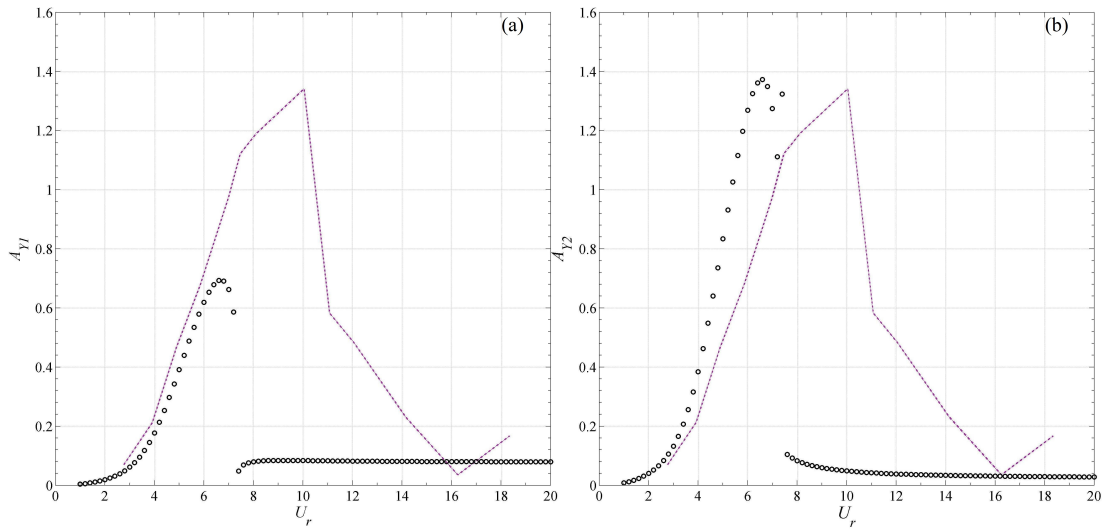

Figure 4.3: Results obtained from VIV experiment conducted by author on a single cylinder (purple -·- line) versus analytical solution of Rayleigh model (○) for (a)leading and (b)trailing cylinders.

and phase difference between cylinder motion and wake force can be calculated from equation 4.40

$$\phi_1 = \arctan\left(\frac{\omega\left(2\xi_1 + \frac{\gamma_1}{\mu_1}\omega_0\right)}{1-\omega^2}\right). \tag{4.40}$$

Then oscillation amplitude can be obtained from any expression in equation 4.37. Same assumption that was made for van der Pol should be made here so it is possible to solve equation 4.36. This expression can be solved for q_2 in the first step then ϕ_2 and θ. Amplitude of trailing cylinder oscillation can be obtained from following equation:

$$y_2 = \frac{q_2\left(\omega_0^2 - \omega^2\right)\sin\phi_2 + \left(\frac{\lambda_1\omega^2}{\omega_0}q_2^2 - \alpha\omega_0\right)q_2\cos\phi_2}{A'\omega\cos\theta} \tag{4.41}$$

Figure 4.3 provides a comparison between analytical solution of Rayleigh model and results obtained in chapter 3 for an isolated cylinder. Empirical coefficients of Rayleigh wake oscillator were considered as $A' = 2$ and $\alpha = 0.3$ (tuned against in-house experiments) in obtaining figure 4.3. Rayleigh model under-predicted the result for leading cylinder similarly to VDP model (figure 4.2) which is because the model is only developed in one DOF. Moreover, both models are simulating a higher amplitude response for the trailing cylinder in comparison to its leading counterpart which is in contrary

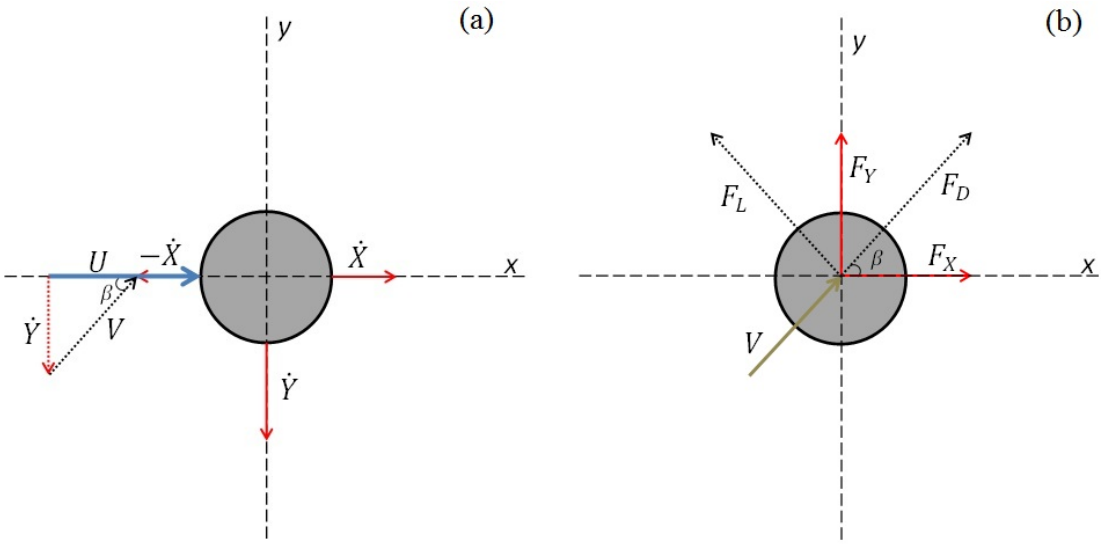

Figure 4.4: (a)Relative velocity and (b)force outcome for an oscillating cylinder with 2DOF

to observations in the previous chapter.

4.3 SimuLink Modelling & Validation

4.3.1 effect of structural non-linearity

Hydrodynamic non-linearities should be accounted to develop a wake oscillator model for a system with two DOF. The relationship between stream-wise and cross-flow motion has been discussed previously in the literature [69]. When a structure is flexibly mounted and allowed to oscillate in both directions, a relative velocity appears between flow stream and motion of the oscillating structure, figure 4.4a, contrary to the case of a fixed cylinder. The direction of the fluid force acting on a oscillating cylinder rotates clockwise (figure 4.4b) or counter-clockwise due to the relative motion of cylinder in respect to flow stream. In other words, drag force(F_D) is not along the stream direction but with an angle of (β) which is time dependent and is a function of cylinder instantaneous velocity. Additionally lift force (F_L) is always perpendicular to the drag. It was observed in figure 3.20 that crescents of both cylinders in this study are pointing downstream. Therefore, right side of motion equation in stream-wise and cross-flow (in

case of counter-clockwise) would become:

$$\begin{cases} F_X = F_D \cos\beta - F_L \sin\beta \\ \\ F_Y = F_D \sin\beta + F_L \cos\beta \end{cases} \tag{4.42}$$

by assuming that angle β is small, it can be defined:

$$\sin\beta = \frac{-\dot{Y}}{U} \tag{4.43}$$

Following the steps explained by Blevins and Coughran [58] equation 4.44 can be obtained.

$$\begin{cases} F_X = F_D + F_L \dfrac{\dot{Y}}{U} \\ \\ F_Y = F_L - F_D \dfrac{\dot{Y}}{U} \end{cases} \tag{4.44}$$

Therefore, by replacing 4.43 into van der Pol model, equations describing fluid-structure interaction for trailing cylinder would become:

$$\begin{cases} \ddot{x}_2 + \left(2\xi_2 + \dfrac{2\gamma_2}{\mu_2}\omega_0\right)\dot{x}_2 + x_2 = a_D\left(p_2 + p_1(\tau_1)\right) + 2\pi a_L q \dfrac{\dot{y_2}}{U_r} \\ \\ \ddot{p}_2 + 2\epsilon\omega_0(p_2^2 - 1)\dot{p}_2 + 4\omega_0^2 p_2 = A\ddot{x}_2 \\ \\ \ddot{y_2} + \left(2\xi_2 + \dfrac{\gamma_2}{\mu_2}\omega_0\right)\dot{y_2} + y_2 = a_L\Big(q_2 + q_1(\tau_1)\Big) - 2\pi a_D p \dfrac{\dot{y_2}}{U_r} \\ \\ \ddot{q}_2 + \epsilon\omega_0(q_2^2 - 1)\dot{q}_2 + \omega_0^2 q_2 = A\ddot{y}_2 \end{cases} \tag{4.45}$$

Analytical solution of such a complex system of equations seems challenging thus it was necessary to solve it using numerical techniques. *Matlab* program provides a suitable environment for such a purpose through *Simulink* Add-on.

4.3.2 SimuLink Model Validation

Two simple Simulink models (figure 4.5) were initially developed so that equations 4.15 and 4.22 as van der Pol model, equations 4.18 and 4.23 as Rayleigh could be solved simultaneously in both stream-wise and cross-flow direction. Fourth-order Runge-Kutta algorithm with variable time step (in order to enhance convergence and stability) was adopted. Reduced velocity was increased gradually with increments of 0.2 from zero. Initial conditions for all reduced velocities were considered similar where at $t = 0, p = q = 2$ and $x = y = 0$. It should be noted that several initial conditions were tried and it was concluded that this model is not sensitive to initial conditions. SimuLink simulation was run for $400s$ for each reduced velocity so that solution could reach the steady state before termination of simulation. Figure 4.6 shows a sample time history of van der Pol SimuLink solution at reduced velocity of 8.

As a validation of the SimuLink models both model solutions (RMS of numerical and analytical) were compared with each other(figure 4.7). It is evident that results from numerical solution and analytical are almost identical which confirms that SimuLink model has been developed accurately. Papaioannou et al. [48] showed that there is hysteresis phenomenon at high Reynolds numbers which velocity coupling term is able to capture it.

Following similar steps, the motion of both cylinders can be extended into stream-wise direction. Figure 4.8 shows a comparison between experiment result of a single cylinder and simulation done by van der Pol model (from here onward due to popularity of van der Pol in the literature only van der Pol model will be discussed). van der Pol simulation of the leading cylinder has some similarities with what was observed during experiments, however it is far from trailing cylinder results. Moreover, it is clear that mathematical model predicts the onset of lock-in range with an acceptable approximation whereas, its full length could not be captured by the model. Zanganeh [28] has addressed this issue in his studies where a pendulum set-up was used for an isolated cylinder test. He suggested that due to geometry non-linearity of the spring-mass system, structural motion equations should be in the form of Duffing oscillator, equation 4.46 [70]. Two terms of $\left(x^3, y^3\right)$ capture the axial non-linear properties and $\left(xy^2, yx^2\right)$

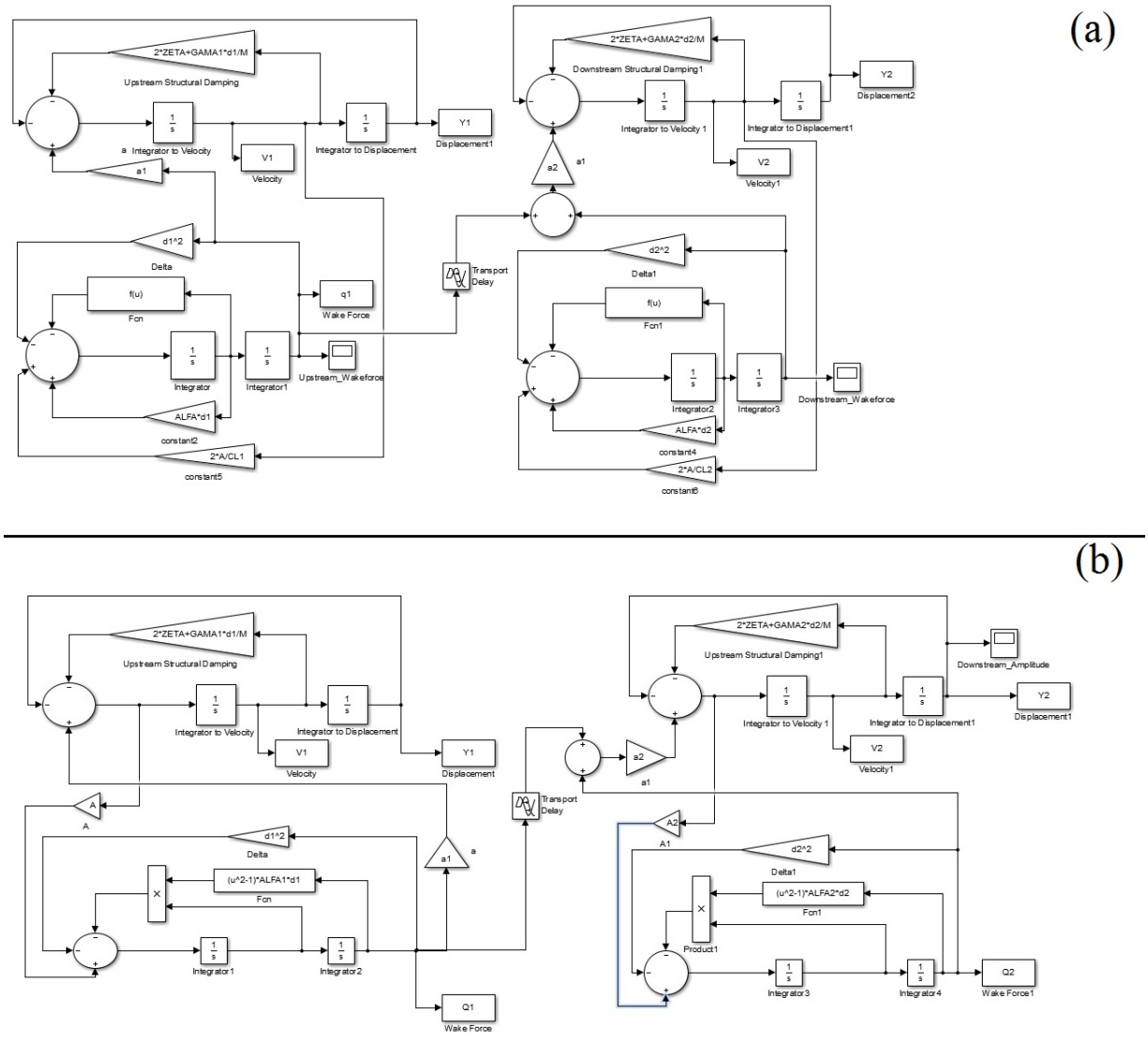

Figure 4.5: (a) Rayleigh and (b) van der Pol simulink models for two cylinders in tandem with 1DOF

can capture physical coupling between cross-flow and stream-wise motions. He also referred to Jian-Shu et al. [71] and Raj and Rajasekar [72] as two other applications of such a coupled system.

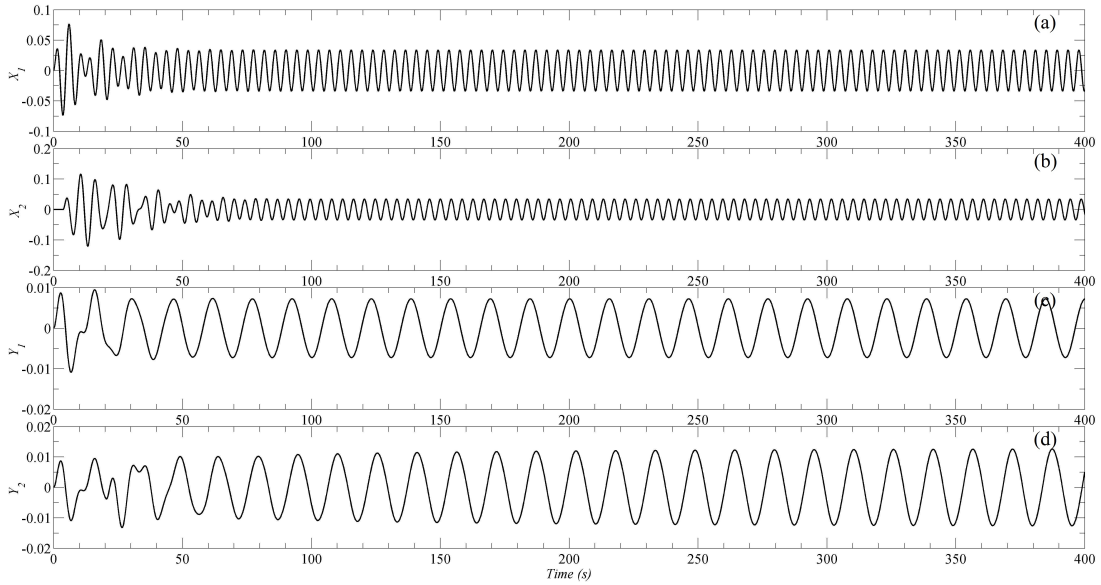

Figure 4.6: Time history of in (a) stream-wise and (c) cross-flow for van der Pal as well as (b) and (d) respectively for Rayleigh SimuLink models

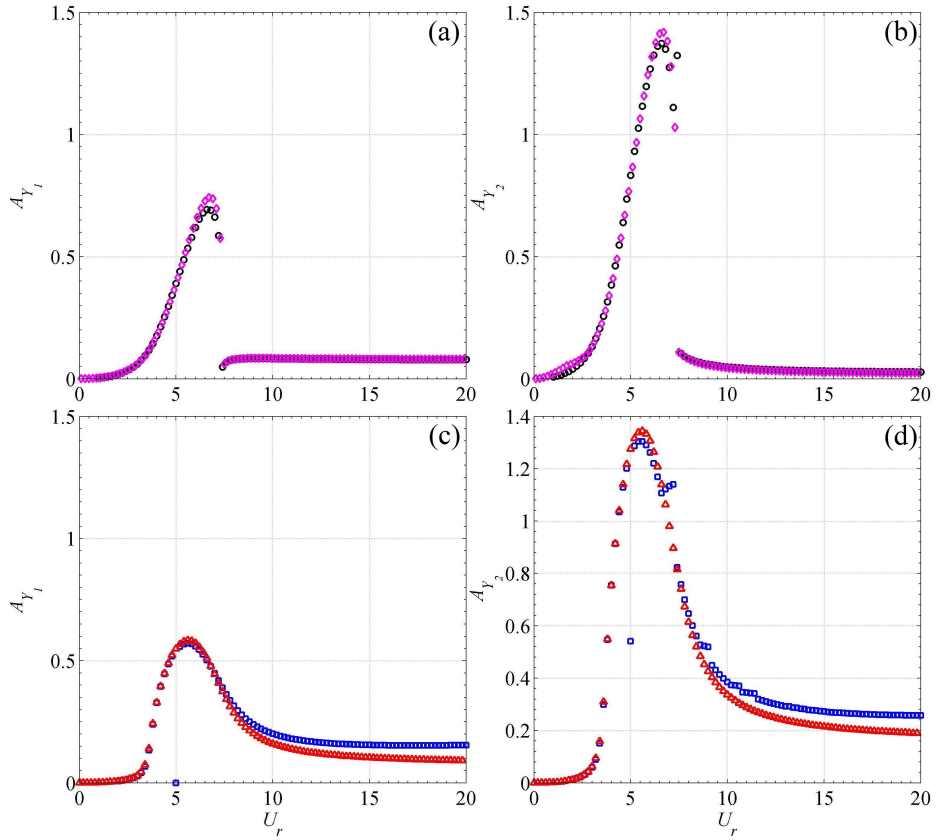

Figure 4.7: (a) Amplitude response of leading cylinder obtained from analytical(○) solution vs. Rayleigh SimuLink model(♢), (b) Amplitude response of trailing cylinder obtained from analytical(○) solution vs. Rayleigh SimuLink model(♢), (c) Amplitude response of leading cylinder obtained from analytical(□) solution vs. van der Pol SimuLink model(△), (d) Amplitude response of trailing cylinder obtained from analytical(□) solution vs. van der Pol SimuLink model(△)

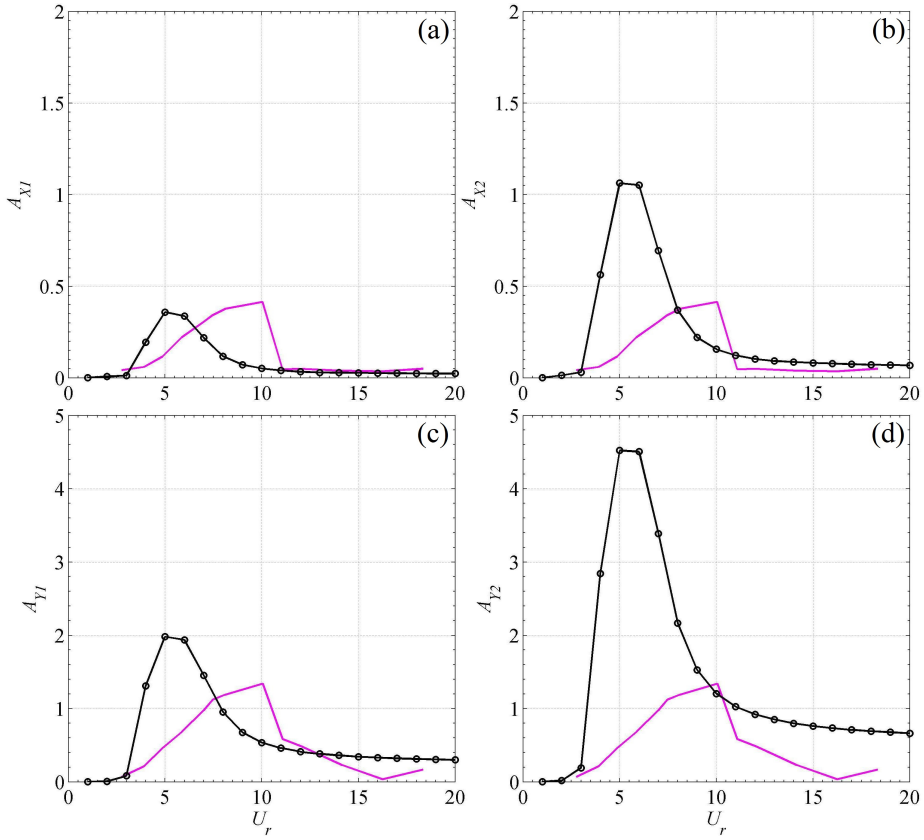

Figure 4.8: Comparison between amplitude response of two cylinders in tandem simulated by van der Pol (○) and experimental result of a single cylinder (purple -·- line)

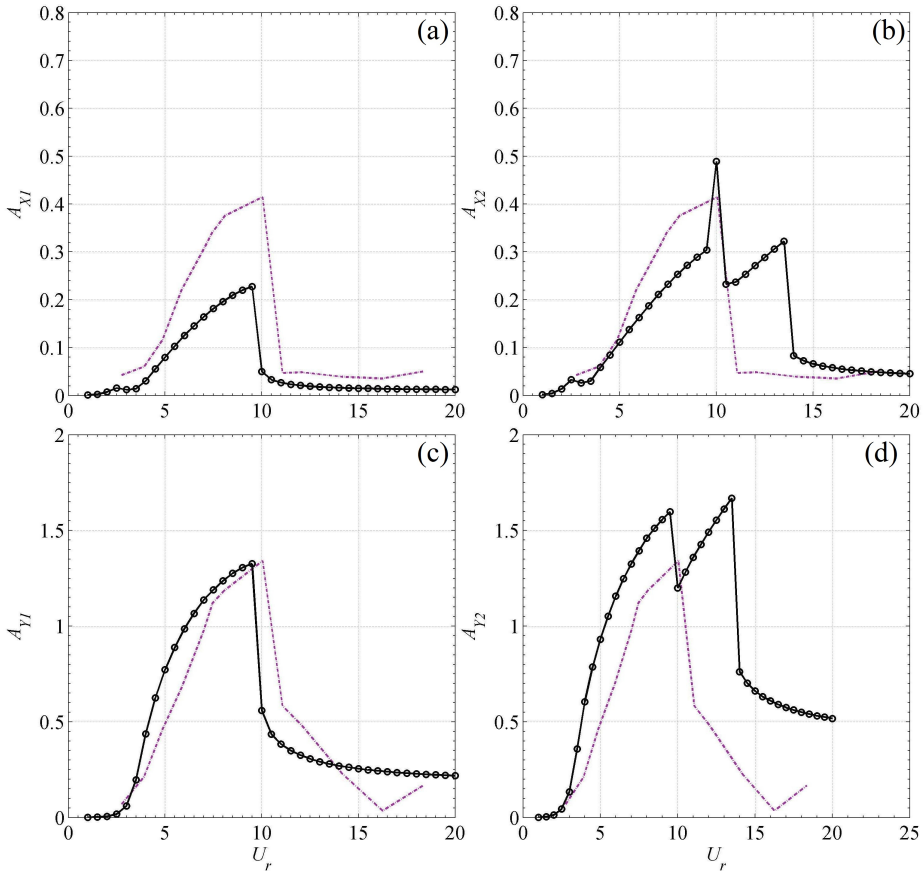

Figure 4.9: Comparison between amplitude response of two cylinders in tandem, simulated by van der Pol and duffing couple(○) and experimental result of a single cylinder (purple -·- line)

$$
\begin{cases}
\ddot{x}_1 + \left(2\xi_1 + \dfrac{2\gamma_1}{\mu_1}\omega_0\right)\dot{x}_1 + \left(x_1 + \alpha_x x_1^3 + \beta_x x_1 y_1^2\right) = a_D p_1 + 2\pi a_L q_1 \dfrac{\dot{y_1}}{U_r} \\
\ddot{p}_1 + 2\epsilon\omega_0(p_1^2 - 1)\dot{p}_1 + 4\omega_0^2 p_1 = A\ddot{x}_1 \\
\ddot{y_1} + \left(2\xi_1 + \dfrac{\gamma_1}{\mu_1}\omega_0\right)\dot{y_1} + \left(y_1 + \alpha_y y_1^3 + \beta_y y_1 x_1^2\right) = a_L q_1 - 2\pi a_D p_1 \dfrac{\dot{y_1}}{U_r} \\
\ddot{q}_1 + \epsilon\omega_0(q_1^2 - 1)\dot{q}_1 + \omega_0^2 q_1 = A\ddot{y}_1
\end{cases}
\tag{4.46}
$$

Coefficients $\alpha_x, \beta_x, \alpha_y$ and β_y are empirical coefficients that are determined by tuning the model against experimental data. In this study these coefficients are assumed to be identical, and their value are equal to 0.7 [26]. Figure 4.9 is obtained by replacing structural motion equation of the model by Duffing oscillator equation. Model simulation of leading cylinder is satisfying since it can capture the onset of lock-in and maximum amplitude in cross-flow. Additionally, stream-wise lock-in range, induced by coinciding of natural frequency with stream-wise oscillation, is captured as well. Nonetheless, the model for trailing cylinder requires modifications to capture its galloping like response. In the next section it is observed that through which parameters this model could be modified.

4.4 Parametric Study

This model could be calibrated against experimental data discussed in chapter 3. Nonetheless, it is crucial to establish how different parameters of the model could influence the model in such a way that enhance the agreement between experiment data and model simulation.

4.4.1 Tuning parameters

Hitherto, all parameters were assumed to have equal values for the leading and trailing cylinders whereas, in practice such an assumption could be misleading. The aim of this

study is to maintain the structure and parameter values similar for as many as possible for both cylinders . Therefore, methodology here was to isolate each parameter and observe the effect of its variation on the trailing cylinder simulation results and then if necessary its value for trailing cylinder would change so that the agreement between simulation results and experimental could be enhanced.

Strouhal number

It has been discussed earlier (section 3.5.1) that some of previous observations in literature concluded that Strouhal number of trailing cylinder is identical to the leading one while other experiments Bokaian and Geoola [73] confirmed that in fact two cylinders have different Strouhal numbers. Other studies, [31], revealed that this number is not a function of Re for the trailing cylinder while OKAJIMA [56] and Igarashi [37] showed that after the critical spacing (approximately $L = 3.5D$) it is not a function of spacing either and is equal to that of a single cylinder.

Overall, based on the experimental observation in the previous chapter and reports in the literature it is concluded that Strouhal number of trailing cylinder should be similar to that of the leading and equal to 0.2 (suggested value for modelling, [27], for wide range of Re). However it is still important to observe how model could be modified to capture the galloping like response of the trailing cylinder. Figure 4.10 shows how increase of St_2 results in lock-in range width reduction in trailing cylinder simulation. This conclusion is in agreement with Bokaian and Geoola [73] observations in which a lower strouhal number were reported for the trailing cylinder. Allen and Henning [74] and Williams and Suaris [75] claimed that variation of Strouhal number also has reverse relation with the velocity at which synchronization commence while analytical simulation cannot confirm this.

Lift coefficient of a stationary cylinder (C_{L_0})

Due to turbulent upstream wake, lift coefficient of trailing cylinder could differ from its leading counterpart. There is no studies on the variation of trailing cylinder C_{L_0}

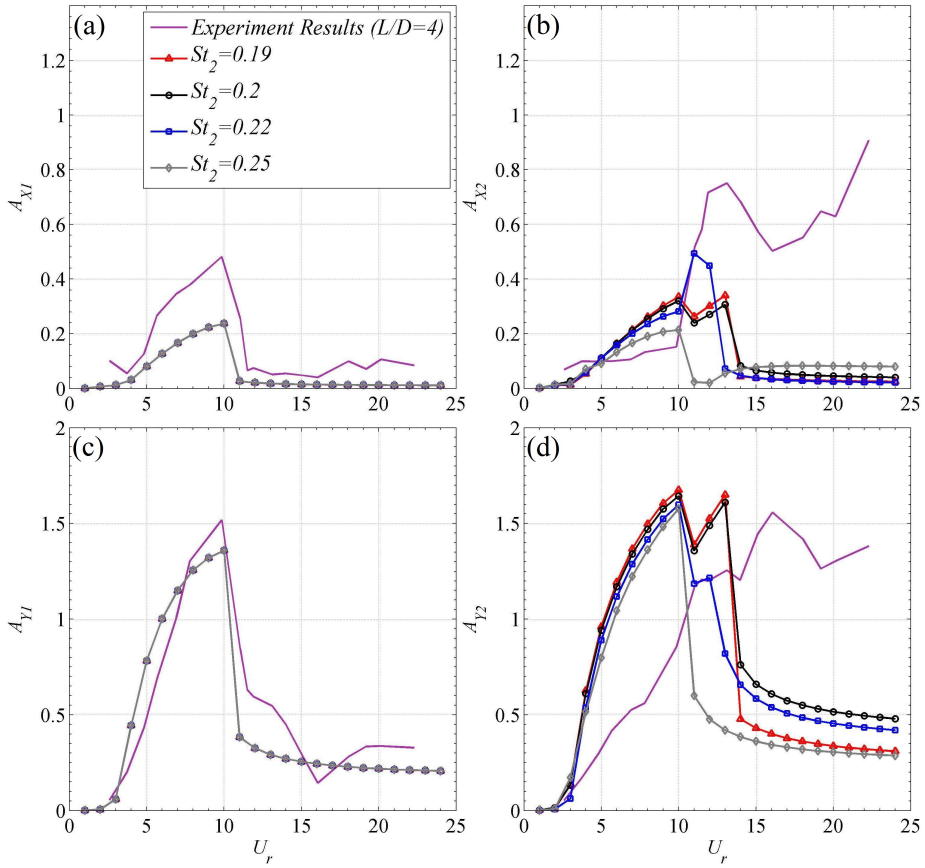

Figure 4.10: (a)stream-wise and (c)cross-flow response of leading cylinder as well as trailing (b, d respectively) obtained from models with different Strouhal numbers. $St_2 = 0.19$ (△), $St_2 = 0.2$ (○), $St_2 = 0.22$ (□), $St_2 = 0.25$ (♢), experimental data (purple solid line)

to correct this parameter in the trailing cylinder model. However, it is important to examine the effect of this parameter on the mathematical model. Figure 4.11 includes the effect of lift coefficient on the response amplitude of trailing cylinder. Effect of C_{L_0} is insignificant in this model as it can be seen in this figure. Although $C_{L_{0_2}}$ is influential on the right side of the Duffing oscillator, the value of a_{L_2} is so small (0.006, 0.018 and 0.03 respectively) that $C_{L_{0_2}}$ effect is insignificant.

Mean drag coefficient

Drag coefficient is highly influential on the response amplitude and width of lock-in range due to its significant influence on fluid added damping (c_a). Increase of turbulence in the wake of an oscillating cylinder results into increase of the drag force

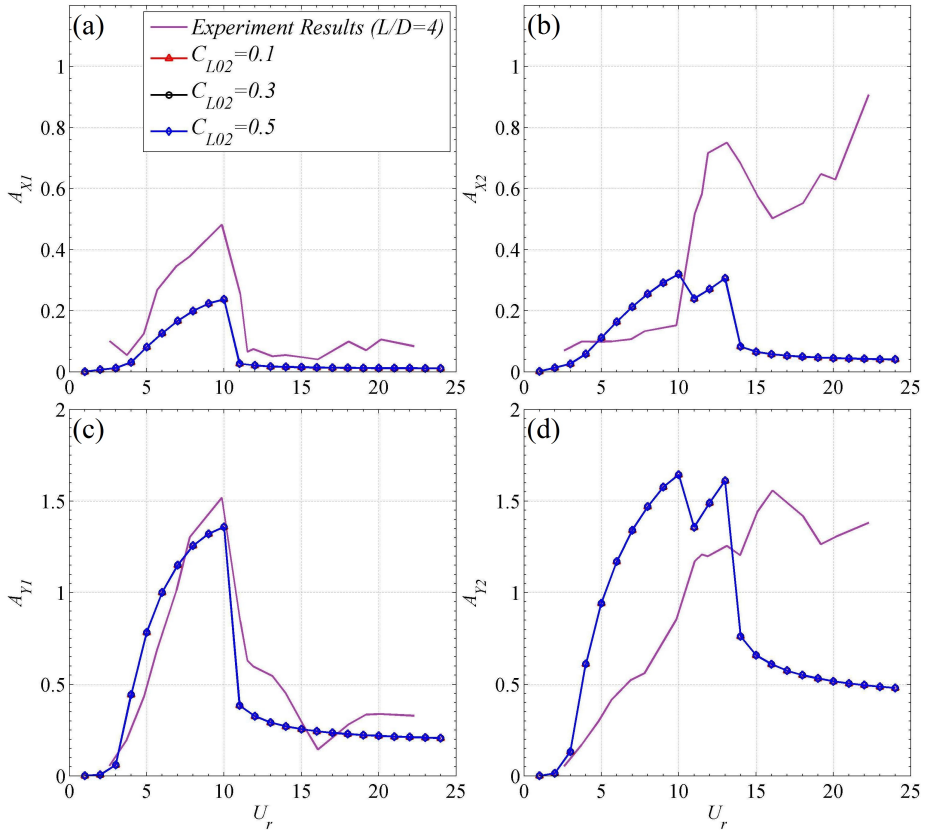

Figure 4.11: (a)stream-wise and (c)cross-flow response of leading cylinder as well as trailing (b, d respectively) obtained from models with different $\left(C_{L_{0_2}}\right)$. $C_{L_{0_2}} = 0.1$ (△), $C_{L_{0_2}} = 0.3$ (○), $C_{L_{0_2}} = 0.5$ (◇), experimental data (purple solid line)

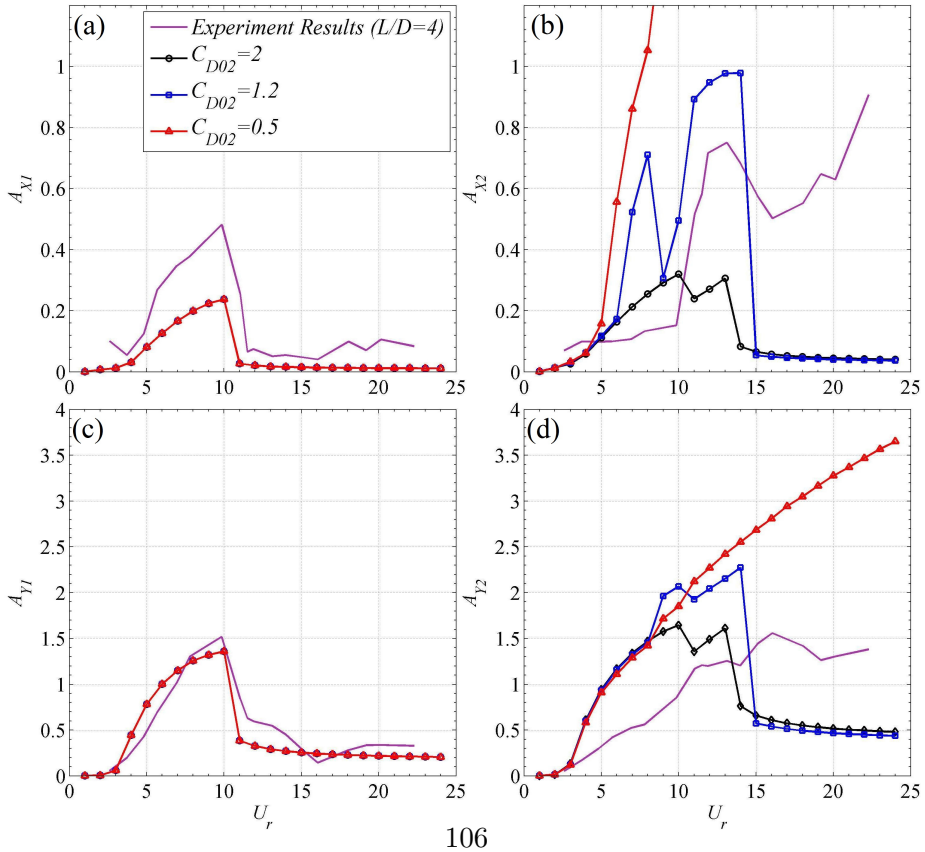

Figure 4.12: (a)stream-wise and (c)cross-flow response of leading cylinder as well as trailing (b, d respectively) obtained from models with different $C_{D_{0_2}}$. $C_{D_{0_2}} = 0.2$ (○), $C_{D_{0_2}} = 1.2$ (□),$C_{D_{0_2}} = 0.5$(△), experimental data (purple solid line)

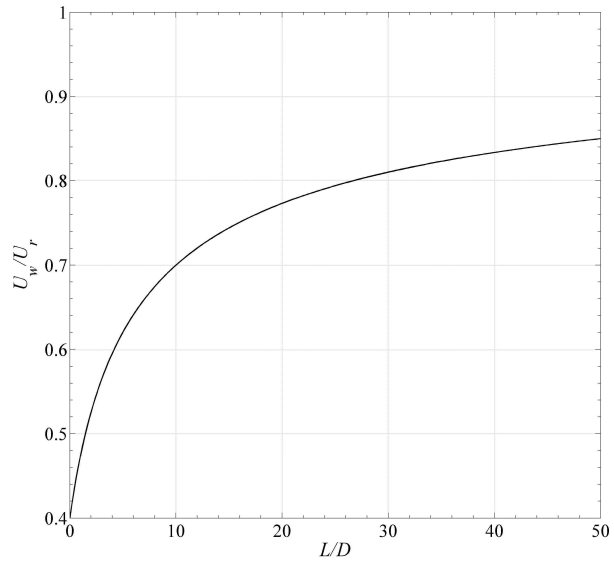

Figure 4.13: Flow velocity profile in the wake of a cylinder with diameter of $0.11m$ as a function of distance,[76].

and consequently, rise of damping. Figure 4.12 includes simulation of three models with different drag coefficient (suggested value for an oscillating cylinder is $C_{D_{0_2}} = 0.2$ by Facchinetti et al. [27]). It is evident that reduction in drag coefficient raises the maximum amplitude as well as lock-in range. Further reduction of $C_{D_{0_2}}$ produces a galloping like response. In the next chapter it will be discussed how the model could be improved by introducing an extra damping term to the duffing equation.

Flow velocity in the gap

Flow velocity in the wake of leading cylinder is less than free stream velocity and follows a exponential trend from zero at the *stagnation point* at the immediate downstream of the cylinder and increases gradually towards downstream. Huse [76] suggested that wake velocity profile is a function of drag coefficient, diameter of the cylinder and distance from its centre which figure 4.13 depicts it. Flow velocity variation in the spacing range that is the focus of this study ($L > 5D$) does not have a significant influence on the simulation, and only results in a small variation of lock-in range in response.

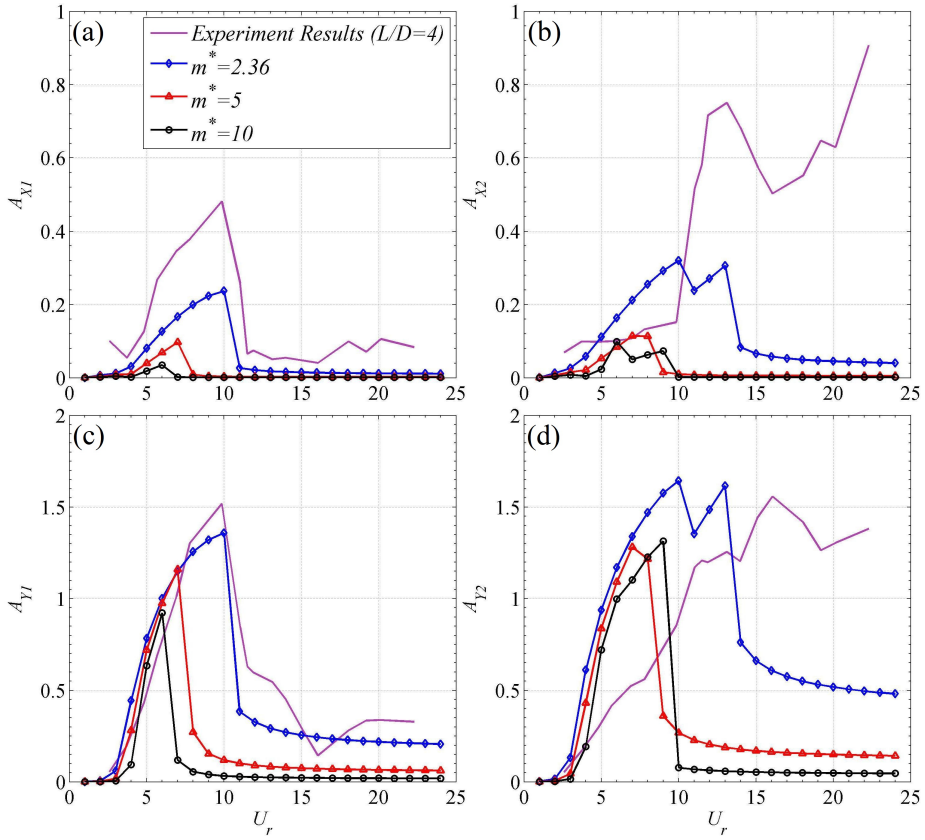

Figure 4.14: (a)stream-wise and (c)cross-flow response of leading cylinder as well as trailing (b, d respectively) obtained with mass ratios of $m^* = 2.36$ (♢)(Low), $m^* = 5$ (△) (Medium), $m^* = 10$ (○) (High), experimental data (purple solid line).

4.4.2 structural properties influence

Effect of structural property (mass and damping ratio) is often demonstrated by *Griffin plot*. The Skop-Griffin parameter, [19], is defined as:

$$S_G = 2\pi^3 St^2 m^* \xi \tag{4.47}$$

which can collect different response amplitude peaks based on the cylinder properties (mass-damping) in order to provide a clear picture of mass-damping effect on the maximum oscillation amplitudes. Based on this parameter, maximum oscillation amplitude of an oscillating cylinder depends on both mass and damping ratio. Figure 4.14 shows how simulation results change in response to variation of the mass ratio. Mass ratio has a direct effect on the maximum amplitude as well as lock-in range which is in agreement with observations in previous studies [11, 14, 24].

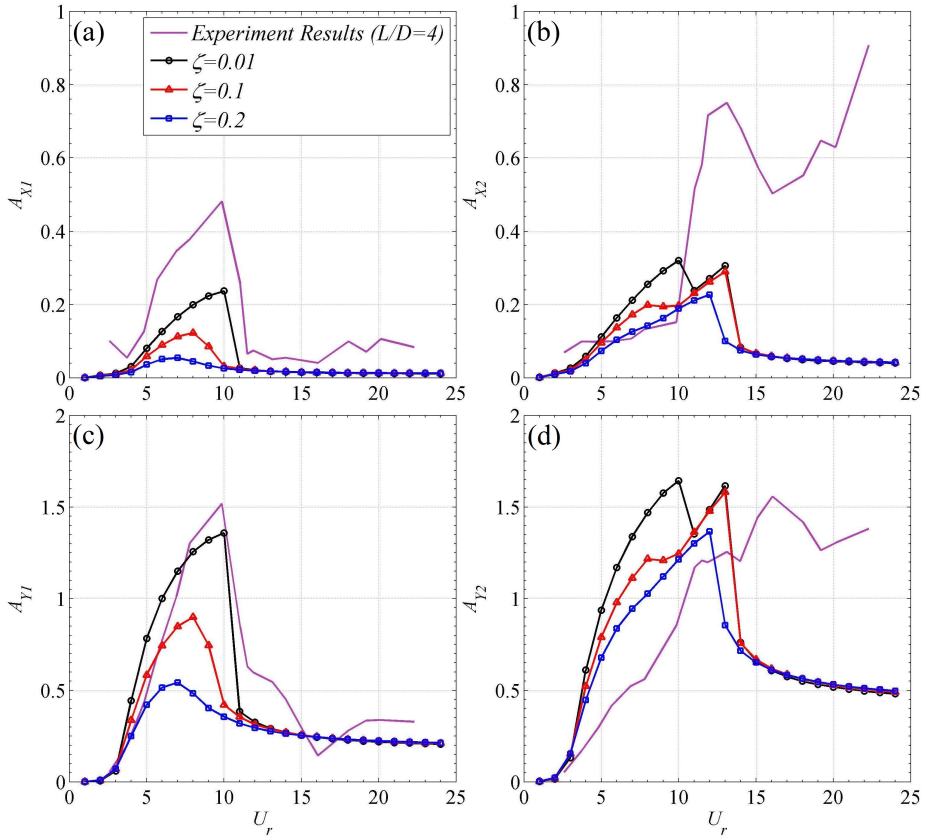

Figure 4.15: (a)stream-wise and (c)cross-flow response of leading cylinder as well as trailing (b, d respectively) obtained with mass ratios of $\xi = 0.01$ (○), $\xi = 0.1$ (△), $\xi = 0.2$ (◇), experimental data (purple solid line).

Additionally, it is necessary to observe the effect of structural damping on the model and compare it with previous studies. Figure 4.15 demonstrates how maximum response amplitude decreases by increase of the structural damping. Blevins and Coughran [15] observed similar trend in his studies. It is clear that lock-in range width is not affected by change of structural damping.

Spacing between two cylinders

Variation of the spacing between two cylinders can be introduced into trailing cylinder equation in this form of the model which is sufficient based on the discussion in chapter 3. Firstly, spacing is influential to time delay (equation 4.21) on the right-hand side of the Duffing equation for trailing cylinder. Nonetheless, an increase of spacing only increases the time required for the downstream cylinder to reach the steady state and

once reached amplitude response would be similar to the other spacings. Secondly, variation of flow velocity could be added to the model with a trend following figure 4.13 which, as discussed earlier, would not be effective in the scope of this research.

4.5 Conclusion

A mathematical model was developed for two identical cylinders in tandem arrangement, based on a coupled system of a van der Pol wake oscillator and a Duffing equation. Two equations were coupled by considering the fluid force, driven from wake oscillator equation, as the source of motion excitation of the structure. Furthermore, wake oscillator was connected to structural motion equation through assuming a function of acceleration on the right-hand side. It was assumed that tandem cylinders are rigid, and flexibly mounted with the identical structural stiffness of k in both directions. Constants in both systems were considered equal for the sake of simplicity and compensating for the lack of experimental measurements for the trailing cylinder hydrodynamic coefficients.

- On the other hand, another force term was added to the Duffing oscillator of trailing cylinder in an attempt to simulate the buffeting upstream vortices [53, 77]. This new term was considered to be the same as the wake force that leading cylinder experienced, assuming that they buffet on the trailing body with the equal force as they exert on the leading cylinder during their generation and dispatch. This extra force term was implemented with a *time delay* of t_1 which is a function of the (L) and spacing between two vortices in Kármán vortex street.

- It was observed that added forcing term to downstream duffing equation is only effective in such a way that upstream force at time t would be added to downstream wake force at the time $t + t_1$ and it does not account for energy loss of the upstream vortex street as it travels further downstream. Additionally, observations during experiments in this study revealed that collision of upstream

vortices and trailing cylinder does not follow a specific pattern and based on the flow velocity it could amplify downstream oscillation amplitude or damp it.

- This method also failed to address this phenomenon which resulted in simulating a higher amplitude response for trailing cylinder in comparison with its leading counterpart regardless of the spacing between them.

- A parametric study was conducted so that the effect of all parameters in the model could be recognised and their values could be modified to fit the best to experimental data. Table 4.1 presents a summary of the parametric study. The effect of each parameter was considered with three indicators of maximum amplitude (A_max), onset velocity (U_r) of lock-in range and the width of lock-in. If the growth of a parameter increases the value of any of these parameters, it is shown by an upward arrow otherwise if it results in reduction it is represented by a downward arrow.

Table 4.1: Summary of parametric study on the mathematical model of trailing cylinder

parameter	A_{Max}	onset U_r	Lock-in width
m^*	$\downarrow$	$\uparrow$	$\downarrow$
ξ	$\downarrow$	–	–
St	$\downarrow$	–	$\downarrow$
C_{L_0}	–	–	–
C_D	$\downarrow$	–	$\downarrow$

- None of the tested parameters (except C_0) could successfully influence the model to capture the galloping like response of the trailing cylinder.

Chapter 5

Model tuning & improvements

5.1 Objective & Methodology

It was discussed in details through out the previous chapter (chapter 4) how to develop a mathematical model for two rigid cylinders in tandem arrangement so that it can simulate their FIV response. However, it was observed in section 4.4 that this model, although successful in simulating the leading cylinder response, was not performing satisfyingly in simulating trailing cylinder. Additionally, the parametric study showed that variation in any of parameters (except $C_{D_{0_2}}$) would not change the nature of equations to produce a galloping-like response for the trailing cylinder.

Such an observation led to an attempt at rearranging and modifying the Duffing oscillator for trailing cylinder so that it becomes capable of capturing the effect of upstream turbulent wake rather than simply accounting and acknowledge the force of coming vortices. This approach is competent for two reasons; One, it eliminates the input from the leading cylinder and necessity to measure the energy loss of Kármán vortex street. Two, it is no longer crucial to know the exact position of trailing cylinder on its trajectory at the time of collision; hence the solution would be less complex.

Since the mathematical model can simulate the leading cylinder behaviour at a satisfactory level it is only required to add an amendatory term to simulate the difference between trailing cylinder and upstream wake forces (F_1 and F_2 respectively). Therefore wake forces of both cylinders were driven in the form of equation 4.44, from the experiment data obtained in chapter 3. Total mass and damping of the structure were

obtained previously. Moreover, velocity and acceleration of each cylinders were calculated by differentiating the the corresponding time history once and twice respectively with respect to time.

Then, few mathematical functions were tried to be fitted to the difference between F_1 and F_2 which resulted in two additional terms of *added mass* and *damping* in the Duffing oscillator. Moreover, these terms were optimised to provide the best fit to RMS amplitude graph in both directions.

Finally, these amendatory terms were introduced as a function of the spacing to represent changes in the wake as it flows downstream.

5.2 Hydrodynamic force of the wake

As it was discussed in section 4.3 due to the relative velocity between flow and the cylinder motion, there is a relative velocity between them which is equal to the resultant of flow and structure velocities in cross-flow and stream-wise directions. Consequently, drag and lift forces are not respectively in line and perpendicular to the flow direction anymore but, they rotate and align with the relative velocity hence, the force in stream-wise and cross-flow direction becomes as described in equation 4.42.

It is possible to calculate F_X and F_Y through dynamic equation (5.1) using experimental data.

$$\begin{cases} F_X = (m_s + m_a)\,\ddot{X} + 2\xi_1\omega_n\,(m_s + m_a)\,\dot{X} + kX \\ \\ F_Y = (m_s + m_a)\,\ddot{Y} + 2\xi_1\omega_n\,(m_s + m_a)\,\dot{Y} + kY \end{cases} \tag{5.1}$$

Then, solving the equation 4.44 for F_D and F_L yields the equation 5.2 through which oscillating drag and lift coefficients can be calculated.

$$\begin{cases} C_D = \dfrac{F_Y \sin\beta - F_X \cos\beta}{\dfrac{1}{2}\rho_w D U^2 L_c} \\ \\ C_L = \dfrac{F_Y \cos\beta + F_X \sin\beta}{\dfrac{1}{2}\rho_w D U^2 L_c} \end{cases} \tag{5.2}$$

Figure 5.1 demonstrates the two force coefficients for different spacings at which experiment one (equal natural frequencies) was conducted. This graph also includes the predicted drag force obtained from Vandiver expression, [17], which has 86% agreement with experimental results of the single cylinder experiment. Figures a and b confirm that rise in oscillation amplitude increases the oscillating drag coefficient for both cylinders [1, 65]. On the other hand, the amplification is not dependent on oscillation amplitude as much, for trailing cylinder. Contrary to previous observations for a single cylinder, an increase in trailing cylinder response amplitude does not result in the rise of drag and lift forces, especially at higher reduced velocities. Additionally, comparing Figure 5.1 and 3.15 (b, d) reveals that wake forces (drag and lift) are independent of U_r during upstream lock-in range. However, a sharp increase can be observed at the reduced velocity corresponding to end of upstream lock-in range which reduces to original value gradually by an increase of U_r. Moreover, this jump is more significant in smaller spacings, whereas in larger gaps ($L/D = 15,\ 20$) it is non-existence. Nevertheless, this figure can confirm that wake force highly depends on the spacing between two cylinders which as it grows large the wake force rises as well.

5.3 Curve fitting

Chapter 4 concluded that proposed mathematical model could produce a satisfactory description of trailing cylinder. However, it requires major modification to provide a better simulation of the leading cylinder FIV. In this regard, first, it should be established how forces on trailing cylinder are different from the leading body, what causes this difference and what can influence it.

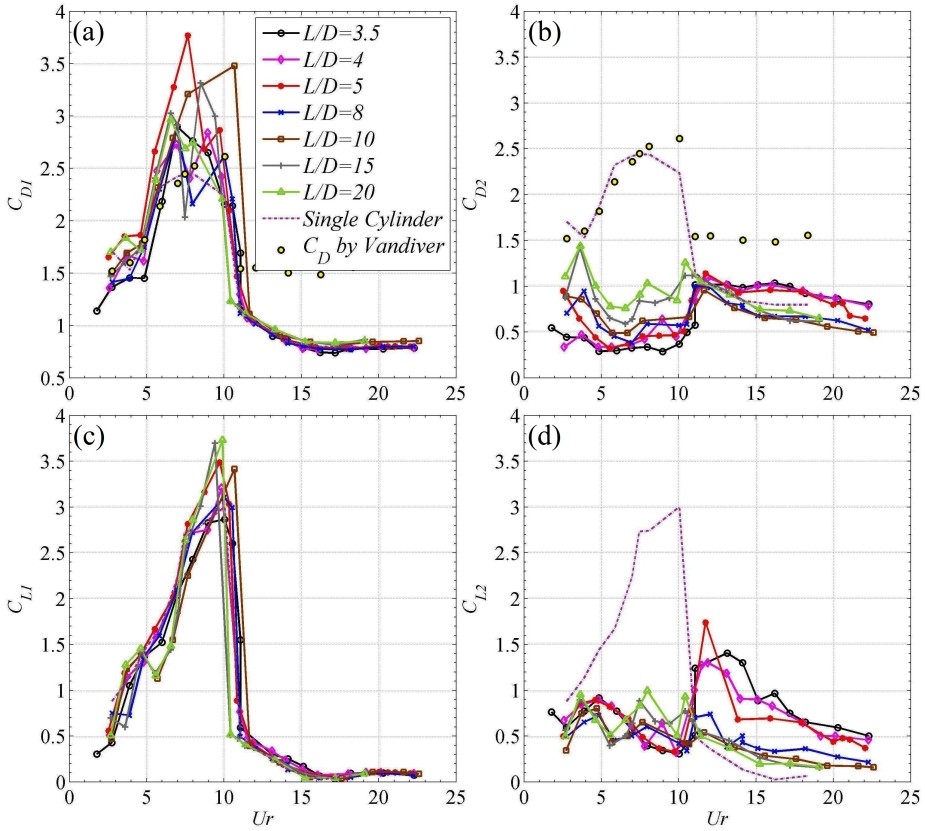

Figure 5.1: Oscillating drag and lift force exerted on leading (a, c respectively) and trailing(b, d respectively) cylinders by passing fluid versus drag force obtained from Vandiver equation.

It was found in section 3.5.1 that two mechanisms of excitation govern the response of trailing cylinder, firstly, VIV motion due to the fluid current in the gap, secondly vortices and turbulent flow regime in the wake of leading body. The model only requires modifications that takes into account the effect of chaotic flow regime in the upstream wake, since the mathematical model can simulate the VIV motion of leading cylinder (it was discussed before that buffeting vortices reach trailing cylinder at different positions hence some of them amplify the VIV motion and some other damp it).

A simple method to identify the influence of wake is to deduct the downstream force from upstream ($C_{D_2} - C_{D_1}$, $C_{L_2} - C_{L_1}$). The distinct upstream wake force would be revealed after deduction since a single cylinder response to undisturbed flow is known (leading cylinder and an isolated one have identical VIV response). It should be emphasised that due to shielding effect, trailing body experiences a lower velocity. However, as the undisturbed flow velocity is being considered in mathematical modelling the

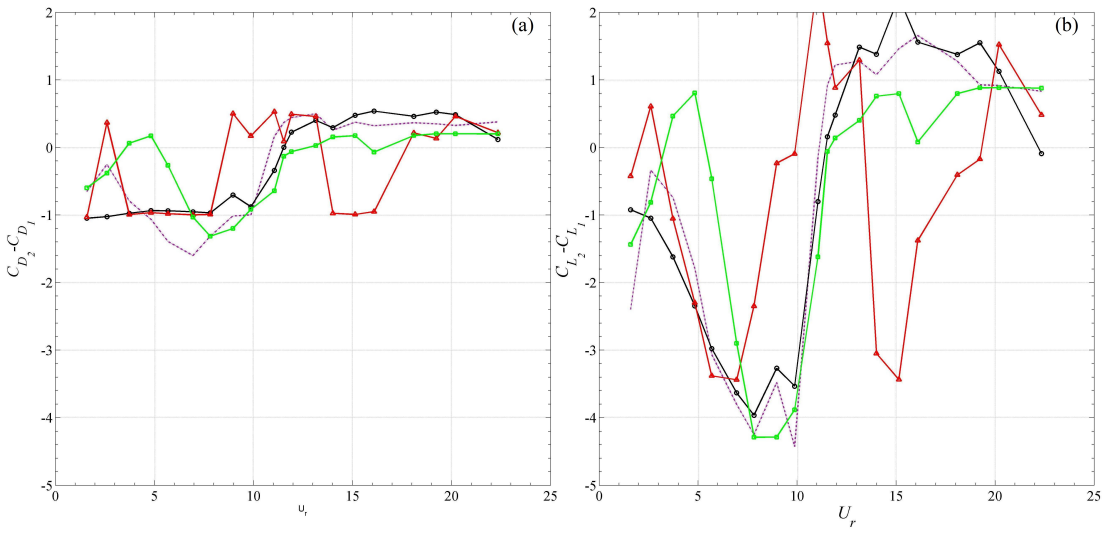

Figure 5.2: Curve fitting to hydrodynamic force ((a) Drag,(b) Lift) variance between up and downstream cylinder at spacing of $L/D = 4$ with a polynomial function of third order. Experiment (purple -·- line), $f(A_{y_1})$ (□), $f(\ddot{x}_2, \ddot{y}_2)$ (○), $f(\dot{x}_2, \dot{y}_2)$ (△).

simulation would yield the VIV response corresponding to that specific speed hence this method provides the exact value of the upstream wake force that is needed to be accounted for in modifying term.

The wake force could be divided into three different components, mean drag, oscillating lift and drag. Figure 5.2 displays oscillating drag and lift components for the spacing of $L/D = 4$. Then it is possible to examine this difference against several variables and find the best fit to this variance. Thus, polynomial functions of leading cylinder cross-flow oscillation amplitude, trailing cylinder acceleration and velocity were fitted, figure 5.2. It is evident that upstream displacement provides the best fit, and the downstream displacement is also satisfactory.

It was assumed that upstream wake force could be modelled by a polynomial function of third order. In this assumption, contrary to Shiau and T. Y. Yang [53], no time delay was implied since the fluid flow is undisturbed hence the wake force is not a function of time, and it reaches steady state after a finite period. The curve fitting yielded the following function to describe the upstream wake force exerted on the trailing cylinder at $L/D = 4$.

$$\begin{cases} F_X = -5.904{y_1}^3 + 6.457{y_1}^2 + 06096y_1 - 1.07 \\ \\ F_Y = -14.22{y_1}^3 + 35.88{y_1}^2 - 20.34y_1 - 0.6537 \end{cases} \tag{5.3}$$

Figure 5.3 demonstrates a comparison between experimental results obtained for $L/D = 4$ and oscillation amplitude simulation produced by amended mathematical model in which equation 5.3 simulated the wake force. All parameters were kept identical between two cylinders.

The dominant peak of trailing cylinder in cross-flow direction, observed in figure 5.3, has no corresponding in experimental results, what is more, this peak location is at the exact reduced velocity (approximately $U_r = 11$) at which maximum upstream response occurs. This conclusion can be drawn that this peak is due to very high response amplitude of leading cylinder. Furthermore, by looking at the previous figures from mathematical model in section 4.4.1, it becomes clear that although system physics suggests that response of the trailing cylinder depends on its leading counterpart, however, in modelling any input from upstream model to downstream one results in appearance of a distinct peak at the same U_r at which maximum amplitude of the leading cylinder occurs.

It can be concluded from the observation above that up and downstream models should be independent of each other, and the effect of chaotic flow regime in the wake should be a function of trailing cylinder response.

5.4 Added mass and damping modification

5.4.1 Added Mass

In the previous section it was observed that the upstream wake force on trailing cylinder can be described as a function of acceleration as well. Results of curve fitting to acceleration was also satisfactory, figure 5.3. However, it is not possible to have any arbitrary function of acceleration in the right hand side of the equation as it creates an algebraic

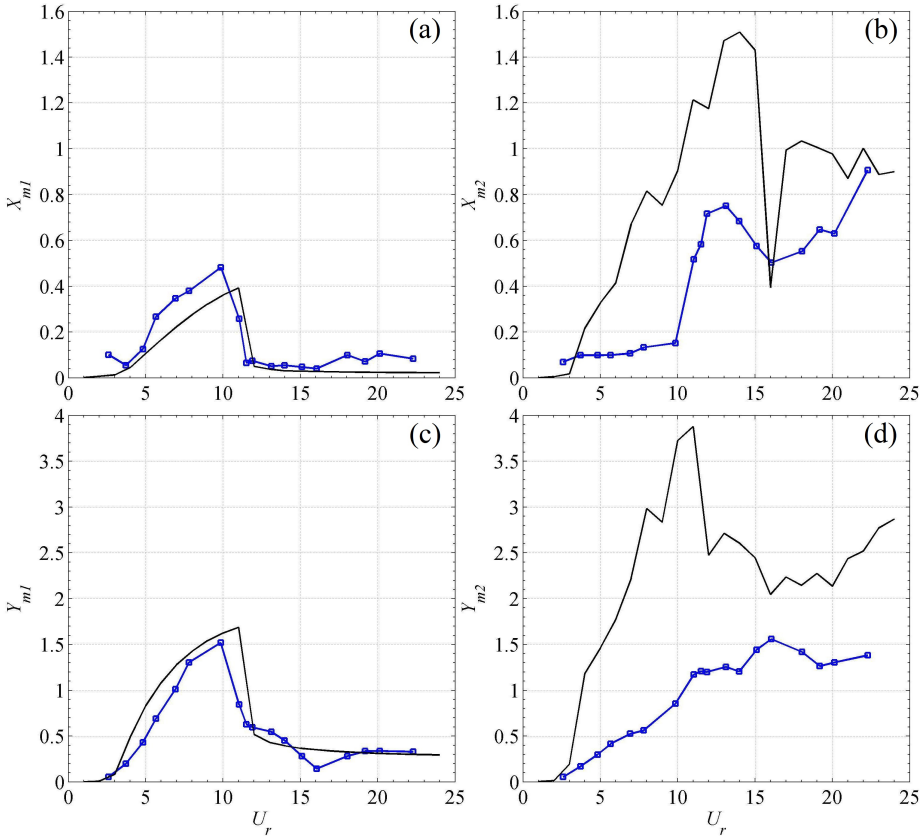

Figure 5.3: Amplitude of oscillation at different reduced velocities obtained from experiment(□) versus mathematical model with a third order polynomial function of upstream cross-flow displacement as the force modification (solid black line).

loop that SimuLink cannot solve. Consequently, a modification term should be considered in such a way that is transferable to the left side which means only a polynomial first order function can be considered. Figure 5.4 includes results of the curve fitting to a first order polynomial function. Nonetheless, this simple function would not yield a non-dimensional term after applying non-dimensional time and distance, instead it is possible to consider the modification terms as $A_X \frac{\ddot{X}_2}{D{\omega_s}^2}$ and $B_Y \frac{\ddot{Y}_2}{D{\omega_s}^2}$ which their non-dimensional process is:

$$\begin{cases} {\omega_n}^2 D\ddot{x}_2 + (2\xi {\omega_n}^2 D + \dfrac{2\gamma\omega_s\omega_n\rho D^3}{M})\dot{x}_2 + {\omega_n}^2 D x_2 = \dfrac{\frac{1}{2}\rho U^2 D C_D}{M} + \dfrac{\frac{1}{2}\rho U^2 D}{M} A_X \dfrac{{\omega_n}^2 D\ddot{x}_2}{D{\omega_s}^2} \\ {\omega_n}^2 D\ddot{y}_2 + (2\xi {\omega_n}^2 D + \dfrac{\gamma\omega_s\omega_n\rho D^3}{M})\dot{y}_2 + {\omega_n}^2 D y_2 = \dfrac{\frac{1}{2}\rho U^2 D C_L}{M} + \dfrac{\frac{1}{2}\rho U^2 D}{M} B_Y \dfrac{{\omega_n}^2 D\ddot{y}_2}{D{\omega_s}^2} \end{cases} \tag{5.4}$$

It should be emphasised that amending terms were added to structural equations as a modification agent to improve force coefficients , as the curve fitting was done to

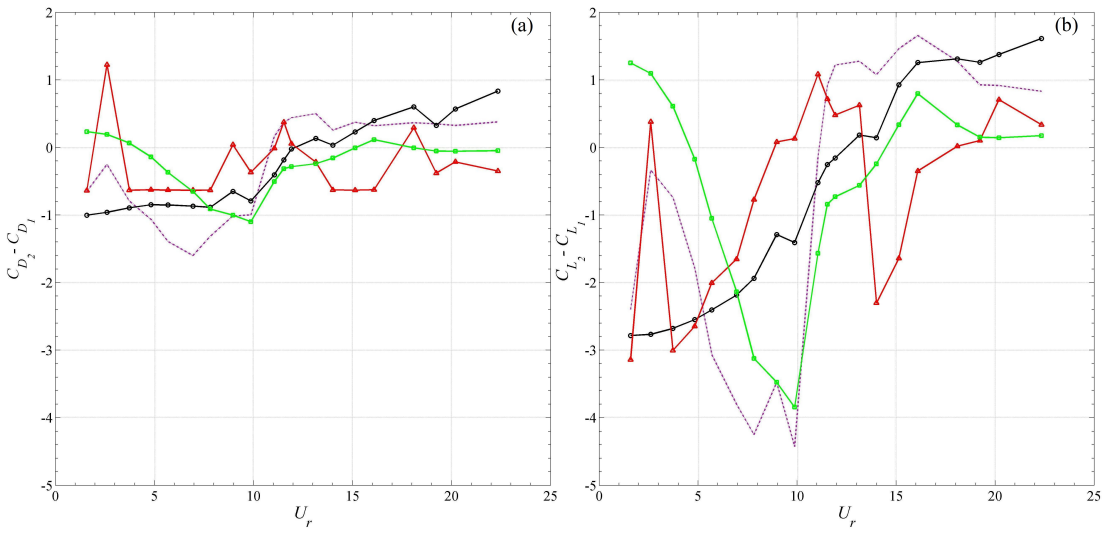

Figure 5.4: Curve fitting to hydrodynamic force ((a) Drag,(b) Lift) variance between leading and trailing cylinders at spacing of $L/D = 4$ with a first order polynomial function. Experiment (purple -·- line), $f(A_{y_1})$ (□), $f(\ddot{x}_2, \ddot{y}_2)$ (○), $f(\dot{x}_2, \dot{y}_2)$ (△).

difference between force coefficient in section 5.3, hence it is important to treat this term as force and multiply it by dynamic pressure of the free stream. In this way the increase of turbulence with rise of Re in the wake can be accounted. By rearranging equation 5.4 structural motion equation becomes:

$$\begin{cases} \ddot{x}_2 + (2\xi + \dfrac{2\gamma\omega_0}{\mu})\dot{x}_2 + x_2 = \dfrac{1}{16}\dfrac{C_{D_0}}{\mu\pi^2 St^2}p_2 + \dfrac{1}{2}\dfrac{A_X}{\mu St^2}\ddot{x}_2 \\ \\ \ddot{y}_2 + (2\xi + \dfrac{2\gamma\omega_0}{\mu})\dot{y}_2 + y_2 = \dfrac{1}{16}\dfrac{C_{L_0}}{\mu\pi^2 St^2}q_2 + \dfrac{1}{2}\dfrac{B_Y}{\mu St^2}\ddot{y}_2 \end{cases} \tag{5.5}$$

$$\begin{cases} \left(1 - \dfrac{1}{2}\dfrac{A_X}{\mu St^2}\right)\ddot{x}_2 + (2\xi + \dfrac{2\gamma\omega_0}{\mu})\dot{x}_2 + x_2 = \dfrac{1}{16}\dfrac{C_{D_0}}{\mu\pi^2 St^2}p_2 \\ \\ \left(1 - \dfrac{1}{2}\dfrac{B_Y}{\mu St^2}\right)\ddot{y}_2 + (2\xi + \dfrac{2\gamma\omega_0}{\mu})\dot{y}_2 + y_2 = \dfrac{1}{16}\dfrac{C_{L_0}}{\mu\pi^2 St^2}q_2 \end{cases} \tag{5.6}$$

Appearance of an extra acceleration term can be explained by change in added mass coefficient due to increase of turbulence in the gap between two cylinders. Chaotic flow regime in the upstream wake changes the added mass coefficient of the cylinder in comparison with the value suggested by Blevins [1]. Table 5.1 includes stream-wise and cross-flow added mass modification coefficient. It should be noted that new added

mass coefficient is dependent on the upstream vortex shedding which is controlled by Strouhal number St_1.

Table 5.1: Added mass modification coefficients obtained from curve fitting for different spacings.

L/D	A_X	B_Y
3.5	0.00007218	0.105
4	0.00009198	0.1207
5	0.000102	0.1103
8	0.0003643	0.0802
10	0.0003336	-0.04664
15	0.00008403	-0.1486
20	0.00007129	-0.1054

Figure 5.5 presents the simulation result with modified added mass for a range of reduced velocities and experimental result at corresponding spacing. Effect of the modification term on mathematical model appears to be similar to that of mass ratio. In section 4.4 it was observed that variation of mass ratio has a significant effect on the width of lock-in range response similar to what can be observed in figure 5.5. Since no experimental results on the cylinders response in tandem at very high Re is available, it cannot be concluded whether the actual response of trailing cylinder is galloping or would calm down at higher reduced velocities, U_r>25.

Nevertheless, oscillation amplitude predicted by the model is greater than experimental results. Additionally, variation in spacing has an insignificant effect on the oscillation amplitude which is in contrast with observations during the experimental investigation. Hence, it is necessary to address this issue through a damping term to control the excitation due to upstream vortices.

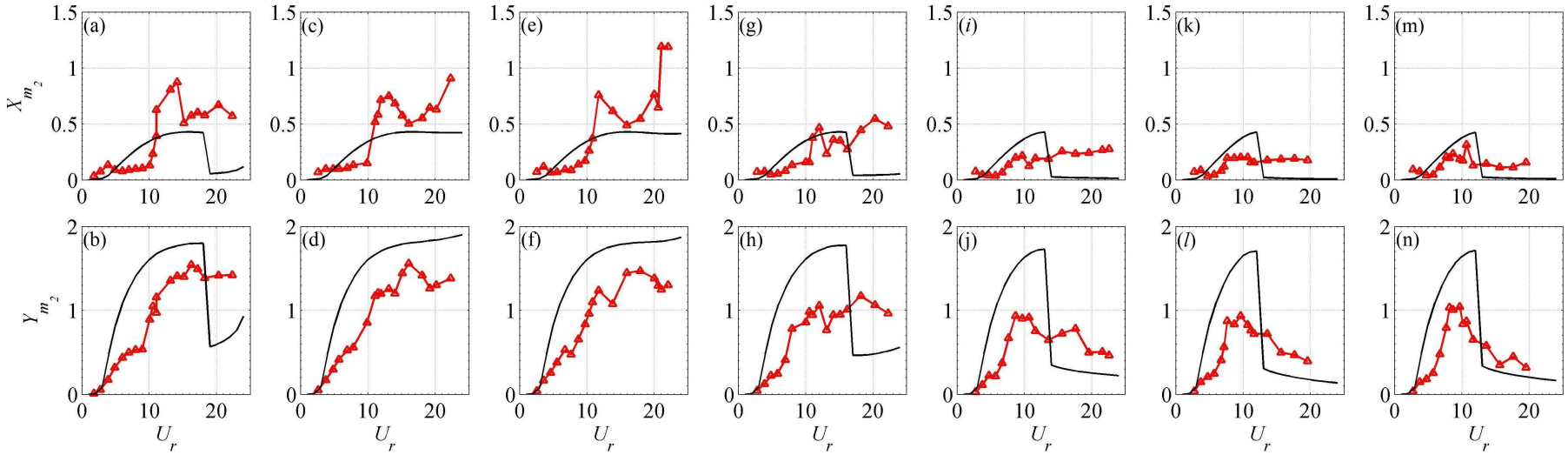

Figure 5.5: Experimental response amplitude (△) versus mathematical model simulation (Black solid line) at various reduced velocity and spacings. (a,b) $L/D = 3.5$, (c,d) $L/D = 4$, (e,f) $L/D = 5$, (g,h) $L/D = 8$, (i,j) $L/D = 10$, (k,l) $L/D = 15$, (m,n) $L/D = 20$.

5.4.2 Damping

The difference observed in figure 5.5 is not constant at various reduced velocities examined, at lower velocities model and experiment have a good agreement whereas intermediately higher velocities the model simulate larger oscillation amplitudes where at very high velocities it drops below experimental results. Such a behaviour is similar to VIV phenomenon itself which suggest that the secondary modification term should be limiting at medium and exciting at higher velocities. Hence, this conclusion can be drawn that this modification term should be a function of cylinders velocity alike the damping term on the left side of the structural motion equation.

A damping term can be considered as a modification term through a similar approach to the one considered for added mass. Such a term should be introduced to motion equation as a force since it is driven from the effect of upstream wake. Moreover, it is was observed in figure 3.19 that mean drag force is not zero for trailing cylinder similar to leading body hence term C_1 was added to the equation so that the difference from an isolated cylinder in mean drag can be considered.

Additionally, since this term is driven from the effect of upstream vortices it should be a function of their shedding frequency so the equation of motion becomes:

$$\begin{cases} M\ddot{X}_2 + (2\xi M\omega_n + \gamma\omega_s\rho D^2)\dot{X}_2 + kX_2 = \frac{1}{2}\rho U^2 D C_D + \frac{1}{2}\rho U^2 D\left(A_X\frac{\ddot{X}_2}{D{\omega_s}^2} + E_X\frac{\dot{X}_2}{D\omega_s} + C_1\right) \\ M\ddot{Y}_2 + (2\xi M\omega_n + \gamma\omega_s\rho D^2)\dot{Y}_2 + kY_2 = \frac{1}{2}\rho U^2 D C_L + \frac{1}{2}\rho U^2 D\left(B_Y\frac{\ddot{Y}_2}{D{\omega_s}^2} + F_Y\frac{\dot{Y}_2}{D\omega_s}\right) \end{cases} \tag{5.7}$$

It should be noted that the reason added mass modification coefficient is a quadratic function of shedding frequency but not damping is that to be able to non-dimensionalise these function with time and distance. Therefore, after introducing two non-dimensional terms the equation 5.7 would be:

$$\begin{cases} \left(1 - \frac{1}{2}\frac{A_X}{\mu St^2}\right)\ddot{x}_2 + \left(2\xi + \frac{\omega_0}{\mu}\left(\gamma - \frac{E_X}{2St^2}\right)\right)\dot{x}_2 + x_2 = a_D\left(p_2 + C_1\right) \\ \left(1 - \frac{1}{2}\frac{B_X}{\mu St^2}\right)\ddot{y}_2 + \left(2\xi + \frac{\omega_0}{\mu}\left(\gamma - \frac{F_Y}{2St^2}\right)\right)\dot{y}_2 + y_2 = a_L q_2 \end{cases} \tag{5.8}$$

Figure 5.6 shows the full SimuLink model of equation 5.8 coupled with van der Pol wake oscillator. It should be noted that this SimuLink model is the full and final model in this study which includes non-linearities from oscillating in two directions and the wake (section 4.3.2).

Value of these three new constants should be determined through a optimisation process in such a way that the difference between experimental results and model simulation becomes minimum.

5.5 Optimisation

Objective of optimisation was to determine the values of E_X, F_Y and C_1 so that the difference between mathematical model simulation and experimental results would be minimized. As the first step, optimisation function (equation 5.9) was designed in such a way that optimisation process could minimize the accumulative error between experiment and model simulation at each velocity in cross-flow direction. Moreover, the error function was limited to transverse direction firstly for the sake of simplicity and secondly, it was observed in chapter 4 and by Srinil and Zanganeh [26] that stream-wise simulation is heavily influenced by cross-flow results hence every change in cross-flow model could significantly alter the simulation in either directions while it is not the case for stream-wise model. Therefore, optimisation in cross-flow motion could be sufficient.

$$e = \frac{\sum |A_{Y_2} - y_2|}{n} \tag{5.9}$$

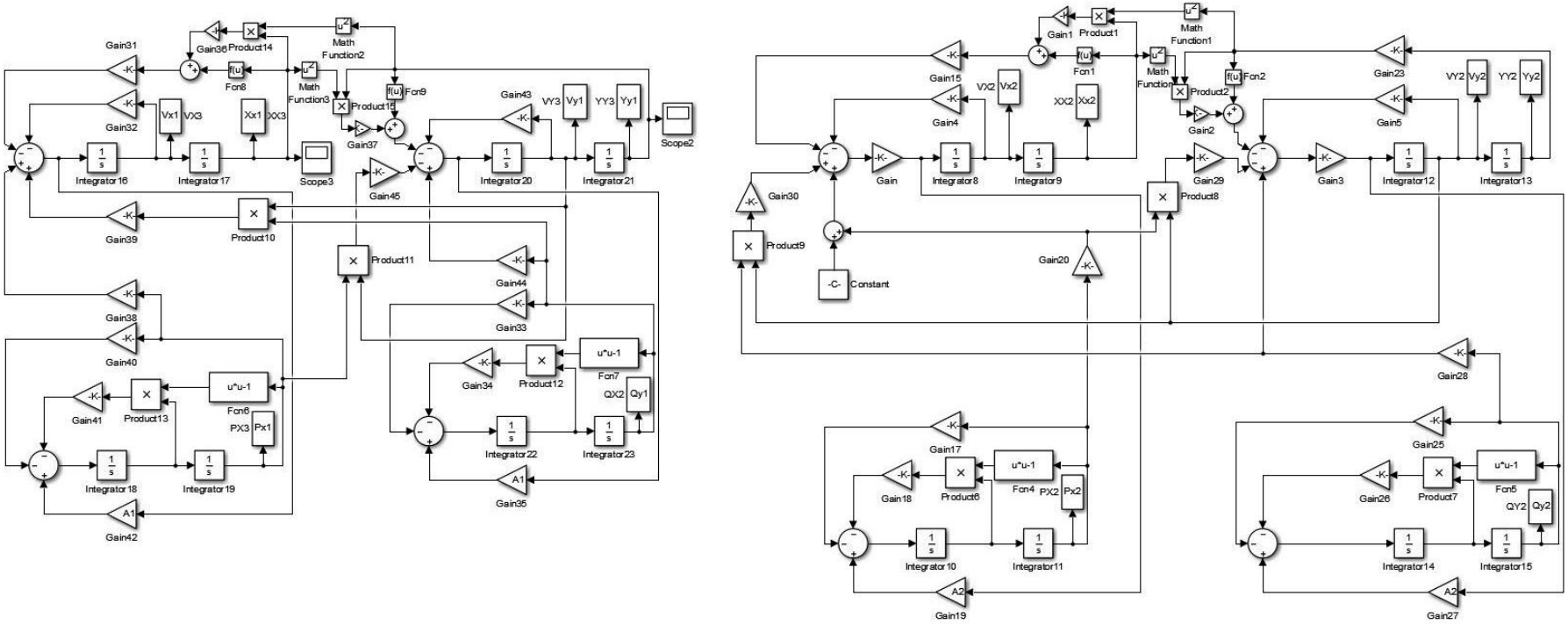

Figure 5.6: Fully modified Duffing oscillator equation with added mass and damping terms coupled with van der Pol wake oscillator for two identical cylinders in tandem

After determining error function, *fminsearch* command in Matlab software was used for optimisation. This command can calculate the local minimum of a discontinuous function with multi-variables using the derivative-free method. The algorithm used for fminsearch is Nelder-Mead simplex algorithm discussed in Lagarias et al. [78]. There was no constraint set for the error function or any of variables. Also, fminsearch command requires no constraint for optimisation function. Moreover, an initial guess was provided for (E_X, F_Y, C_1) in fminsearch code which was considered (0,0,0) for initial spacing of $L/D = 3.5$ and then its optimisation results was used as the initial guess for the next spacing and so on. Options chosen for optimisation can be seen in table 5.2. It should be noted that fminsearch terminates optimisation process when both conditional tolerances on variables and function value are satisfied simultaneously.

Table 5.2: Options and their designated values for optimisation

Option	Value
Maximum number of function evaluations	1e6
Termination tolerance on variables	1e-6
Termination tolerance on the function value	1e-4

The result of optimisation can be seen in table 5.3 with their corresponding spacing. Figure 5.7 demonstrated simulation results using table 5.3 values in equation 5.8.

Table 5.3: Optimisation output for three modification parameter of E_X, F_Y and C_1

L/D	E_X	F_Y	C_1
3.5	0.7042	-0.1598	-31.0758
4	0.5947	-0.1788	-29.444
5	0.6152	-0.1878	-30.5058
8	0.2066	-0.2980	-26.8924
10	0.2398	-0.4318	-18.8942
15	0.0933	-0.4552	-17.2843
20	0.0929	-0.4191	-14.0297

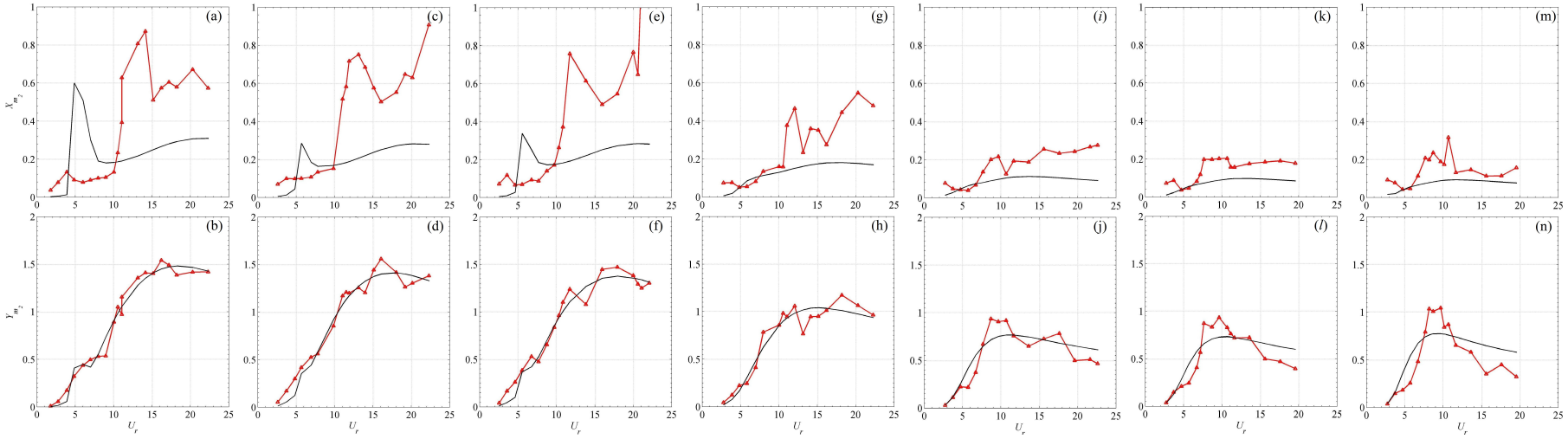

Figure 5.7: Experimental response amplitude (△) versus fully modified mathematical model simulation (Black solid line) at vs. reduced velocity and spacings. (a,b) $L/D = 3.5$, (c,d) $L/D = 4$, (e,f) $L/D = 5$, (g,h) $L/D = 8$, (i,j) $L/D = 10$, (k,l) $L/D = 15$, (m,n) $L/D = 20$.

It can be observed that mathematical model has a good agreement with experimental data in cross-flow direction, however, their agreement with stream-wise response is relatively poor. Moreover, if the capability of model in simulation of downstream FIV response is to be evaluated by its ability to accurately simulate four parameters of lock-in range width, velocities at which lock-in onsets, maximum amplitude occurs and its magnitude, following observations can be made:

- Velocity onset of lock-in range is predicted correctly for both cylinders.
- Lock-in range width is simulated successfully for both cylinders. However, it is less accurate for the trailing cylinder in very large spacings.
- Reduced velocity at which maximum amplitude occurs is predicted accurately for both cylinders at all spacings.
- Magnitudes of oscillation amplitude at corresponding reduced velocities are simulated successfully comparing with existing mathematical models for an isolated cylinder [26, 27]. Although it is evident that the model under-predicts the results, nevertheless, the error is less than that of existing models in the literature for a single cylinder. Table 5.4 compares the overall error of the model against experimental results at different spacings for both cylinders.

Table 5.4: Value of error between experimental and modelling results for leading and trailing cylinders.

	Leading cylinder			Trailing cylinder		
L/D	e_y	e_x	e_t	e_y	e_x	e_t
3.5	0.6225	0.4978	0.4978	0.1689	1.25	1.214
4	0.4599	0.7385	0.9489	0.1723	0.6759	0.7238
5	0.4038	0.4409	0.6769	0.1761	0.8509	0.8984
8	0.7135	0.6125	0.4308	0.1637	0.4975	0.1383
10	0.5373	0.3756	0.2337	0.2130	0.4752	0.1504
15	0.8432	1.1705	0.6973	0.2475	0.4746	0.1509
20	0.7573	0.7262	0.12203	0.3782	0.4725	0.6956

This error is the variance between experimental results and values predicted by the analytical model.

- The first peak in cross-flow response of the trailing cylinder is captured by the model as well. However, it disappears earlier in model simulation as the spacing grows large, in comparison with experimental result which could be due to under-prediction.

- The reduction of amplitude due to increase in spacing can be captured by model successfully.

Figure 5.7 includes the total response of the trailing cylinder which consists of VIV motion and displacement induced by wake instability. However, if the motion caused by wake instability was to be eliminated as it was discussed in section 3.5.1 (figure 3.22) and model was compared with solely VIV motion response component of the experimental result, model simulation could be more appreciated. Figure 5.8 provides such a comparison. It is clear that under-prediction problem in simulation results is no longer an issue.

Moreover, simulation in stream-wise direction is more successful. Although it fails to capture the maximum amplitude value in this direction, the behaviour of the cylinder is captured in all spacings. As mentioned in previous chapter, cross-flow model has a significant affect on stream-wise response. Hence, the large pick at approximately $U_r = 6$ at small spacings occurs due to existence of a peak in cross-flow response at the corresponding reduced velocity. It is observed that this peak disappears at large spacings where the cross-flow response peak at low reduced velocities does not exist.

5.6 Final model

At this stage model simulation has been compared against experiment at seven different spacings it is possible to introduce universal modification coefficients for added mass and damping where they are function of the distance between two cylinders as

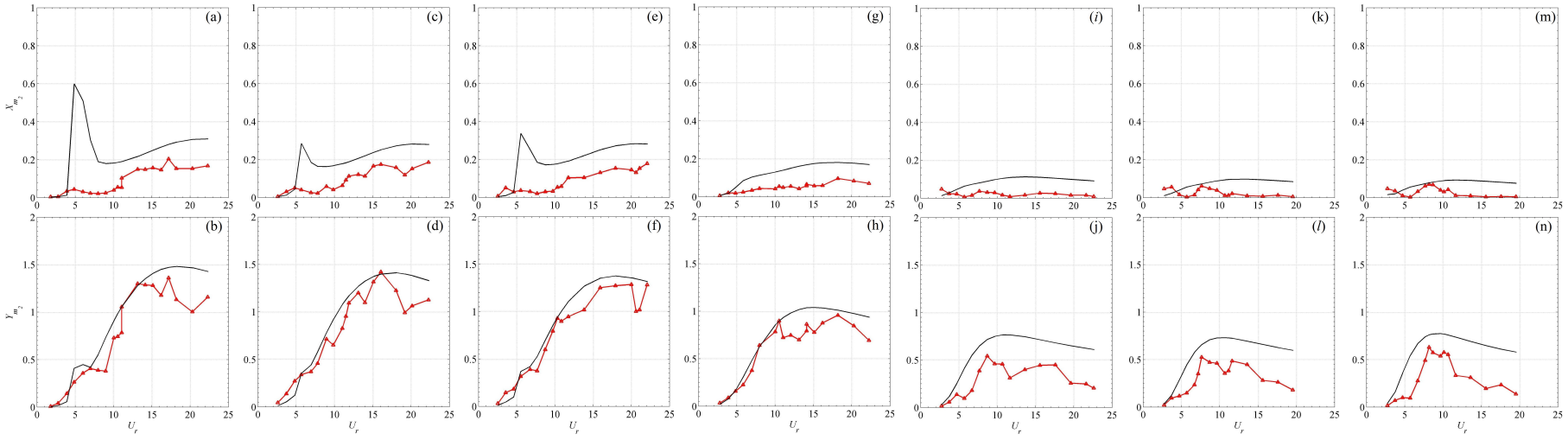

Figure 5.8: Experimental VIV response amplitude (△) versus fully modified mathematical model simulation (Black solid line) at various reduced velocity and spacings. (a,b) $L/D = 3.5$, (c,d) $L/D = 4$, (e,f) $L/D = 5$, (g,h) $L/D = 8$, (i,j) $L/D = 10$, (k,l) $L/D = 15$, (m,n) $L/D = 20$.

it is shown in equation 5.10.

$$\begin{cases} A_X = f(L/D) \\ B_Y = f(L/D) \\ E_X = f(L/D) \\ F_Y = f(L/D) \\ C_1 = f(L/D) \end{cases} \tag{5.10}$$

Such a task can be accomplished by curve fitting to seven values of each parameter that were obtained in previous section (table 5.1 and 5.3). Figure 5.9 demonstrate result of Gaussian function fitted to those four values and a linear function to C_1. result of the curve fitting process can be found in table 5.5.

Table 5.5: Modification coefficients as a function of spacing

Coefficient	Expression
A_X	$0.0004228 \exp\left(-\left(\frac{L/D-8}{2.627}\right)^2\right)$
B_Y	$0.1267 \exp\left(-\left(\frac{L/D-5.018}{3.152}\right)^2\right)$
E_X	$2.605 \times 10^{209} \exp\left(-\left(\frac{L/D+5242}{238.8}\right)^2\right)$
F_Y	$-0.484 \exp\left(-\left(\frac{L/D-15.37}{11.25}\right)^2\right)$
C_1	$1.0908\frac{L}{D} - 34.224$

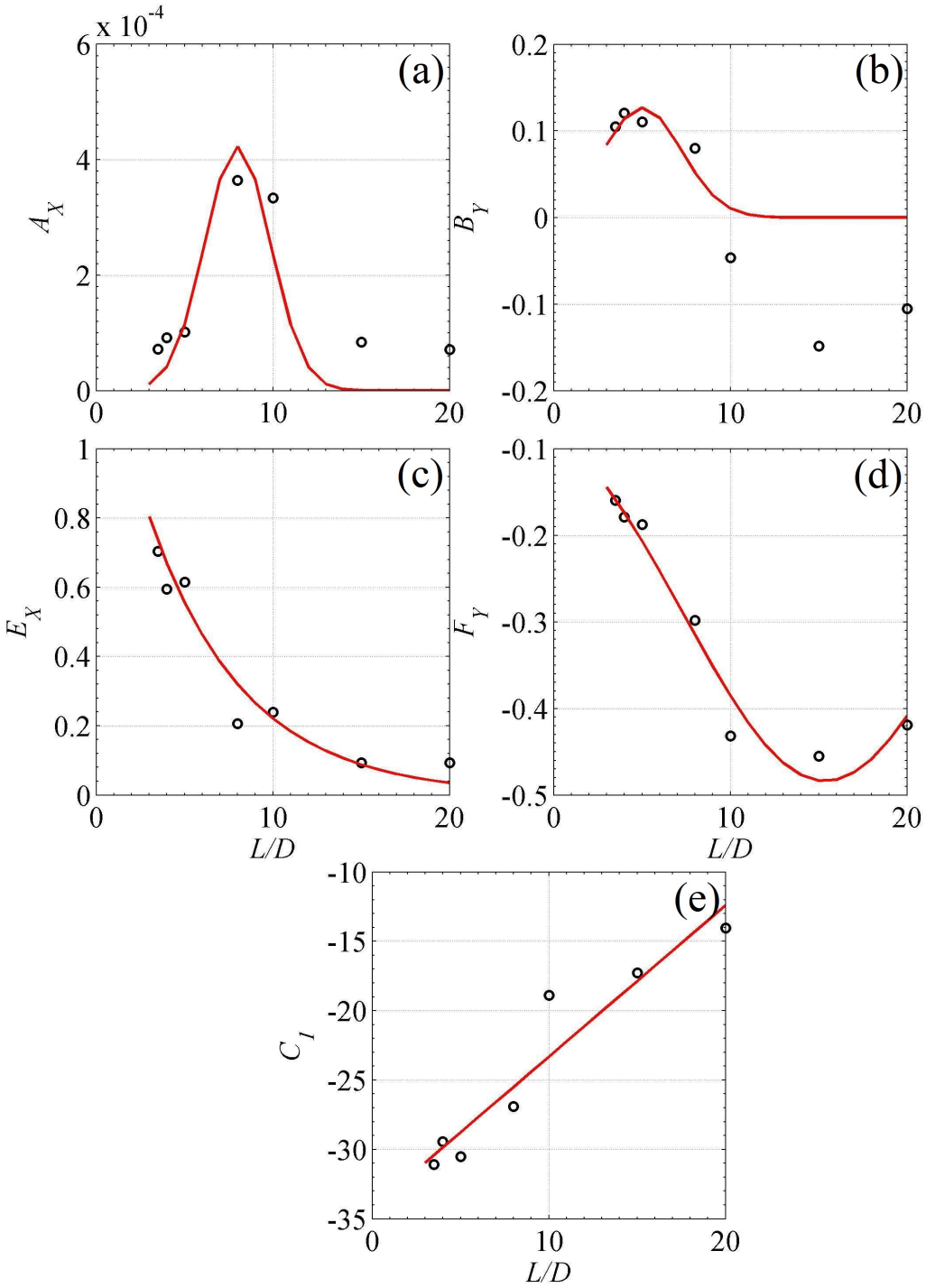

Figure 5.9: Modification coefficients (○) curve fitting results to Gaussian function (red solid line). (a) A_X, (b) B_Y, (c)E_X, (d)F_Y and (e) linear function to C_1.

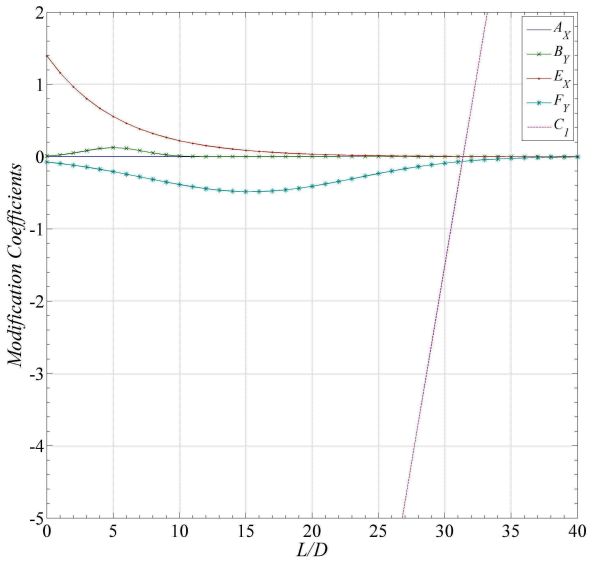

Figure 5.10: Variation of modification coefficients as a function of spacing

Moreover, figure 5.10 depicts the variation of each coefficient as the gap between two cylinders changes. Based on the experimental data it is not clear at what distance influence of upstream wake is insignificant and trailing cylinder behaves as an isolated body, however the fact that all coefficients reach zero at large spacings (approximately $32D$) is reaffirmed.

5.7 Conclusion

The main objective of this chapter was to improve the mathematical model obtained in chapter 4, so that it can simulate the response amplitude of the trailing cylinder more accurately.

- It was concluded that the objective of this chapter could be achieved by adding two modification terms to adjust the added mass coefficient and added fluid damping so that they account the effect of upstream wake instability.

- Hydrodynamic forces applied to leading and trailing cylinders were calculated from experimental data through a simple motion equation for a rigid body. The difference between upstream and downstream hydrodynamic forces was calculated to reveal the additional force due to upstream wake instability. Several functions of upstream displacement, downstream acceleration and velocity were fitted to

this variation.

- It was concluded that acceleration of trailing cylinder governs this extra force. Since the source of this force was upstream vortices, a linear equation was fitted to the wake force as a function of $A_X \frac{\ddot{X}_2}{D{\omega_s}^2}$ and $B_Y \frac{\ddot{Y}_2}{D{\omega_s}^2}$. New modification function was considered as a force in duffing oscillator equation.

- By rearranging the equation and moving the function to left-hand side of the equation it revealed that the new function changes the added mass from a constant suggested by Blevins [1] to a variable depending on the upstream shedding frequency and distance between two cylinders.

- It was observed from simulation results obtained from the new model that predicted maximum amplitude is significantly higher than that obtained from the experiment. It was concluded that this discrepancy is due to increase of damping caused by the turbulent flow in the wake. In order to adjust the damping, a secondary force modification term was added to the left side of Duffing equation $\frac{\dot{X}_2}{D\omega_s}$ and $\frac{\dot{Y}_2}{D\omega_s}$.

- Values of the modification functions for each spacing were derived through optimisation of the error between experimental and simulation results. It should be mentioned that optimisation was carried out by fminsearch command in Matlab software with no constraint on the function value or any of the variables.

- In order to conclude and introduce a universal model through which any spacing can be simulated a Gaussian function with variable of spacing was fitted to each added mass and damping modification coefficients. The function acquired through this method can be used to calculate the value of modification coefficients in any given spacing.

Chapter 6

Conclusion

This study tried to offer a better understanding of a pair of cylinders behaviour in a flow stream. Two cylinders were considered to be in line and free to oscillate in stream-wise and cross-flow directions. The model was examined through two methods, experimental investigation and mathematical modelling. The main objective of the study was to observe the effect of spacing between two cylinders on the response of each cylinder. Experimental investigation was conducted in two occasions on identical and non-identical pair of cylinders at various spacings. Two cylinders were towed at several reduced velocities at each spacing so that the effect of Re on the cylinders response could be observed. Additionally, further investigation was conducted to observe the effect of natural frequency on the behaviour of non-identical cylinders (two sets of similar structures but with 15 and 30% of difference in their natural frequencies).
A mathematical model was developed using a structural dynamic equation coupled with van der Pol wake oscillator. The downstream wake oscillator was modified to capture the effect of upstream wake on the trailing cylinder.
After these investigations these following remarks can be drawn:

6.1 Concluding remarks

6.1.1 Experimental Investigation

- Throughout the experiment it was observed that leading cylinder response is similar to that of an isolated cylinder. Based on the obtained results, it is not

possible to determine whether this behaviour is due to strong wake force or vortex formation in the gap. Due to limitation that 2Dof test set-up it was not possible to conduct the experiment at any smaller spacing where two fixed cylinder had been observed to generate only one wake.

- Trailing Cylinder response was observed to be excited by two mechanisms. This conclusion were drawn by observing time history of trailing cylinder where two different motions with distinct high and low frequencies were detectable. By separating the high and low frequencies from each other, it was observed that high frequency motion was excited by separation of vortices where the low frequency counterpart was excited by buffeting upstream vortices. Moreover, it was noted that VIV is the dominant motion in cross-flow direction while WIV is overriding in stream-wise.

- Contribution of two excitation mechanisms to total response varies as the distance between cylinders grow larger. WIV motion builds up a larger portion of response in small and medium spacings which resulted in reduction of response amplitude with increase of spacing, while flow velocity increased in the gap and an increase of amplitude was expected. At the largest spacing, total fade of WIV was observed and response amplitude starts to rise again.

- Frequency of VIV motion did not depend on spacing and followed the same trend as an isolated cylinder. Downstream cylinder oscillation frequency was dictated by its leading counterpart up to the end of lock-in range after which it broke away and continued to oscillate at lower frequency due to lower flow velocity in the gap. However, in cases that trailing cylinder had higher natural frequency, this difference was not clear.

- Similar natural frequency in the first set-up led to multiple peaks in amplitude response graph of trailing cylinder. Additional to dominant peak which occurred at higher reduced velocity than that of leading cylinder, there is another peak that occurred at a lower reduced velocity, corresponding to high amplitude in upstream lock-in range, which was excited by buffeting vortices with frequency

equal to trailing cylinder natural frequency.

6.1.2 Mathematical Modelling

- It can be concluded that the non-linearity observed by Srinil and Zanganeh [26], which was explained by geometrical non-linearity of spring system, is due to wake since this phenomenon was noted in this study as well although no spring was utilised and apparatus was designed in a way that stiffness was omnidirectional. Nevertheless, suggested quadratic terms to account for this non-linearity in modelling were still valid for this study.

- Through curve fitting, it was concluded that the effect of upstream wake on the trailing cylinder is a function of cylinder acceleration which can be interpreted as modification of the added mass coefficient. A linear function of acceleration was considered to modify force term in the equation of motion.

- It was concluded that fluid added damping is significantly influenced in the upstream wake in comparison to a body in an undisturbed flow. It was assumed that this variation could be addressed by a modification of force term as well. A linear function of cylinder speed was considered which its value was determined by optimising the difference between mathematical model and experimental results of each spacing.

- It was assumed that upstream wake could be characterised by shedding frequency of the leading cylinder and distance from its centre. After non-dimensionalising the modified equation of motion, Strouhal number was appeared in the new acceleration term. Therefore, both modification coefficients (acceleration and velocity) was assumed to be a function of distance.

6.2 Future studies

Despite broad application of multiple bodies in close proximity this area is relatively under explored. Mostly, in industrial practice it is assumed that each body is oscillating independently as an isolated cylinder. In this regard, the author found the following subjects suitable suggestions to be explored and to offer a better understanding of the topic and take this study forward.

- Further free oscillation experimental investigation on un-identical cylinders with different physical properties such as external diameter or mass ratio.
- Further free oscillation experimental investigation on identical cylinders to measure the pressure distribution on the surface of the trailing cylinder.
- Further forced oscillation experimental investigation so that a better understanding of variation in added mass due to turbulent flow could be obtained.
- Further flow visualisation (using experimental results or CFD) in order to find a better understanding of fundamental mechanics.
- Experimental investigation on the effectiveness of standard VIV suppression devices such as strakes, fairings etc.
- Investigation on the fatigue damage rate of structure undergoing free vibration such as that observed in this study.
- Comparison between the obtained results in this study (modelling and experiment) and CFD model of this phenomenon.
- Expansion of the mathematical model for flexible structures to observe the effect of spacing on the oscillation mode.
- Effect of marine growth (surface roughness) on VIV and WIV.
- Investigation on the merits of three-spring supported pendulum system to existing concept with four springs in FIV (VIV and/or WIV) tests.

Appendix A

Static analysis of supporting rods with various length

Table A.1: Bending moment and deflection of an aluminium rod with length of $L_r = 1.5m$ and Diameter of $D_r = 0.01905mm$ due to static drag force at various flow velocities.

U_r	$V(m/s)$	Drag (N/m)	Rod Deflection(m)	Deflection angle	Maximum Deflection(m)	Maximum Stress(Pa)	Furthest Point(m)
1	0.08239	0.448015399	0.001694876	0.044289568	0.165008705	48.19904262	0.174546009
2	0.16478	1.792061594	0.006779502	0.177158273	0.165139219	48.23716587	0.176522099
2.25	0.1853775	2.268077955	0.008580307	0.22421594	0.165222945	48.26162234	0.177262155
2.5	0.205975	2.800096241	0.010592972	0.276809802	0.165339684	48.29572166	0.17811365
2.75	0.2265725	3.388116452	0.012817496	0.334939861	0.165497094	48.34170124	0.179084281

3	0.24717	4.032138587	0.01525388	0.398606115	0.165703593	48.40201962	0.180182325
4	0.32956	7.168246378	0.027118009	0.708633094	0.167213595	48.84309114	0.186030207
4.5	0.370755	9.072311822	0.03432123	0.896863759	0.168531738	49.22812076	0.189963243
5	0.41195	11.20038497	0.042371889	1.107239209	0.170353682	49.76031049	0.194675261
5.25	0.4325475	12.34842442	0.046715007	1.220731228	0.171485544	50.09092748	0.197347893
5.5	0.453145	13.55246581	0.051269985	1.339759443	0.172781976	50.46961532	0.200244164
5.75	0.4737425	14.81250912	0.056036823	1.464323854	.17425592	50.9001541	0.203373028
6	0.49434	16.12855435	0.06101552	1.594424461	0.175920134	51.38627121	0.206742975
6.25	0.5149375	17.50060151	0.066206076	1.730061264	0.177787076	51.93160498	0.210361976
6.5	0.535535	18.92865059	0.071608492	1.871234263	0.179868775	52.53966907	0.214237427
7	0.57673	21.95275453	0.083048902	2.17018885	0.184721737	53.95721934	0.222784201
8	0.65912	28.67298551	0.108472035	2.834532375	0.19746185	57.67860649	0.243210759
9	0.74151	36.28924729	0.137284919	3.587455037	0.214644238	62.69758199	0.268273918
10	0.8239	44.80153986	0.169487554	4.428956836	0.236539703	69.09324726	0.298082057
11	0.90629	54.20986323	0.205079941	5.359037772	0.263216227	76.88545991	0.332639447
12	0.98868	64.5142174	0.244062078	6.377697844	0.294603629	86.05371998	0.371887441
13	1.07107	75.71460236	0.286433967	7.484937053	0.33055925	96.55635679	0.415737233

14	1.15346	87.81101813	0.332195607	8.680755399	0.370916326	108.3446589	0.464091477
15	1.23585	100.8034647	0.381346998	9.965152882	0.415512373	121.3711643	0.516856479
16	1.31824	114.691942	0.433888139	11.3381295	0.464202453	135.5935366	0.573947932
17	1.40063	129.4764502	0.489819032	12.79968526	0.516863313	150.9757738	0.635292828
18	1.48302	145.1569891	0.549139676	14.34982015	0.573392871	167.4880575	0.700829326
19	1.56541	161.7335589	0.611850072	15.98853418	0.633707748	185.1060332	0.770505704
20	1.6478	179.2061594	0.677950218	17.71582735	0.69774028	203.8099357	0.844278982

Table A.2: Bending moment and deflection of an aluminium rod with length of $L_r = 2m$ and Diameter of $D_r = 0.01905mm$ due to static drag force at various flow velocities.

U_r	$V(m/s)$	Drag (N/m)	Rod Deflection(m)	Deflection angle	Maximum Deflection(m)	Maximum Stress(Pa)	Furthest Point(m)
1	0.048752	0.156865995	0.001289441	0.020852286	0.165005038	27.11135907	0.174273614
2	0.097504	0.627463981	0.005157762	0.083409146	0.165080594	27.12377335	0.175355283
2.25	0.109692	0.794134101	0.006527793	0.1055647	0.165129077	27.13173941	0.175751417
2.5	0.12188	0.98041247	0.008059004	0.13032679	0.165196693	27.14284922	0.17620214
2.75	0.134068	1.186299089	0.009751394	0.157695416	0.165287899	27.15783492	0.176710037
3	0.146256	1.411793957	0.011604965	0.187670578	0.165407603	27.17750301	0.177277927
4	0.195008	2.509855924	0.020631049	0.333636583	0.166284816	27.32163463	0.180213154
4.5	0.219384	3.176536404	0.026111172	0.422258801	0.167053265	27.44789549	0.182128698
5	0.24376	3.921649882	0.032236014	0.521307162	0.168119483	27.62308183	0.184384279
5.25	0.255948	4.323618994	0.035540206	0.574741146	0.1687842	27.73229899	0.185649893
5.5	0.268136	4.745196357	0.039005577	0.630781666	0.169547737	27.85775283	0.187013014
5.75	0.280324	5.186381968	0.042632129	0.689428721	0.170418598	28.0008407	0.188477901
6	0.292512	5.64717583	0.046419861	0.750682313	0.171405378	28.16297481	0.190048816
6.25	0.3047	6.12757794	0.050368772	0.81454244	0.172516704	28.34557272	0.191730003
6.5	0.316888	6.6275883	0.054478864	0.881009103	0.173761177	28.55004739	0.193525661

7	0.341264	7.686433768	0.063182588	1.021762037	0.176683444	29.03019414	0.197476849
8	0.390016	10.0394237	0.082524196	1.334546334	0.18448643	30.31227355	0.206927973
9	0.438768	12.70614562	0.104444686	1.689035204	0.1952785	32.085478	0.218630664
10	0.48752	15.68659953	0.128944057	2.085228646	0.209407664	34.40698802	0.232767766
11	0.536272	18.98078543	0.156022309	2.523126662	0.227085801	37.31161634	0.249470194
12	0.585024	22.58870332	0.185679442	3.002729251	0.248398581	40.8134394	0.268818535
13	0.633776	26.5103532	0.217915456	3.524036413	0.273335227	44.91068607	0.290850352
14	0.682528	30.74573507	0.252730352	4.087048147	0.30182384	49.59154338	0.315570229
15	0.73128	35.29484893	0.290124128	4.691764455	0.333761906	54.83916713	0.342960002
16	0.780032	40.15769479	0.330096786	5.338185335	0.369037787	60.63521484	0.372987604
17	0.828784	45.33427263	0.372648325	6.026310788	0.407543585	66.96195819	0.405613844
18	0.877536	50.82458247	0.417778745	6.756140815	0.449181566	73.8033387	0.440797164
19	0.926288	56.62862429	0.465488046	7.527675414	0.493866501	81.14535274	0.47849668
20	0.97504	62.74639811	0.515776228	8.340914586	0.541525731	88.97606211	0.518673955

References

[1] R. D. Blevins, *Flow–induced vibration.* New York, NY (USA); Van Nostrand Reinhold Co., Inc.

[2] J. H. Gerrard, "The mechanics of the formation region of vortices behind bluff bodies," *Journal of Fluid Mechanics*, vol. 25, pp. 401–413, 6 1966. [Online]. Available: http://journals.cambridge.org/article_S0022112066001721

[3] K. H. Halse, *On Vortex shedding and prediction of Vortex induced vibrations of circular cylinders.* Norges Teknisk Naturvitenskapelige Universitet: Department of Marine Structures, 1977.

[4] P. W. Bearman, "On vortex street wakes," *Journal of Fluid Mechanics*, vol. 28, pp. 625–641, 6 1967. [Online]. Available: http://journals.cambridge.org/article_S0022112067002368

[5] B. M. Sumer and J. Fredsøe, *Hydrodynamics around cylindrical structures.* World Scientific, 1997, vol. 12.

[6] M. Zdravkovich, *Flow around Circular Cylinders; Volume 1. Fundamentals.* Oxford Science Press, 1997.

[7] R. Govardhan and C. H. K. Williamson, "Modes of vortex formation and frequency response of a freely vibrating cylinder," *Journal of Fluid Mechanics*, vol. 420, pp. 85–130, 10 2000. [Online]. Available: http://journals.cambridge.org/article_S0022112000001233

[8] R. Gabbai and H. Benaroya, "An overview of modeling and experiments of vortex-induced vibration of circular cylinders," *Journal of Sound and*

Vibration, vol. 282, no. 35, pp. 575 – 616, 2005. [Online]. Available: http://www.sciencedirect.com/science/article/pii/S0022460X04004845

[9] C. Williamson, , and R. Govardhan, "Vortex-induced vibrations," *Annual Review of Fluid Mechanics*, vol. 36, no. 1, pp. 413–455, 2004. [Online]. Available: http://dx.doi.org/10.1146/annurev.fluid.36.050802.122128

[10] R. King, "Vortex excited oscillations of yawed circular cylinders," *ASME.J. Fluids Eng*, vol. 99(3), pp. 495–501, 1977.

[11] A. Khalak and C. Williamson, "Motions, forces and mode transitions in vortex-induced vibrations at low mass-damping," *Journal of Fluids and Structures*, vol. 13, no. 78, pp. 813 – 851, 1999. [Online]. Available: http://www.sciencedirect.com/science/article/pii/S0889974699902360

[12] K. Vikestad, J. Vandiver, and C. Larsen, "Added mass and oscillation frequency for a circular cylinder subjected to vortex-induced vibrations and external disturbance," *Journal of Fluids and Structures*, vol. 14, no. 7, pp. 1071 – 1088, 2000. [Online]. Available: http://www.sciencedirect.com/science/article/pii/S0889974600903086

[13] R. Govardhan and C. H. K. Williamson, "Resonance forever: existence of a critical mass and an infinite regime of resonance in vortex-induced vibration," *Journal of Fluid Mechanics*, vol. 473, pp. 147–166, 12 2002. [Online]. Available: http://journals.cambridge.org/article_S0022112002002318

[14] R. Govardhan and C. Williamson, "Critical mass in vortex-induced vibration of a cylinder," *European Journal of Mechanics - B/Fluids*, vol. 23, no. 1, pp. 17 – 27, 2004, bluff Body Wakes and Vortex-Induced Vibrations. [Online]. Available: http://www.sciencedirect.com/science/article/pii/S0997754603000852

[15] R. D. Blevins and C. S. Coughran, "Experimental investigation of vortex-induced vibration in one and two dimensions with variable mass, damping, and reynolds number," *Journal of Fluids Engineering*, vol. 131, no. 10, p. 101202, 2009.

[16] T. Sarpkaya, "Fluid forces on oscillating cylinders," *NASA STI/Recon Technical Report A*, vol. 78, pp. 275–290, Aug. 1978.

[17] J. K. Vandiver, "Drag coefficients of long flexible cylinders," in *Offshore technology conference*. Offshore Technology Conference, 1983.

[18] R. E. D. Bishop and A. Y. Hassan, "The lift and drag forces on a circular cylinder oscillating in a flowing fluid," *Proceedings of the Royal Society of London A: Mathematical, Physical and Engineering Sciences*, vol. 277, no. 1368, pp. 51–75, 1964. [Online]. Available: http://rspa.royalsocietypublishing.org/content/277/1368/51

[19] C. Williamson and R. Govardhan, "A brief review of recent results in vortex-induced vibrations," *Journal of Wind Engineering and Industrial Aerodynamics*, vol. 96, no. 67, pp. 713 – 735, 2008, 5th International Colloquium on Bluff Body Aerodynamics and Applications. [Online]. Available: http://www.sciencedirect.com/science/article/pii/S0167610507001262

[20] T. Sarpkaya, "A critical review of the intrinsic nature of vortex-induced vibrations," *Journal of Fluids and Structures*, vol. 19, no. 4, pp. 389 – 447, 2004. [Online]. Available: http://www.sciencedirect.com/science/article/pii/S0889974604000350

[21] P. Bearman, "Circular cylinder wakes and vortex-induced vibrations," *Journal of Fluids and Structures*, vol. 27, no. 56, pp. 648 – 658, 2011, {IUTAM} Symposium on Bluff Body Wakes and Vortex-Induced Vibrations (BBVIV-6). [Online]. Available: http://www.sciencedirect.com/science/article/pii/S0889974611000600

[22] G. Moe and Z. Wu, "The lift force on a cylinder vibrating in a current," *Journal of Offshore Mechanics and Arctic Engineering*, vol. 112, no. 4, pp. 297–303, 1990.

[23] T. Sarpkaya, "Hydrodynamic damping, flow-induced oscillations, and biharmonic response," *Journal of Offshore Mechanics and Arctic Engineering*, vol. 114, no. 4, pp. 232–238, 1995.

[24] R. Govardhan and C. H. K. Williamson, "Resonance forever: existence of a critical mass and an infinite regime of resonance in vortex-induced vibration," *Journal of Fluid Mechanics*, vol. 473, pp. 147–166, Dec. 2002.

[25] N. Jauvtis and C. H. K. Williamson, "The effect of two degrees of freedom on vortex-induced vibration at low mass and damping," *Journal of Fluid Mechanics*, vol. 509, pp. 23–62, 6 2004. [Online]. Available: http://journals.cambridge.org/article_S0022112004008778

[26] N. Srinil and H. Zanganeh, "Modelling of coupled cross–flow/in-line vortex-induced vibrations using double duffing and van der pol oscillators," *Ocean Engineering*, vol. 53, pp. 83 – 97, 2012. [Online]. Available: http://www.sciencedirect.com/science/article/pii/S0029801812002296

[27] M. Facchinetti, E. de Langre, and F. Biolley, "Coupling of structure and wake oscillators in vortex–induced vibrations," *Journal of Fluids and Structures*, vol. 19, no. 2, pp. 123 – 140, 2004. [Online]. Available: http://www.sciencedirect.com/science/article/pii/S0889974603001853

[28] H. Zanganeh, "Modelling and analysis of vortex-induced vibrations of rigid and flexible cylinders," Ph.D. dissertation, University of Strathclyde, 2015.

[29] M. Zdravkovich, "The effects of interference between circular cylinders in cross flow," *Journal of Fluids and Structures*, vol. 1, no. 2, pp. 239 – 261, 1987. [Online]. Available: http://www.sciencedirect.com/science/article/pii/S0889974687903550

[30] D. Sumner, S. J. Price, and M. P. Padoussis, "Flow-pattern identification for two staggered circular cylinders in cross-flow," *Journal of Fluid Mechanics*, vol. 411, pp. 263–303, 5 2000. [Online]. Available: http://journals.cambridge.org/article_S0022112099008137

[31] D. Sumner, M. Richards, and O. Akosile, "Two staggered circular cylinders of equal diameter in cross-flow," *Journal of Fluids and Structures*, vol. 20, no. 2, pp. 255 – 276, 2005. [Online]. Available: http://www.sciencedirect.com/science/article/pii/S0889974604001331

[32] S. Huang and K. Herfjord, "Experimental investigation of the forces and motion responses of two interfering viv circular cylinders at various tandem and staggered positions," *Applied Ocean Research*, vol. 43, pp. 264 – 273, 2013. [Online]. Available: http://www.sciencedirect.com/science/article/pii/S0141118713000801

[33] S. Huang and A. Sworn, "Some observations of two interfering viv circular cylinders of unequal diameters in tandem," *Journal of Hydrodynamics, Ser. B*, vol. 23, no. 5, pp. 535 – 543, 2011. [Online]. Available: http://www.sciencedirect.com/science/article/pii/S1001605810601473

[34] D. Sumner, S. Wong, S. Price, and M. Padoussis, "Fluid behaviour of side-by-side circular cylinders in steady cross-flow," *Journal of Fluids and Structures*, vol. 13, no. 3, pp. 309 – 338, 1999. [Online]. Available: http://www.sciencedirect.com/science/article/pii/S0889974699902050

[35] P. W. Bearman and A. J. Wadcock, "The interaction between a pair of circular cylinders normal to a stream," *Journal of Fluid Mechanics*, vol. 61, pp. 499–511, 11 1973. [Online]. Available: http://journals.cambridge.org/article_S0022112073000832

[36] C. H. K. Williamson, "Evolution of a single wake behind a pair of bluff bodies," *Journal of Fluid Mechanics*, vol. 159, pp. 1–18, 10 1985. [Online]. Available: http://journals.cambridge.org/article_S002211208500307X

[37] T. Igarashi, "Characteristics of the flow around two circular cylinders arranged in tandem. I," *JSME International Journal Series B*, vol. 24, pp. 323–331, Feb. 1981.

[38] Y. Zhou and M. W. Yiu, "Flow structure, momentum and heat transport in a two-tandem-cylinder wake," *Journal of Fluid Mechanics*, vol. 548, pp. 17–48, 2 2006. [Online]. Available: http://journals.cambridge.org/article_S002211200500738X

[39] M. M. Alam, M. Moriya, and H. Sakamoto, "Aerodynamic characteristics of two side-by-side circular cylinders and application of wavelet analysis on the switching phenomenon," *Journal of Fluids and Structures*, vol. 18, no.

34, pp. 325 – 346, 2003, bluff-body/Flow interactions. [Online]. Available: http://www.sciencedirect.com/science/article/pii/S0889974603001075

[40] M. Alam, M. Moriya, K. Takai, and H. Sakamoto, "Fluctuating fluid forces acting on two circular cylinders in a tandem arrangement at a subcritical reynolds number," *Journal of Wind Engineering and Industrial Aerodynamics*, vol. 91, no. 12, pp. 139 – 154, 2003, fifth Asia-Pacific Conference on Wind Engineering. [Online]. Available: http://www.sciencedirect.com/science/article/pii/S0167610502003410

[41] T. Kitagawa and H. Ohta, "Numerical investigation on flow around circular cylinders in tandem arrangement at a subcritical reynolds number," *Journal of Fluids and Structures*, vol. 24, no. 5, pp. 680 – 699, 2008. [Online]. Available: http://www.sciencedirect.com/science/article/pii/S0889974607001028

[42] G. Xu and Y. Zhou, "Strouhal numbers in the wake of two inline cylinders," *Experiments in Fluids*, vol. 37, no. 2, pp. 248–256, 2004. [Online]. Available: http://dx.doi.org/10.1007/s00348-004-0808-0

[43] S. Ishigai, E. Nishikawa, K. Nishimura, and K. Cho, "Experimental study on structure of gas flow in tube banks with tube axes normal to flow : Part 1, karman vortex flow from two tubes at various spacings," *Bulletin of JSME*, vol. 15, no. 86, pp. 949–956, 1972.

[44] A. OKAJIMA, "Flows around two tandem circular cylinders at very high reynolds numbers," *Bulletin of JSME*, vol. 22, no. 166, pp. 504–511, 1979.

[45] F. HOVER and M. TRIANTAFYLLOU, "Galloping response of a cylinder with upstream wake interference," *Journal of Fluids and Structures*, vol. 15, no. 34, pp. 503 – 512, 2001. [Online]. Available: http://www.sciencedirect.com/science/article/pii/S0889974600903645

[46] Y. Yang, T. B. Aydin, and A. Ekmekci, "Flow past tandem cylinders under forced vibration," *Journal of Fluids and Structures*, vol. 44, pp. 292 – 309, 2014. [Online]. Available: http://www.sciencedirect.com/science/article/pii/S0889974613002454

[47] G. R. S. Assi, P. W. Bearman, and J. R. Meneghini, "On the wake-induced vibration of tandem circular cylinders: the vortex interaction excitation mechanism," *Journal of Fluid Mechanics*, vol. 661, pp. 365–401, 10 2010. [Online]. Available: http://journals.cambridge.org/article_S0022112010003095

[48] G. Papaioannou, D. Yue, M. Triantafyllou, and G. Karniadakis, "On the effect of spacing on the vortex–induced vibrations of two tandem cylinders," *Journal of Fluids and Structures*, vol. 24, no. 6, pp. 833 – 854, 2008. [Online]. Available: http://www.sciencedirect.com/science/article/pii/S0889974607001132

[49] T. Prasanth and S. Mittal, "Flow-induced oscillation of two circular cylinders in tandem arrangement at low re," *Journal of Fluids and Structures*, vol. 25, no. 6, pp. 1029 – 1048, 2009. [Online]. Available: http://www.sciencedirect.com/science/article/pii/S0889974609000450

[50] G. Assi, J. Meneghini, J. Aranha, P. Bearman, and E. Casaprima, "Experimental investigation of flow–induced vibration interference between two circular cylinders," *Journal of Fluids and Structures*, vol. 22, no. 67, pp. 819 – 827, 2006.

[51] J. Lin, R. Jiang, Z. Chen, and X. Ku, "Poiseuille flow-induced vibrations of two cylinders in tandem," *Journal of Fluids and Structures*, vol. 40, pp. 70 – 85, 2013. [Online]. Available: http://www.sciencedirect.com/science/article/pii/S088997461300087X

[52] J. Dahl, F. Hover, and M. Triantafyllou, "Two–degree–of–freedom vortex-induced vibrations using a force assisted apparatus," *Journal of Fluids and Structures*, vol. 22, no. 67, pp. 807 – 818, 2006.

[53] L. Shiau and M. A. T. Y. Yang, "Two–cylinder model for wind vortex–induced vibration," *Journal of Engineering Mechanics*, vol. 113, no. 5, pp. 780–789, 1987. [Online]. Available: http://dx.doi.org/10.1061/(ASCE)0733-9399(1987)113:5(780)

[54] N. Srinil, H. Zanganeh, and A. Day, "Two-degree-of-freedom viv of circular cylin-

der with variable natural frequency ratio: Experimental and numerical investigations," *Ocean Engineering*, vol. 73, pp. 179 – 194, 2013.

[55] S. Rao, *Vibration of Continuous Systems*. Wiley, 2007. [Online]. Available: https://books.google.co.uk/books?id=kWja9NTH0bEC

[56] A. OKAJIMA, "Flows around two tandem circular cylinders at very high reynolds numbers," *Bulletin of JSME*, vol. 22, no. 166, pp. 504–511, apr 1979. [Online]. Available: http://ci.nii.ac.jp/naid/110002358986/en/

[57] D. Inman and R. Singh, *Engineering Vibration*, ser. Always Learning. Pearson, 2014.

[58] R. D. Blevins and C. S. Coughran, "Experimental investigation of vortex-induced vibration in one and two dimensions with variable mass, damping, and reynolds number," vol. 131, October date.

[59] B. Stappenbelt, F. Lalji, and G. Tan, "Low mass ratio vortex-induced motion," in *16th Australia Fluid Mechanics Conference*, S. o. E. The University of Queensland, Ed.

[60] L. Tan and J. Jiang, "Chapter 8 - infinite impulse response filter design," in *Digital Signal Processing (Second Edition)*, second edition ed., L. T. Jiang, Ed. Boston: Academic Press, 2013, pp. 301 – 403. [Online]. Available: http://www.sciencedirect.com/science/article/pii/B9780124158931000081

[61] ——, "Chapter 4 - discrete fourier transform and signal spectrum," in *Digital Signal Processing (Second Edition)*, second edition ed., L. T. Jiang, Ed. Boston: Academic Press, 2013, pp. 87 – 136. [Online]. Available: http://www.sciencedirect.com/science/article/pii/B9780124158931000044

[62] P. W. Bearman, "Vortex shedding from oscillating bluff bodies," *Annual Review of Fluid Mechanics*, vol. 16, no. 1, pp. 195–222, 1984.

[63] R. King, "A review of vortex shedding research and its application," *Ocean Engineering*, vol. 4, no. 3, pp. 141 – 171, 1977. [Online]. Available: http://www.sciencedirect.com/science/article/pii/0029801877900026

[64] H. Benaroya and R. D. Gabbai, "Modelling vortex-induced fluid–structure interaction," *Philosophical Transactions of the Royal Society of London A: Mathematical, Physical and Engineering Sciences*, vol. 366, no. 1868, pp. 1231–1274, 2008. [Online]. Available: http://rsta.royalsocietypublishing.org/content/366/1868/1231

[65] M. S. Pantazopoulos, "Vortex-induced vibration parameters: critical review," in *American Society of Mechanical Engineers, New York, NY (United States)*, 1994.

[66] L. Shiau, "Wind–induced vibration of two flexible cylindrical structures," *Journal of Engineering Mechanics*, vol. 115, no. 9, pp. 2089–2098, 1989. [Online]. Available: http://dx.doi.org/10.1061/(ASCE)0733-9399(1989)115:9(2089)

[67] O. M. Griffin and S. E. Ramberg, "Vortex shedding from a cylinder vibrating in line with an incident uniform flow," *Journal of Fluid Mechanics*, vol. 75, pp. 257–271, 5 1976. [Online]. Available: http://journals.cambridge.org/article_S0022112076000207

[68] T. Tsutsui, "Experimental study on the instantaneous fluid force acting on two circular cylinders closely arranged in tandem," *Journal of Wind Engineering and Industrial Aerodynamics*, vol. 109, pp. 46 – 54, 2012. [Online]. Available: http://www.sciencedirect.com/science/article/pii/S0167610512001912

[69] J. Vandiver and J.-Y. Jong, "The relationship between in-line and cross-flow vortex-induced vibration of cylinders," *Journal of Fluids and Structures*, vol. 1, no. 4, pp. 381 – 399, 1987. [Online]. Available: http://www.sciencedirect.com/science/article/pii/S0889974687902799

[70] A. H. Nayfeh, *Introduction to perturbation techniques*. John Wiley & Sons, 2011.

[71] F. Jian-Shu, F. Zhuo, L. Xiao-Juan, and R. Man-Sheng, "Chaos synchronization in two coupled duffing oscillators," *Chinese Physics Letters*, vol. 18, no. 11, p. 1438, 2001. [Online]. Available: http://stacks.iop.org/0256-307X/18/i=11/a=304

[72] S. P. Raj and S. Rajasekar, "Migration control in two coupled duffing

oscillators," *Phys. Rev. E*, vol. 55, pp. 6237–6240, May 1997. [Online]. Available: http://link.aps.org/doi/10.1103/PhysRevE.55.6237

[73] A. Bokaian and F. Geoola, "Vortex shedding from two interfering circular cylinders," *Journal of Engineering Mechanics*, vol. 110, no. 4, pp. 623–628, 1984.

[74] D. Allen and D. Henning, "Vortex-induced vibration current tank tests of two equal-diameter cylinders in tandem," *Journal of Fluids and Structures*, vol. 17, no. 6, pp. 767 – 781, 2003. [Online]. Available: http://www.sciencedirect.com/science/article/pii/S0889974603000197

[75] R. G. Williams and W. Suaris, "An analytical approach to wake interference effects on circular cylindrical structures," *Journal of Sound and Vibration*, vol. 295, no. 12, pp. 266 – 281, 2006. [Online]. Available: http://www.sciencedirect.com/science/article/pii/S0022460X06001003

[76] E. Huse, "Interaction in deep-sea riser arrays," in *Offshore Technology Conference*, 1993.

[77] M. L. Facchinetti, E. de Langre, E. Fontaine, P. A. Bonnet, F. Biolley, and S. Etienne, "Viv of two cylinders in tandem arrangement: Analytical and numerical modeling," in *International Society of Offshore and Polar Engineers*, 2002.

[78] J. C. Lagarias, J. A. Reeds, M. H. Wright, and P. E. Wright, "Convergence properties of the nelder–mead simplex method in low dimensions," *SIAM Journal on Optimization*, vol. 9, no. 1, pp. 112–147, 1998. [Online]. Available: http://dx.doi.org/10.1137/S1052623496303470